Poster ID： 1 The 2024 International Workshop on the High Energy Circular Electron Positron Collider (CEPC2024), Nanjing, China, Oct 23-27, 2024

CEPC Megawatt-level High Power Density High Voltage Power System

LIU J.D, ZHOU Z.S, LI J.Y, CHI Y.L

1. Institute of High Energy Physics, Chinese Academy of Sciences, Beijing, China
2. University of Chinese Academy of Sciences, Beijing 100049, China

INTRODUCTION

The cost of large particle accelerator devices is expensive (up to billions), and the operating energy consumption is huge (hundreds of megawatts). Green, environmental economics and sustainability are hot topics in accelerator research. For the CEPC CDR/TDR, a high-efficiency RF power source system is planned. This system adopts a 1-to-1 scheme, necessitating 96 sets of 650MHz 800kW high-efficiency klystrons and PSM (Pulse Step Modulation) high-voltage power supply systems. This paper introduces a novel design scheme for high-voltage power supplies (HVPS) and explores the feasibility of using a 1-to-2 or 1-to-4 configuration, where a single megawatt high-power HVPS could drive multiple klystrons. The proposed design features high power density and hybrid modulation methods.

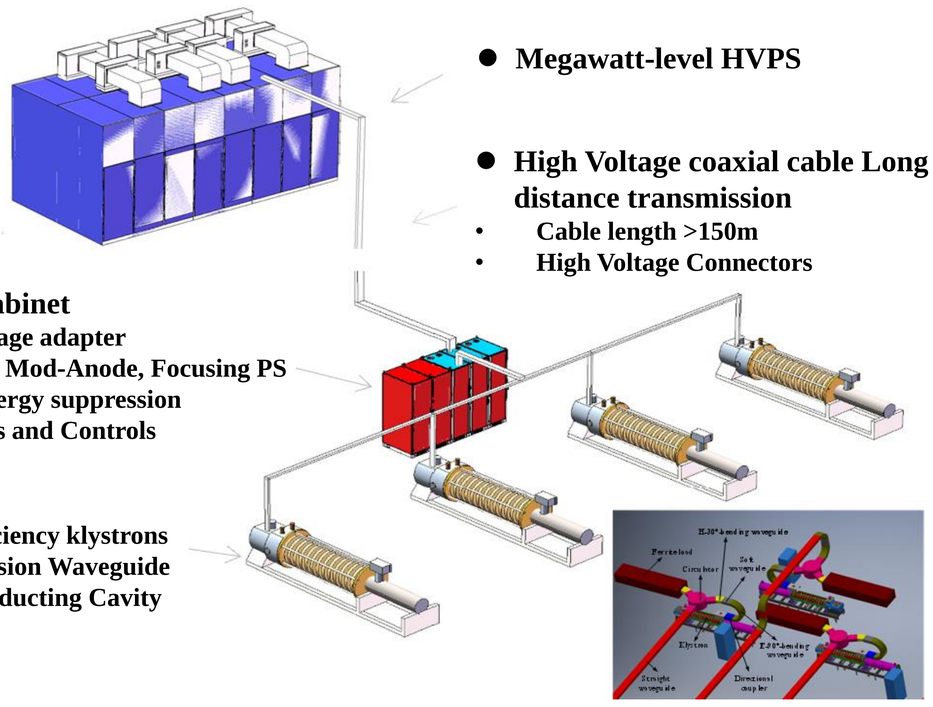

RF Power System Megawatt-level HVPS to Klystron with 1 to 2 or 1 to 4 Layout Schematic

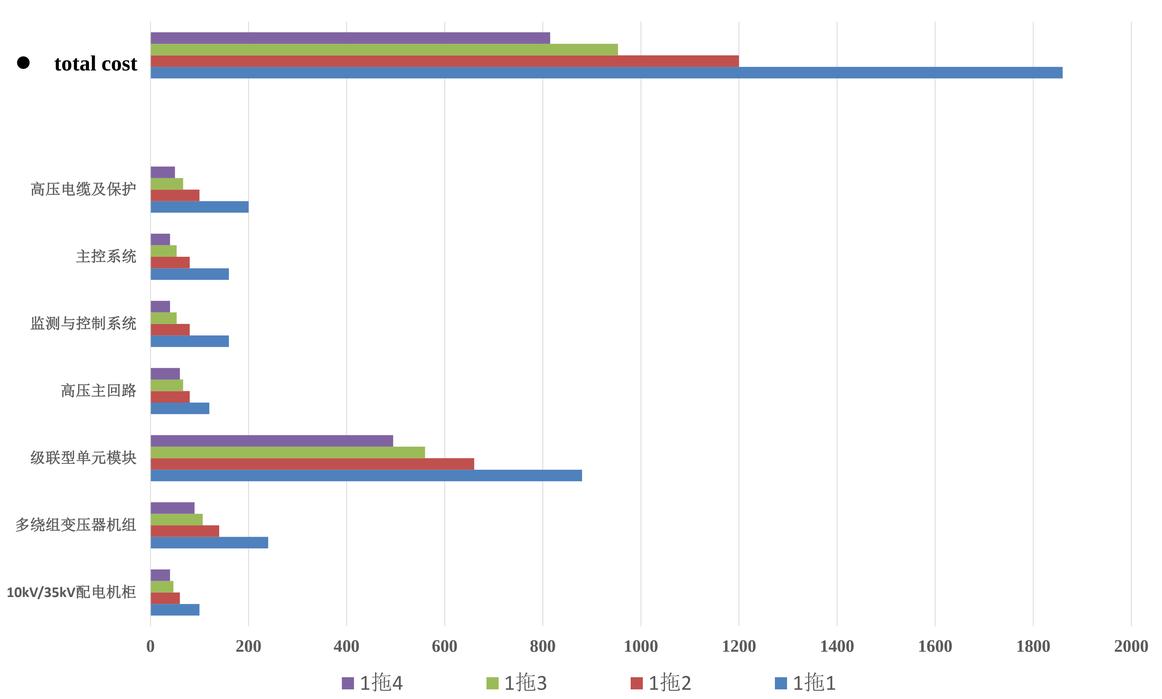

Estimated cost of one high-voltage power supply/total cost for different scheme

The key advantages of this scheme include:

1) Cost Reduction: The new design is expected to cut project costs by 50%, making it a more economical choice for large-scale accelerator projects.

2) Improved Reliability: By increasing the Mean Time Between Failures (MTBF), the system's overall reliability is significantly enhanced.

3) Enhanced Performance: The power supply performance for continuous-wave applications is improved, ensuring more stable and efficient operation.

4) Additionally, this new HVPS scheme can be utilized for power factor correction in large power grids. It offers a reactive power compensation capacity ranging from 2.19 to 5.475 Mvar（User-defined）, potentially reducing annual operating expenses by 15.33 to 38.32 million RMB.

The proposed design scheme not only supports the green, energy-saving, and sustainable development of CEPC, but also applicable to others projects such as the Compact Linear Collider (CLIC) and the Future Circular Collider (FCC).

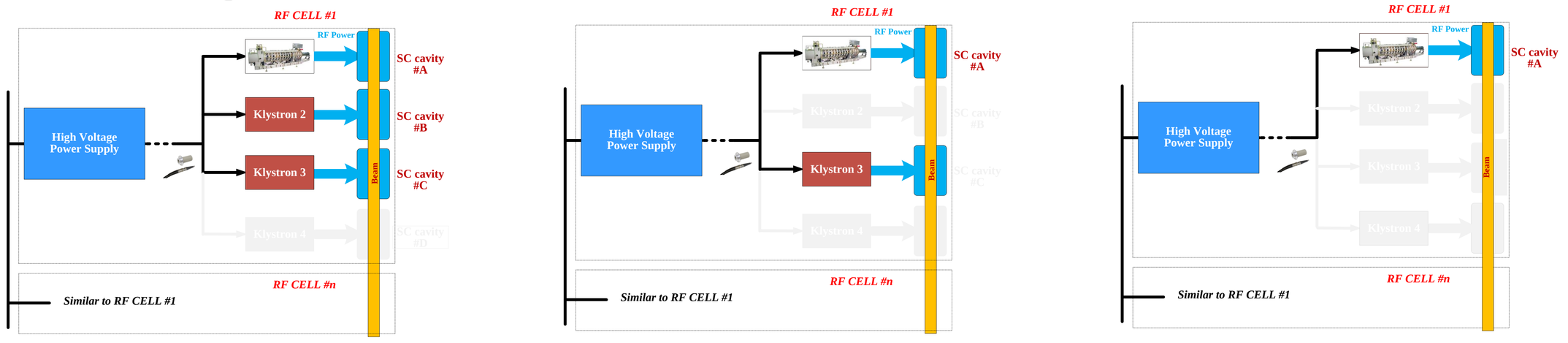

1 to 4, 1 to 3, 1 to 2, 1 to 1, can be customizable configured for redundancy

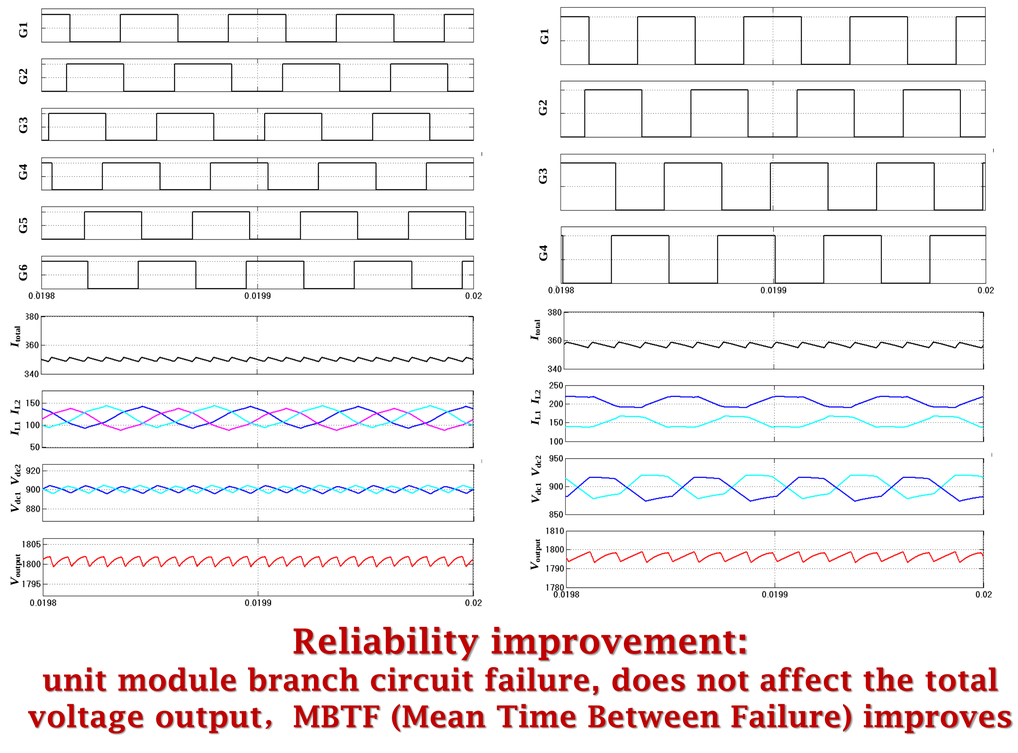

Reliability improvement:
unit module branch circuit failure, does not affect the total voltage output，MBTF (Mean Time Between Failure) improves

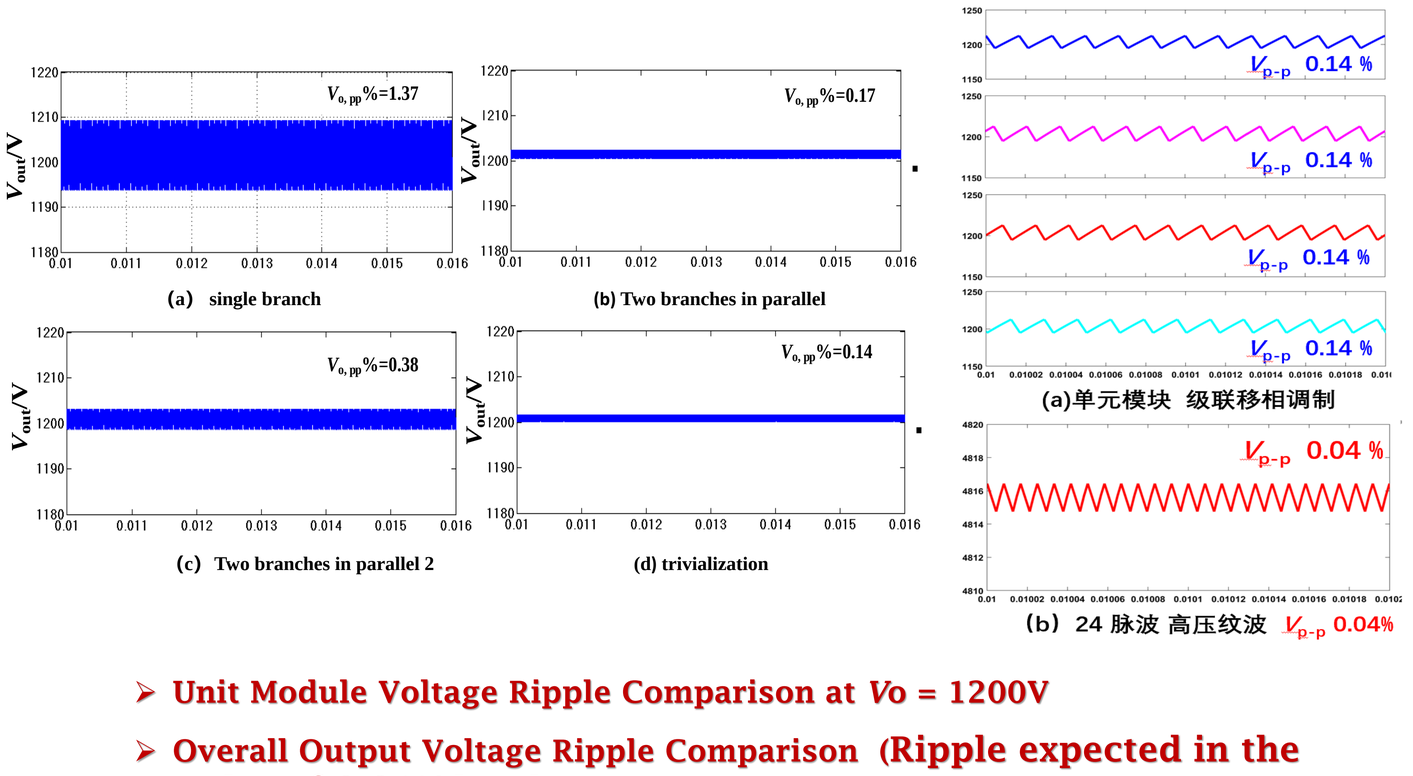

- **Unit Module Voltage Ripple Comparison at *Vo* = 1200V**
- **Overall Output Voltage Ripple Comparison (Ripple expected in the order of 0.01% level, 1% for conventional HVPS)**

REFERENCE

[1] Gao, J. CEPC Technical Design Report: Accelerator. Radiat Detect Technol Methods 8, 1–1105 (2024). https://doi.org/10.1007/s41605-024-00463-y

Poster ID:2

The 2024 International Workshop on the High Energy Circular Electron Positron Collider (CEPC202), Hangzhou, China, Oct 22-27, 2024

An External Injected Driver-witness Bunch Pair Merge System with Femtosecond Timescale Jitter

Wei Li[1], Cai Meng[1]

Institute of High Energy Physics, Chinese Academy of Sciences, Beijing 100049, China

[1]also at University of Chinese Academy of Sciences, Beijing 100049, China

中国科学院高能物理研究所
Institute of High Energy Physics
Chinese Academy of Sciences

Beam-driven plasma-wakefield accelerators (PWFA) rely on the precise energy transfer from a leading drive bunch to a trailing witness bunch, with the separation between the two typically on the order of 100 fs. To achieve high transformer ratios and maintain long-distance acceleration, it is crucial to precisely control this separation. We propose and demonstrate a novel system that merges two bunches from separate beamlines using a common dipole magnet. Through optimized parameter sets, we show that the energy jitter-induced separation time jitter can be reduced to femtosecond levels, while accounting for coherent synchrotron radiation (CSR) and longitudinal space charge (LSC) effects. Furthermore, we address emittance growth during beam merging, incorporating design strategies to mitigate its impact and preserve beam quality. Our system is compatible with other longitudinal modulation methods and can utilize the initial energy difference between bunches for further beam compression in high-energy accelerators.

INTRODUCTION

To ensure efficient energy transfer in Beam-driven plasma-wakefield accelerators (PWFA), the double-bunch structure must meet three key requirements:

- precise temporal separation of around 100 fs with fs-level tof jitter control
- longitudinal alignment of both bunches along the same axis
- controlled emittance to minimize growth, especially from CSR.

Existing methods to generate such a structure include splitting a single bunch with a mask, which causes emittance degradation and charge loss, and generating two bunches at the photocathode , which faces challenges in achieving high charge and precise timing.

In our scheme, two bunches with energies of 200 MeV and 400 MeV are transported through two separate beamlines into our designed system and are ultimately merged into a double-bunch structure via a single dipole magnet, which avoids charge loss and enables high-charge (nC-level) bunch generation.

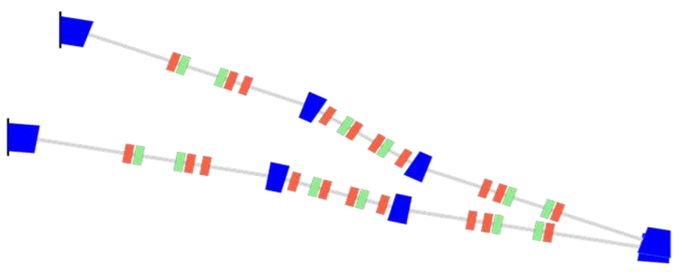

Figure 1:layout of the merge system

SYSTEM DESIGN AND PRINCIPLES

To reach our goal, we have to take energy variation induced by CSR and LSC into consideration. By introducing the energy variation terms into the transport matrices, we notice that the higher order transport matrix element can contribute to residual dispersions.

$$\Delta x = R_{16}\delta \quad \Delta x' = R_{26}\delta \quad \Delta z = R_{56}\delta$$

Modified Dispersions

Emittance growth

$$\Delta x = \int_{s_1}^{s_f} R_{16}^{s\to s_f}\frac{d\delta}{ds}ds + \left(R_{16} + 2\int_{s_i}^{s_f} T_{166}^{s\to s_f}\frac{d\delta}{ds}ds\right)\delta$$

$$\Delta x' = \int_{s_i}^{s_f} R_{26}^{s\to s_f}\frac{d\delta}{ds}ds + \left(R_{26} + 2\int_{s_i}^{s_f} T_{266}^{s\to s_f}\frac{d\delta ds}{ds}\right)\delta$$

$$\Delta z = \int_{s_i}^{s_f} R_{56}^{s\to s_f}\frac{d\delta}{ds}ds + \left(R_{56} + 2\int_{s_i}^{s_f} T_{566}^{s\to s_f}\frac{d\delta}{ds}ds\right)\delta$$

Equation 1:Modified transportation equations

Table 1: Witness/Driver parameters

Energy	200/400 MeV
Charge	1/5 nC
Beam length	0.3/0.3 mm
Energy spread(rms)	0.1/0.1 %
Emittance(normalized)	20/20 μm

OPTIMIZATION RESULT

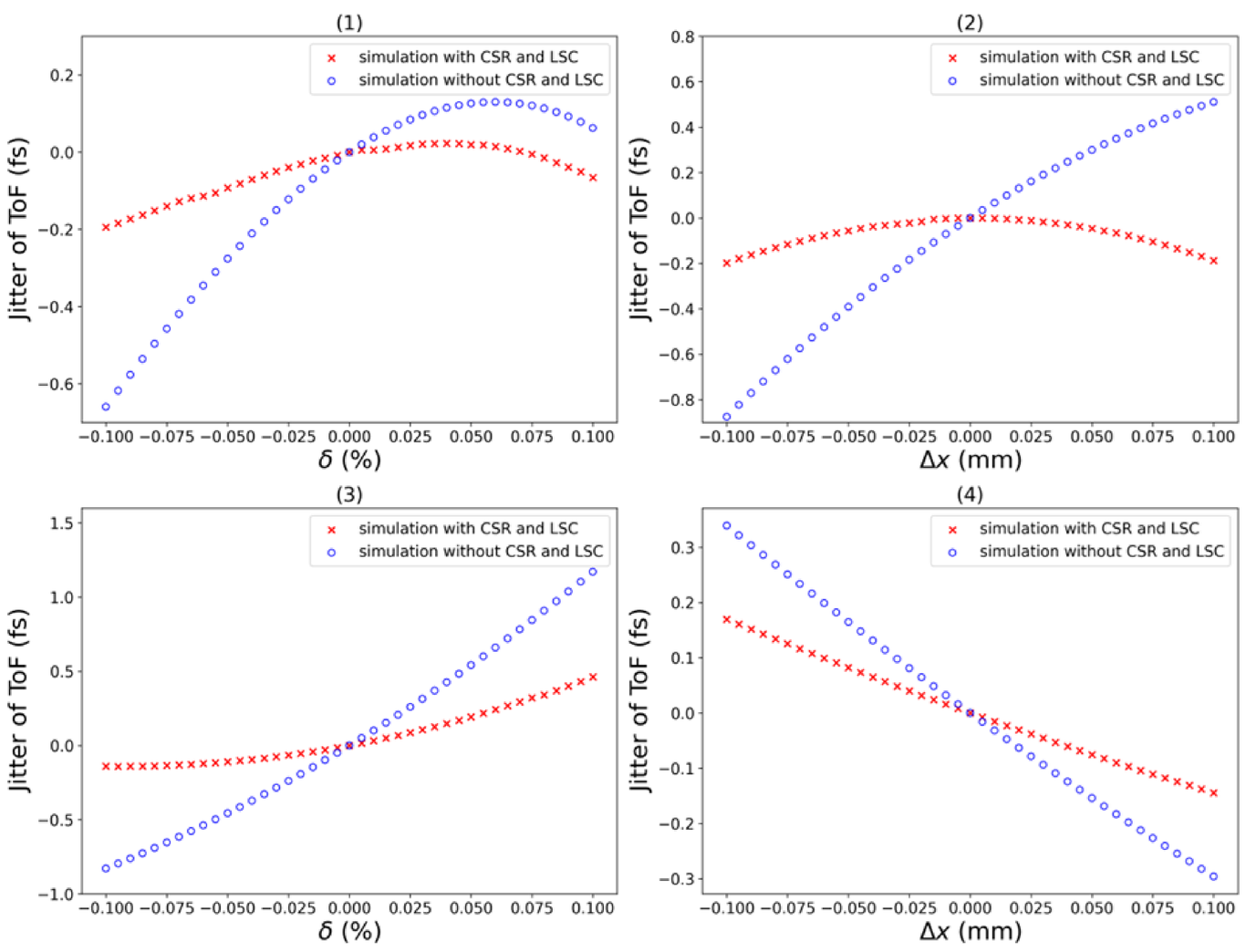

Figure 2: tof jitter induced by energy jitter and initial x offset

By simulation of ELEGANT, we optimize both beamlines, controlling the tof jitter below 1fs with 0.1% energy jitter and 0.1 mm transverse offset at the entrance. Also the effect of the magnetic field error caused by power supply of dipoles are considered.

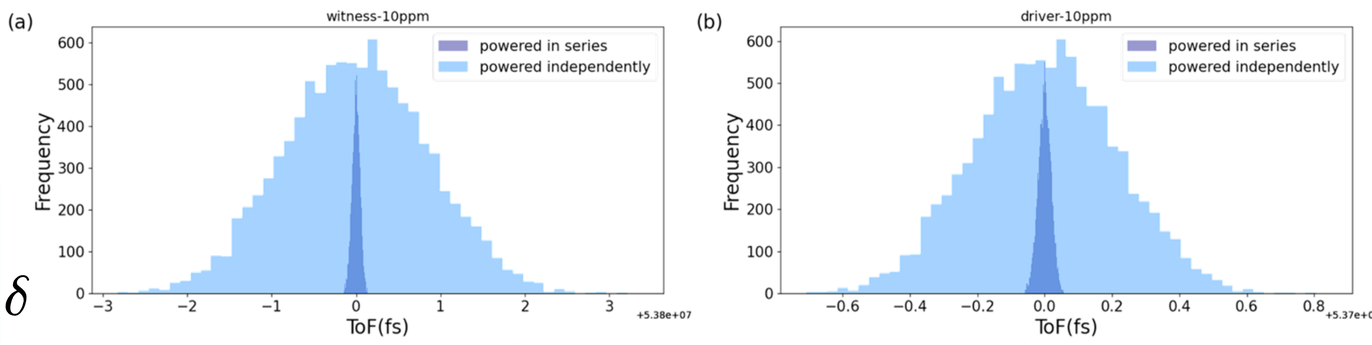

Figure 3: tof jitter induced by power supply error of the dipoles

CONCULSION

This study propose a design which effectively merges two high-charge bunches with energies of 100 MeV and 200 MeV, achieving femtosecond-level timing stability and minimal emittance growth, making it a highly suitable solution for advanced PWFA applications and compatible with other longitudinal modulation methods.

REFERENCES

[1] P. Chen, J. M. Dawson, R. W. Huff, and T. Katsouleas,Acceleration of electrons by the interaction of a bunched electron beam with a plasma, Phys. Rev. Lett. 54, 693 (1985).
[2] N. Majernik, G. Andonian, W. Lynn, S. Kim, C. Lorch, R. Roussel, S. Doran, E. Wisniewski, C. Whiteford, P. Piot, J. Power, and J. B. Rosenzweig, Beam shaping using an ultrahigh vacuum multileaf collimator and emit-
tance exchange beamline, Phys. Rev. Accel. Beams 26, 022801 (2023).
[3] C. M. Entrena Utrilla, Generation and transport of double-bunch electron beams in the FLASH beamline, Master's thesis, U. Hamburg, Dept. Phys. (2014).
[4] R Pompili et al 2016 New J. Phys. 18 083033
[5] M. Venturini, Design of a triple-bend isochronous achromat with minimum coherent-synchrotron-radiation-induced emittance growth, Phys. Rev. Accel. Beams 19,064401 (2016).

† email address: weili@ihep.ac.cn mengc@ihep.ac.cn

Design of S-band high efficiency klystron

Y. A. Wang[1,2], Z. S. Zhou[1,2], O. Z. Xiao[1], Y. Liu[1,2], H. Xiao[1,2], F. Li[1], W. B. Gao[1,2], M. Iqbal[1], A. Aleem[1], F. Y. Wang[1,2], Y. L. Chi[1], Noman Habib[1,2]

[1]Institute of High Energy Physics, Chinese Academy of Sciences, Beijing 100049, China
[2]University of Chinese Academy of Sciences, Beijing 100049, China

中国科学院高能物理研究所
Institute of High Energy Physics
Chinese Academy of Sciences

Abstract

This paper focuses on designing S-band klystrons with higher efficiency to reduce energy consumption and costs in particle accelerators. Two novel bunching methods, Core Oscillation Method (COM) and Bunching Alignment and Collecting (BAC), have been applied to the S-band klystron at the Beijing Electron Positron Collider II (BEPCII). These methods have increased the klystron's efficiency from 45% to 55% and its output power to 80 MW. The design has been optimized using 1-D, 2-D, and 3-D simulation codes, which have improved electron injection and RF conversion efficiency. This design aligns with the goal of reducing energy consumption and promoting environmental sustainability.

Background

The development of large particle accelerators necessitates klystrons capable of providing megawatt-level power, which results in high energy consumption and operational costs. Therefore, enhancing the efficiency of klystrons can enable higher RF power generation while simultaneously reducing energy consumption and operating costs, thereby promoting environmentally friendly and sustainable solutions.

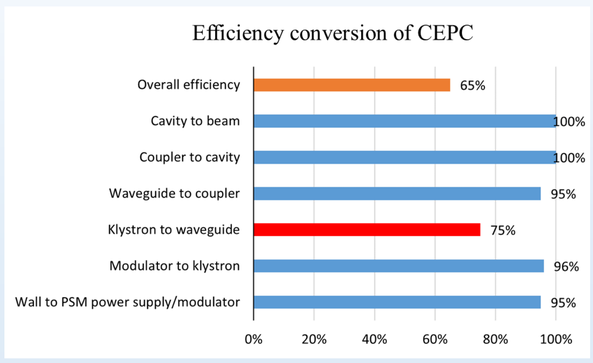

Figure 1 Overall efficiency of CEPC power sources

Method

The BAC method utilizes a resonant cavity to generate oscillations at the bunching center, reducing the length of high-frequency interactions. This leads to improved RF conversion efficiency and reduced energy losses. In contrast, the COM increases the drift length between the cavities to leverage the oscillation properties of the electron beam plasma, allowing for the oscillation of the bunching center electrons.

Design of electronic optical system

The required parameters for the electron gun in this design are a voltage of 350 kV, a current of 415 A, and a beam radius of 8.65 mm. The electron gun is modeled in DGUN based on Pierce electron gun theory.

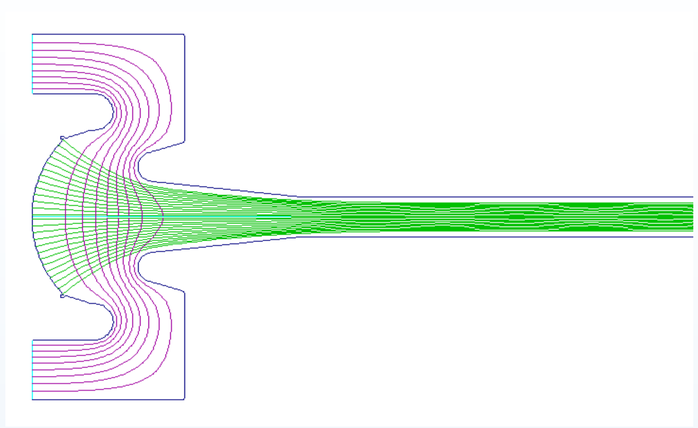

Figure 2 The electron gun in DGUN

The focusing magnetic field for the electron gun is provided by the coil structure designed using Poisson.

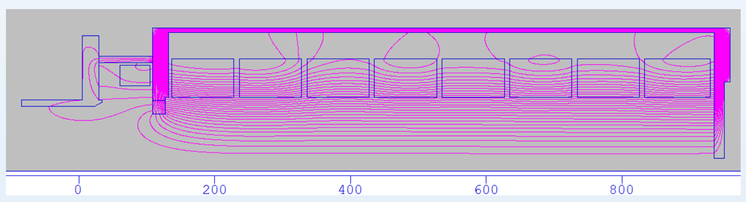

Figure 3 The coil structure in Poisson

The coil structure and magnetic field distribution are verified in CST.

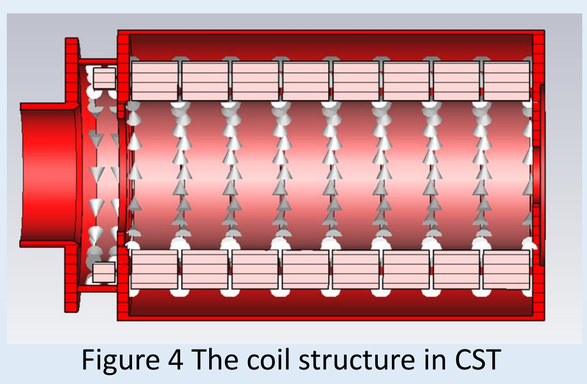

Figure 4 The coil structure in CST

Design of electronic optical system

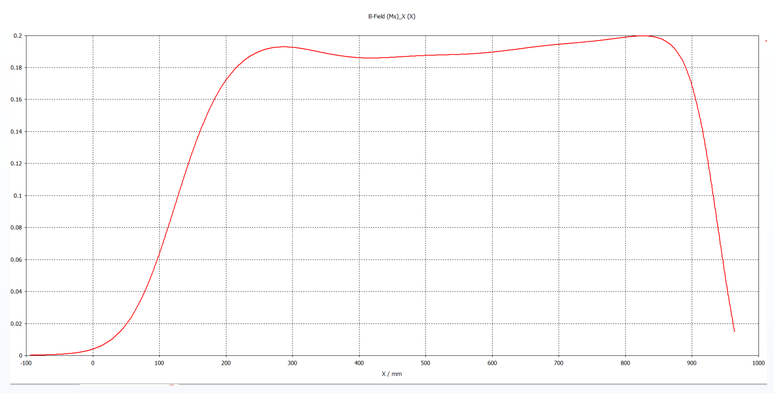

Figure 5 Magnetic field distribution in CST

The electron gun is verified in CST to achieve a current of 415 A, a maximum beam radius of 8.67 mm, and a beam fluctuation rate of 5.1%.

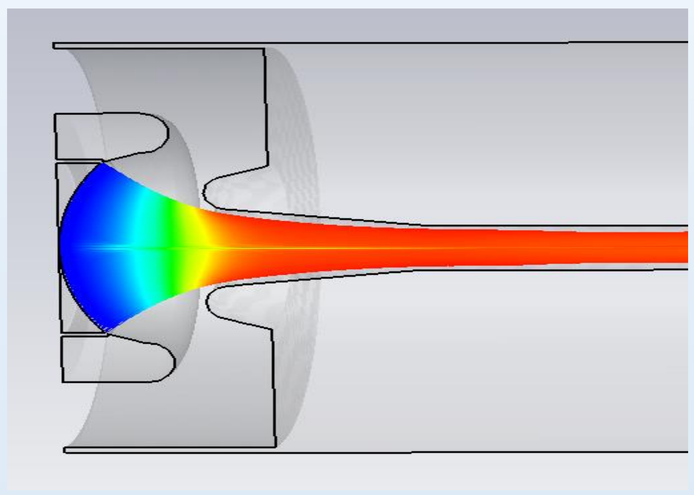

Figure 6 The electron gun in CST.

Beam dynamic

Using 8 resonant cavities, the resonant cavity array is designed using the BAC and COM methods. The fifth resonant cavity is a second harmonic cavity.

By optimizing the parameters of the resonant cavities and the distances between them using a genetic algorithm, the relationship between efficiency and the length of the klystron can be determined.

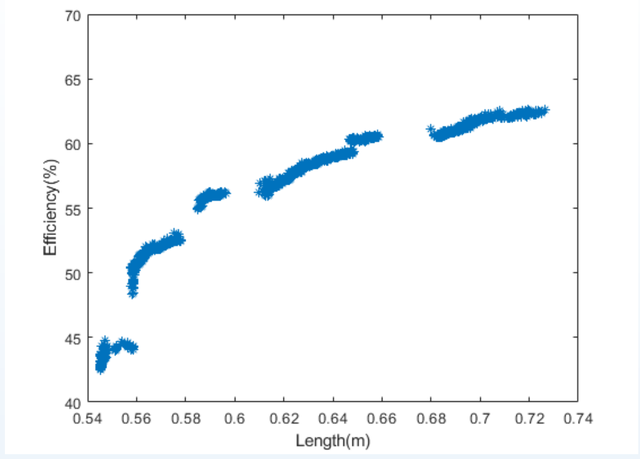

Figure 7 Relationship between efficiency and length

The parameters of the 8 resonant cavities are simulated in 1-D AJDISK. The RF conversion efficiency of the klystron is 61.5%, and the output power is 89 MW.

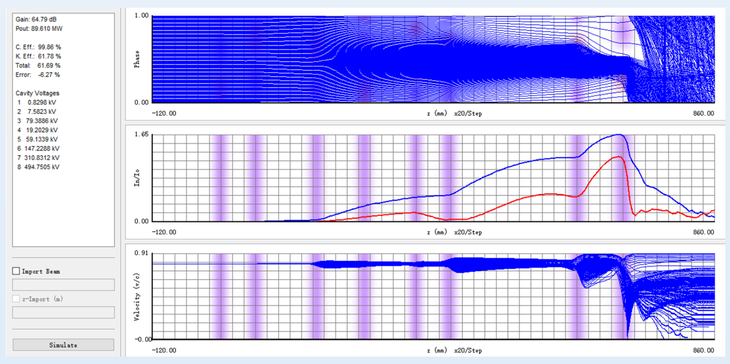

Figure 8 1-D simulation result in AJDISK

In 2-D EMSYS, the RF conversion efficiency of the klystron was determined to be 58%, with an output power of 84 MW. Figure 9 displays the beam current, energy, and current distribution of the klystron.

Beam dynamic

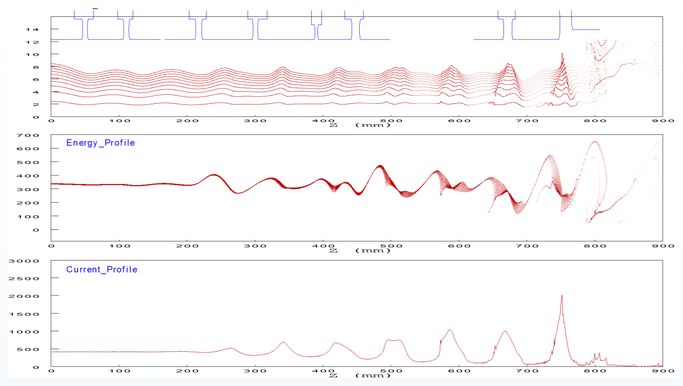

Figure 9 Beam and energy profile simulated by EMSYS

In 3-D CST, the RF conversion efficiency of the klystron was determined to be 55%, with an output power of 80 MW.

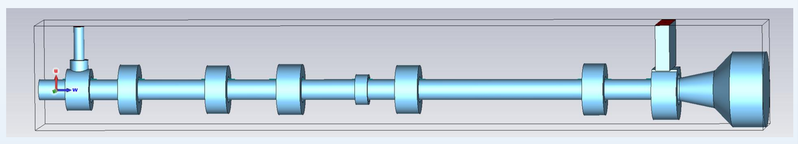

Figure 10 Structure of the klystron

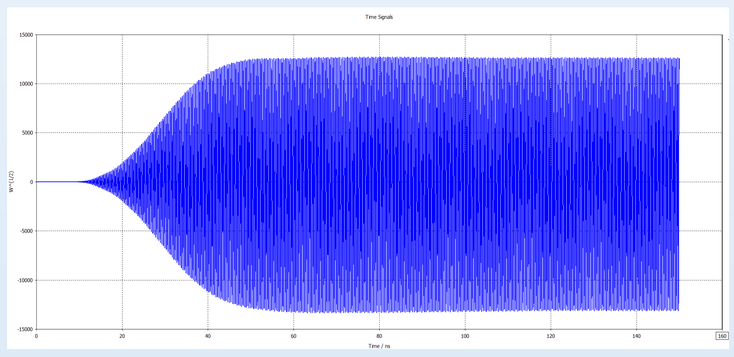

Figure 11 The power output in CST

Conclusion

The electron gun is modeled and optimized based on Pierce electron gun theory for the electron optical system. The electron gun structure is optimized using 2-D DGUN and 3-D CST, while the coil structure is optimized using 2-D Poisson and 3-D CST. Currently, the electron beam current, beam radius, and beam fluctuation rate all meet the design requirements.

For the design of S-band high-efficiency klystrons, two novel beam focusing methods—Core Oscillation Method (COM) and Bunching Alignment and Collecting (BAC)—have been employed. The 1-D simulation efficiency is 61.5%, the 2-D simulation efficiency is 58%, and the 3-D simulation efficiency is 55%.

In the future, overall optimization, thermal analysis, and cooling system design will be carried out. After the design is completed, mechanical machining and high-power testing will be conducted.

References

[1] R.V. Egorov,I.A.Guzilov,“BAC-klystron: a new generation of klystrons in vacuum electronics”, Moscow University Physics Bulletin, Vol. 74, No.1, pp 38-42,2019.

[2] Gao, Jie . "CEPC Technical Design Report: Accelerator." Radiation Detection Technology and Methods 8.1(2024):1-1105.

[3] Guzilov, I. A. . "BAC method of increasing the efficiency in klystrons." Vacuum Electron Sources Conference IEEE, 2014.

[4] CST GmbH, Darmstadt, Germany.

[5] Guzilov, Igor , et al. "Comparison of 6 MW S-band pulsed BAC MBK with the existing SBKs." (2017).

[6]S. G. Tantawi, et al. "Beam-wave interaction studies for the development of high-efficiency klystrons." IEEE Transactions on Electron Devices 60.6 (2013): 2014-2022.

* Work supported by Dr. Yifang Wang’s Science Studio of the Thousand Talents Project

† email address: zhouzs@ihep.ac.cn wangya@ihep.ac.cn

Poster ID:5 The 2024 International Workshop on the High Energy Circular Electron Positron Collider (CEPC2024), Hangzhou, China, Oct 23-27, 2024

A Low-Level Radio Frequency (LLRF) Control System for Multiple Superconducting Cavities Based on MicroTCA.4*

Wenbin Gao[1,2], Nan Gan†[1], Zusheng Zhou[1,2], Jiyuan Zhai[1,2], Xinpeng Ma[1], Fei Li[1], Yu Liu[1,2], Yiao Wang[1,2], Han Xiao[1,2], Fanyu Wang[1,2]

Institute of High Energy Physics, Chinese Academy of Sciences, Beijing 100049, China[1]

University of Chinese Academy of Sciences, Beijing 100049, China[2]

中国科学院高能物理研究所 Institute of High Energy Physics Chinese Academy of Sciences

In modern particle accelerators, multiple superconducting cavities are often driven simultaneously by one high-power klystron, thereby reducing the cost of the power sources. The CEPC RF system contains 96 cryomodules for 650 MHz 2-cell cavities. Each cryomodule contains six 650 MHz 2-cell cavities. In the CEPC EDR horizontal test, it is planned to use a single power source to drive a superconducting module (6×2-cell cavities), set up a testing platform, and verify its feasibility. This approach significantly reduces the cost of the power source but introduces several challenges for high-precision control of superconducting cavities, such as gradient differences due to individual cavity variations, frequency offsets caused by Lorentz force detuning, and the calibration of vector sum of amplitudes and phases for multiple cavities. This paper introduces the design of a MicroTCA.4 based Low-Level Radio Frequency (LLRF) control system for multi-cavity control, which will be used for the horizontal testing of the CEPC 650MHz superconducting cavities. Based on the vector-sum control principle, the system utilizes IQ sampling, feedforward-feedback control, and other techniques, eventually achieved high-precision amplitude and phase control and frequency tuning of six superconducting cavities.

BACKGROUND & INTRODUCTION

The control of multiple superconducting cavities is based on vector sum control principles, where the energy gain of the beam results from the integration of the accelerating voltage along the acceleration path. The calibrated amplitude and phase vectors of multiple cavities are summed to form a single equivalent amplitude and phase signal, which is applied to all control loops. Individual cavities undergo separate coupling adjustments and tuning without individual feedback control. This approach reduces the number of feedback control loops, and consequently, the number of LLRF systems, thereby lowering costs and simplifying the system.

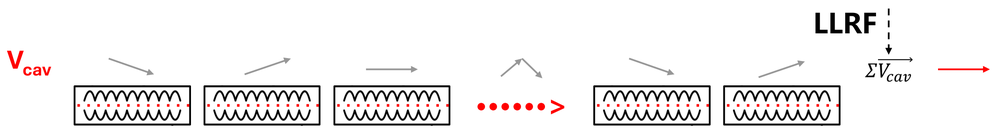

Figure 1:The Vector Sum Control Principle

The key focus of vector sum control lies in calibrating the measurement signals. Small measurement errors in each cavity can be negligible when controlled individually, but when the measurement signals from multiple cavities are summed, the error in the vector sum can significantly increase to an unacceptable level. If the measurement signals are not corrected, even perfect control of the vector sum would still result in substantial errors. Therefore, the prerequisite for everything is the calibration of the vector sum.

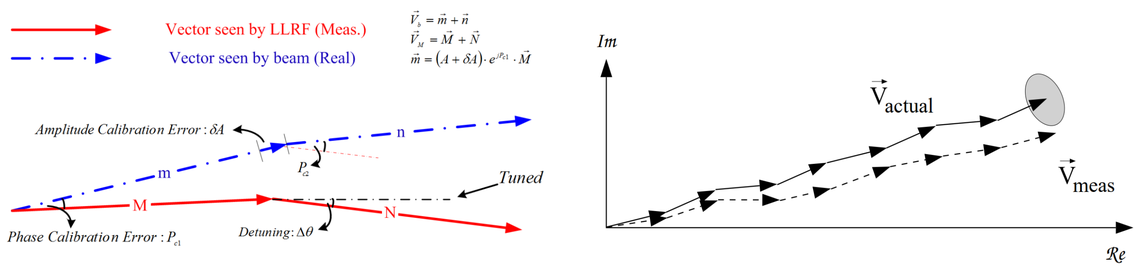

Figure 2: The actual vector seen by the beam and the uncalibrated measurement vector

DESIGN OF THE LLRF FOR MULTI-CAVITY

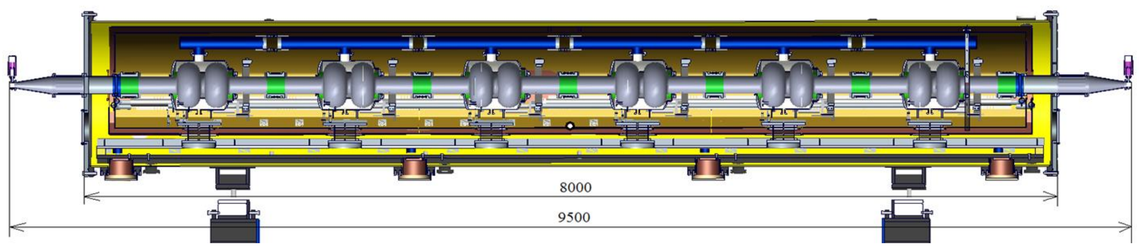

Figure 3: CEPC 650 MHz 6×2-cell superconducting module

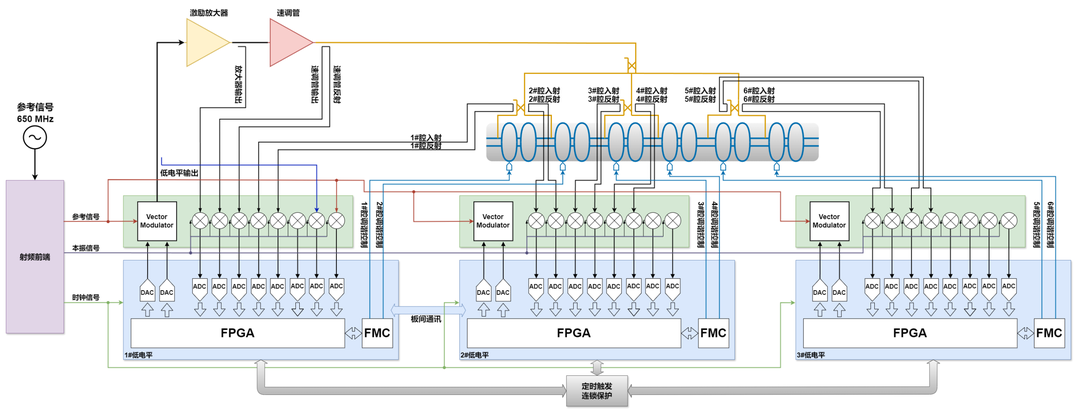

Figure 4: CEPC 650 MHz 6×2-cell superconducting module LLRF system design scheme

- Six 2-cell superconducting cavities are driven by **a klystron power source** system
- The LLRF adopts the domestic MicroTCA platform, including **3** sets of control boards
- A multi-cavity control algorithm based on **vector sum** is used to achieve synchronous control of the amplitude, phase and frequency of six superconducting cavities driven by a set of power source.

DESIGN PROGRESS

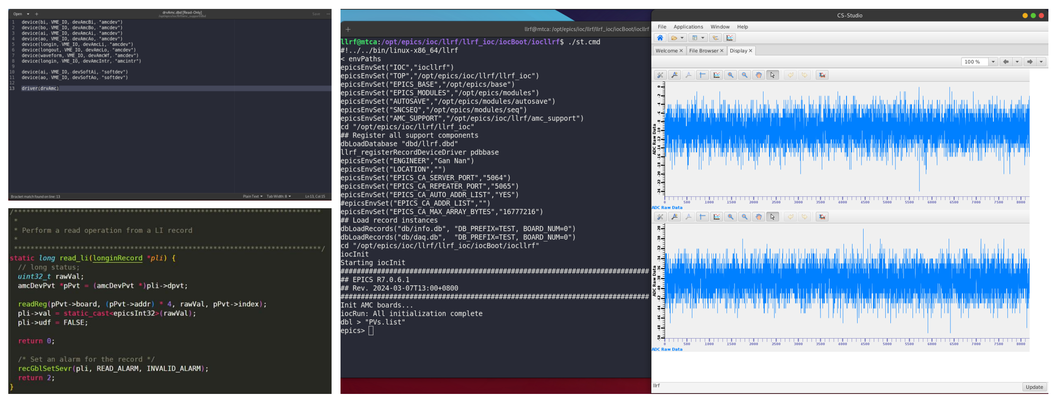

Figure 5: A portion of the firmware and IOC programs

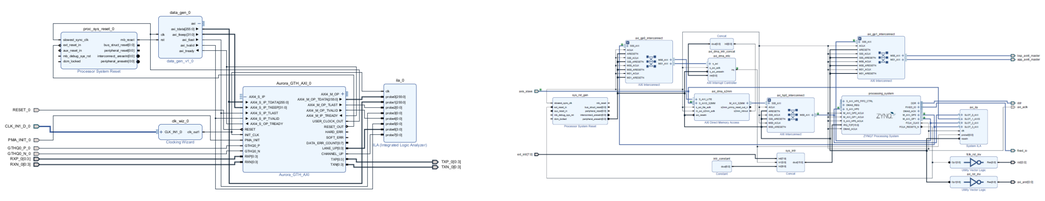

Figure 6: Inter-board communication module and processing system block design

Figure 7: tuning control board and partial domestic hardware resources

CONCLUSION

Currently, the project team has completed the development of the LLRF firmware for the domestically produced MicroTCA control board and the development of the upper-layer EPICS application, as well as successfully finished the development and debugging of the inter-board communication program. Moving forward, it is planned to complete the migration of the LLRF algorithms by the end of March 2025. This includes the research and development of multi-cavity control algorithms and the transplantation of firmware and upper-layer applications. At the same time, the procurement of domestically produced MicroTCA hardware, including chassis power sources, CPU boards, and FPGA control boards, will be completed by the same deadline. Additionally, the team plans to set up a horizontal test platform in Huairou in June 2025 for the installation and debugging of the low-level control system. These advancements indicate that the project is steadily progressing according to the scheduled timeline, laying a solid foundation for subsequent testing and practical application.

REFERENCES

[1] Schilcher, T., Schmueser, P., & Gamp, A. (1998). Vector sum control of pulsed accelerating fields in Lorentz force detuned superconducting cavities.

[2] Brandt, A. (2007). Development of a finite state machine for the automated operation of the LLRF control at FLASH (DESY-THESIS--2007-024). Germany

[3] Hoffmann, Matthias (2008). Development of a multichannel RF field detector for the low-level RF control of the free-electron laser at Hamburg (DESY-THESIS--2008-028). Germany

[4] I. Rutkowski, K. Czuba, D. Makowski, A. Mielczarek, H. Schlarb and F. Ludwig, "Vector Modulator Card for MTCA-Based LLRF Control System for Linear Accelerators," in IEEE Transactions on Nuclear Science, vol. 60, no. 5, pp. 3609-3614, Oct. 2013, doi: 10.1109/TNS.2013.2278372.

[5] Gao, J. CEPC Technical Design Report: Accelerator. Radiat Detect Technol Methods 8, 1–1105 (2024). https://doi.org/10.1007/s41605-024-00463-y

* Work supported by Dr. Yifang Wang's Science Studio of the Thousand Talents Project

† email address: gann@ihep.ac.cn

Poster ID：7 The 2024 International Workshop on the High Energy Circular Electron Positron Collider (CEPC2024), Hangzhou, China, Oct 23-27, 2024

*Preliminary design of energy recovery scheme for high-power klystron**

Yu Liu[1,2], Zusheng Zhou[1,2†], Fei Li[1], Ouzheng Xiao[2],Yiao Wang[1,2], Munawar Iqbal[1], Abid Aleem[1], Han Xiao[1,2], Wenbing Gao[1,2], Fanyu Wang[1,2], Noman Habib[1], Yunlong Chi[1,2]

1Institute of High Energy Physics, Chinese Academy of Sciences, Beijing 100049

2University of Chinese Academy of Sciences, Beijing 100049, China

中国科学院高能物理研究所
Institute of High Energy Physics
Chinese Academy of Sciences

Based on the high efficiency klystron scheme of circular electron positron collider (CEPC), the depressed collector design is proposed to improve the overall efficiency of RF power source. The depressed collector technology has been applied in low power microwave electronic vacuum devices such as traveling-wave tube(TWT) and klystron for TV communications. The velocity of electrons entering the klystron collector is scattered, and it is difficult to use the depressed collector to sort the velocity of electrons. This paper describes a detailed theoretical analysis of the depressed collector and determine its basic design scheme for CEPC high efficiency klystron. In order to verify the klystron energy recovery scheme, an energy recovery verification device is designed. Currently, the mechanical fabrication and the setup of the testing platform have been completed. The verification device is expected to be completed by the end of the year to carry out high-power experiments.

INTRODUCTION

The depressed collector is an important method to improve the efficiency of microwave tubes by recovering the energy of waste electrons. This technology has been widely used in TWT, and its collector recovery efficiency is more than 70%. Fig. 1 shows the basic principle of an energy recovery device. At present, the application of depressed collector on klystron is mainly used in low power klystron for TV and communication, but there is a little research on depressed collector technology of high power klystron. The characteristics of klystron bring some difficulties to the design of depressed collector. The proposal of depressed accelerator puts forward higher demand for high power klystron efficiency. The application of step-down collector technology in high power klystron further improves the overall efficiency of power source system. In order to verify the feasibility of klystron energy recovery scheme, we complete the design of energy recovery verification device. The mechanical machining was completed, and preliminary tests were conducted.

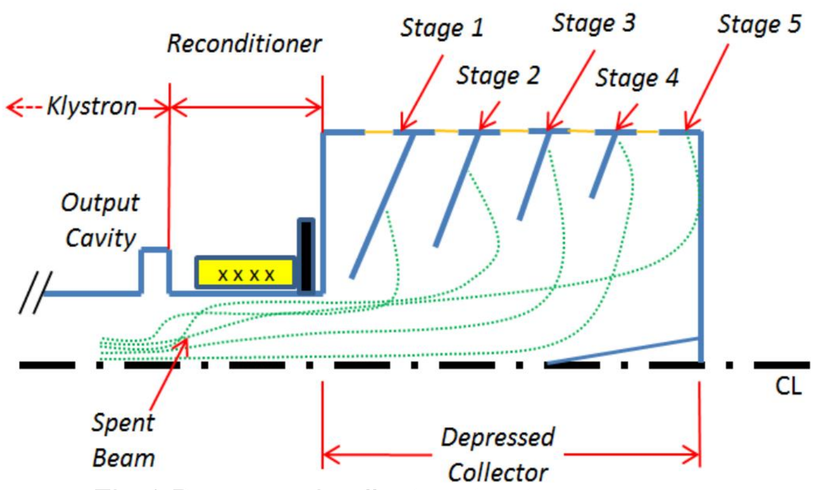

Fig.1.Depressed collector structure

DEPRESSED COLLECTOR PRINCIPLE

The recovery power of depressed collector is related to the selection of collector potential. A deceleration field is established in space by providing the collector with a lower potential than the tube body, after which the waste electrons will be decelerated by the electric field force upon entering the collector. The efficiency of the klystron is improved by the energy recovery on the electrode, and the heat dissipation pressure of the collector is also reduced.

Based on the high efficiency klystron of CEPC, the depressed collector scheme is designed. The high efficiency tube has a saturated output power of 800kW and a design efficiency of more than 75%. The main design parameters of the high-efficiency klystron are shown in Table 1.

Table 1: Klystron parameters of CEPC

Operating frequency	650 MHz
Output power	≥800 KW
Beam voltage	113 kV
Beam current	9.5 A
Beam perveance	0.25 μP
Efficiency	≥75%

Due to the need of low-level feedback control, the klystron usually works in the approximately linear region, and its output power is based on 700 kW. The probability distribution of its energy entering the collecting pole waste electron is shown in Fig. 2.

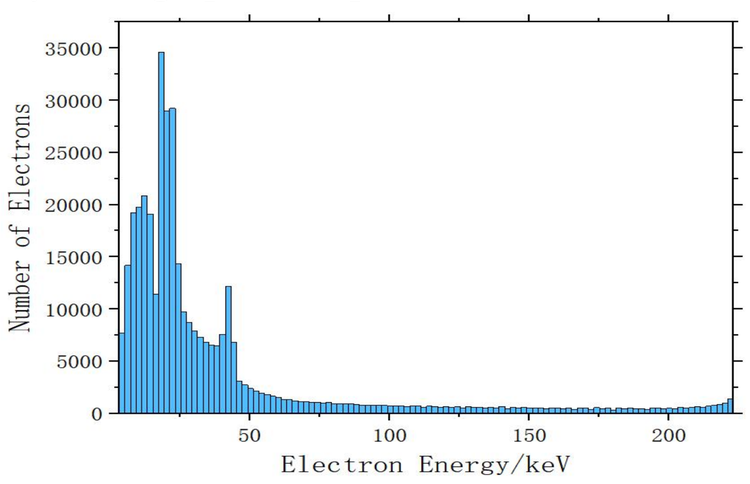

Fig.2.Energy distribution of waste electrons

The following formula is used to obtain the recovery power of the multi-stage depressed collector:

$$P_{rec} = \sum_{1}^{N-1} \int_{Vi}^{Vi+1} J_{waste}(V) I_0 V_i dV + \int_{V_N}^{\infty} J_{waste}(V) I_0 V_N dV$$

where Jwaste is the probability density function of electron energy distribution. We can calculate the relationship between the klystron efficiency of depressed collector and the number of electrodes, and the result is depicted in Fig. 3.

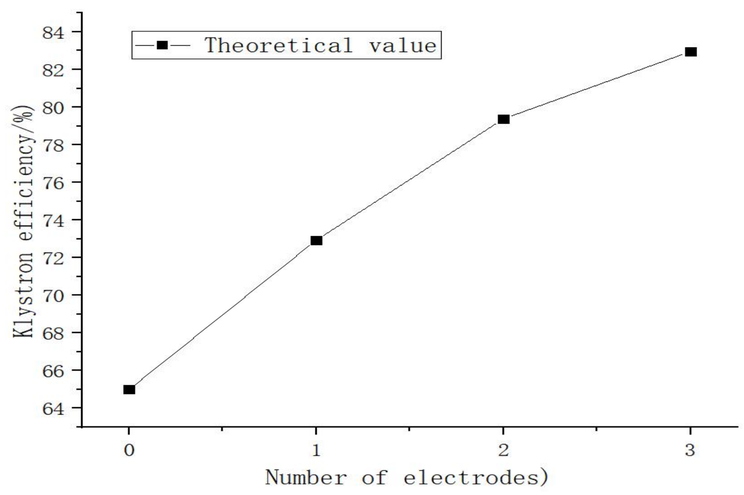

Fig.2.Number of electrodes vs efficiency

VERIFICATION DEVICE

Before processing the depressed collector klystron, we use the energy recovery verification device to verify the key technology. The basic structure and machining of the verification device are shown in Fig. 3 and Fig. 4.

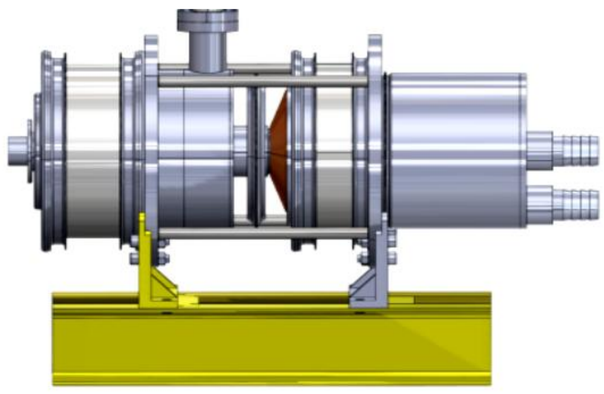

Fig. 3. Structure of energy recovery verification device

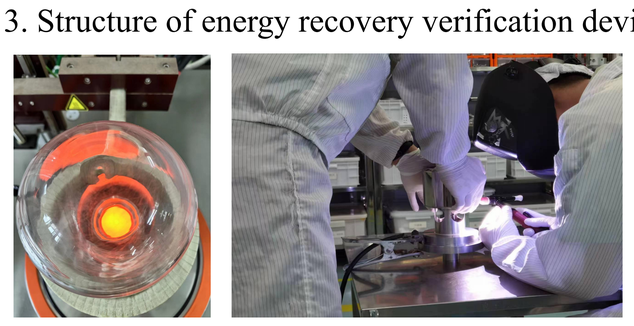

Fig. 4. Mechanical machining

After the mechanical machining was completed, we proceeded with the setup of the test platform, as shown in Fig. 5. Additionally, ceramic pressure resistance tests were conducted, as shown in Figure 6. The verification device is expected to undergo high-power testing by the end of this year.

Fig. 5. Test platform

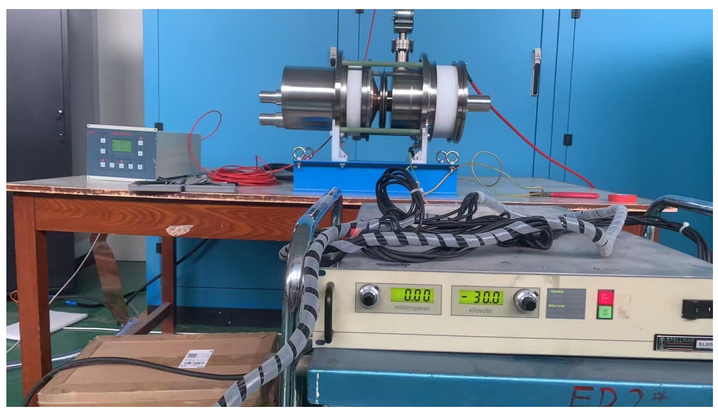

Fig. 6. Ceramic pressure testing

SUMMARY AND OUTLOOK

This paper focuses on the high-efficiency CEPC klystron and conducts a theoretical analysis of the collector suppression, determining the electrode parameters. To validate the key technologies of the energy recovery klystron, an energy recovery verification device consisting of an electron gun and a collector was designed and fabricated. After completing the high-power testing, we will proceed with the design of a high-efficiency klystron with a depressed collector, aiming to increase the efficiency from 65% to over 75%.

REFERENCES

[1]Kosmahl H G. Modern multistage depressed collectors—A review[J]. Proceedings of the IEEE, 1982, 70(11): 1325-1334.

[2]DAYTON J A. System efficiency of a microwave power tube with a multistage depressed collector(Current distribution estimates for microwave power tube with depressed multistage collector)[J]. 1972.

[3]Jiang Y, Teryaev V E, Hirshfield J L. Partially grounded depressed beam collector[J]. IEEE Transactions on Electron Devices, 2015, 62(12): 4265-4270.

[4]Vaughan J R M. Synthesis of the Pierce gun[J]. IEEE Transactions on Electron Devices, 1981, 28(1): 37-41.

[5]Hamme F, Becker U, Hammes P. Simulation of secondary electron emission with CST PARTICLE STUDIOTM[C]//Proc. ICAP. 2006: 160-163.

*** Work supported by Yifang Wang's Science Studio of the Thousand Talents Project**

† email address: zhouzs@ihep.ac.cn

Design of periodic permanent magnet for S-band high efficiency klystron†

Han Xiao[1,2], Zusheng Zhou[1,2]*, Ouzheng Xiao[1], Yu Liu[1,2], Yiao Wang[1,2], Wenbin Gao[1,2],
Noman Habib[1,2], Fanyu Wang[1,2], Xiaobo Zhou[1,2], Munawar Iqbal[1], Abid Aleem[1]

[1]Institute of High Energy Physics, Chinese Academy of Sciences, Beijing 100049, China
[2]University of Chinese Academy of Sciences, Beijing 100049, China
*email address: zhouzs@ihep.ac.cn

ABSTRACT

The efficiency of klystrons is critical in determining the operational costs of particle accelerators. This study introduces the design of an S-band 50MW high-efficiency klystron, utilizing permanent magnet focusing technology. We emphasize innovative design methodologies aimed at improving klystron efficiency through advanced magnetic field configurations and the optimization of cavity string structures.These innovations not only enhance operational performance but also facilitate the integration of permanent magnets, maximizing spatial efficiency within the klystron design. The development of this high-efficiency S-band klystron marks a significant advancement in klystron technology, providing a sustainable and cost-effective solution for high-power applications. By enhancing performance and reducing power consumption, this design aligns with broader objectives of energy efficiency and cost reduction in accelerator technology.

INTRODUCTION

High power and high efficiency are critical areas of focus in klystron research. The development of large scientific facilities such as the International Linear Collider (ILC), Compact Linear Collider (CLIC), Future Circular Collider (FCC), and Circular Electron Positron Collider (CEPC) underscores the significance of high-efficiency klystrons as essential technologies for these endeavors. Improving klystron efficiency involves effectively bunching peripheral electrons and minimizing velocity dispersion. Common strategies to achieve this include reducing electrical conductivity and employing second harmonic cavities.

The adoption of permanent magnet focusing technology offers several advantages: it reduces power consumption associated with focusing coils, decreases the overall size and weight of the klystron, and eliminates the need for coil power supplies and cooling systems. These enhancements are crucial for achieving klystron miniaturization and operational simplicity.

This study presents a design that integrates high efficiency with permanent magnet focusing, aiming to enhance klystron performance while facilitating system miniaturization.

PERIODIC PERMANENT MAGNET FOCUSING

The periodic permanent magnet (PPM) focusing system consists of a positive and negative periodic arrangement of axially magnetized permanent magnet rings. Within this periodic magnetic field, the beam can still maintain the focus, but there is a fluctuation in the envelope, and the fluctuation increases with the decrease of the beam voltage, and the beam is completely divergent below a certain voltage. The periodic magnetic field enhances the utilization of the reverse magnetic fields adjacent to the permanent magnet rings, resulting in a more compact and lightweight focusing system.

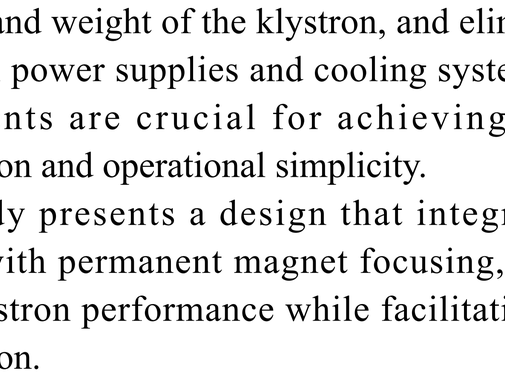

Figure 1 Periodic permanent magnet focusing structure

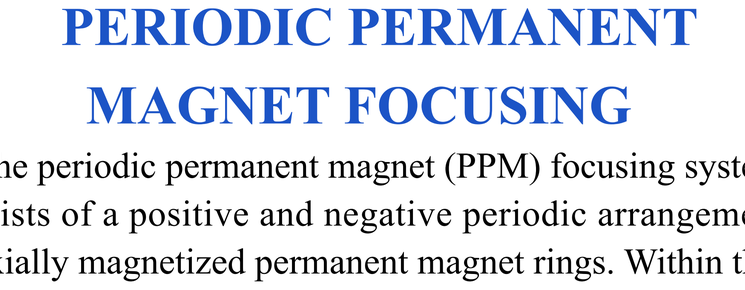

Figure 2 Focusing structure and vacuum inside the klystron

FOUNDATION DESIGN

This design uses 7 cavities, including 2 second harmonic cavities. The two second harmonic cavities are placed adjacent to each other in an unconventional manner. The first cavity corrects the velocity, while the second cavity collects peripheral electrons and provides spatial convenience for the focusing structure.

The focusing structure is mainly divided into three sections. The first section has a small fundamental current of the beam and is designed as a long-period magnetic field that is easy to process. At the same time, considering the water cooling space, a large inner diameter magnetic ring is used. In the second section, the pole shoe extends into the vacuum inside the klystron, and considering the cavity size, it is designed as a medium-period medium inner diameter structure. The third section has a large fundamental current and is designed as a short-period small inner diamete structure.

Table 1 Main parameters of klystron

Frequency	2856Mhz
Output power	50MW
Voltage	373kV
Current	245A
Beam radius	7.1mm
Drift tube radius	11.8mm
Efficiency	55%

ELECTRON OPTICS

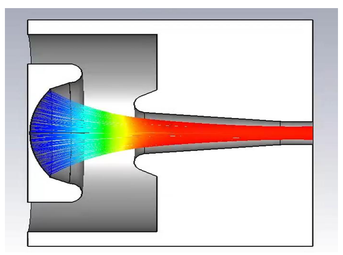

Figure 3 The electron gun in CST

In CST simulation, the electron gun current is 245A, the waist radius is 6.6mm, the minimum period length of the focusing structure is 24mm, and the maximum magnetic field along the axis is 1703Gs.

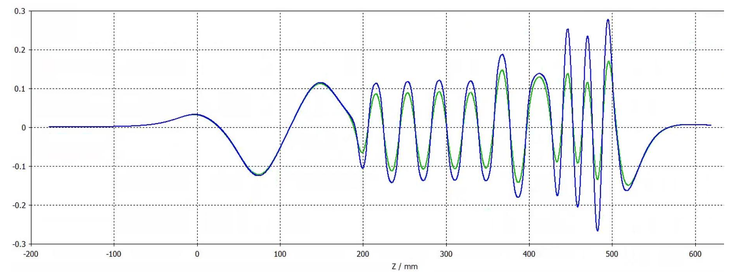

Figure 4 Magnetic field distribution at the axis and beam radius

BEAM DYNAMIC

In CST simulation, the performance of cavities was optimized and the field asymmetry caused by the output cavity coupling port was reduced by off-axis. The final output power in PIC simulation is 50MW with an efficiency of 55%.

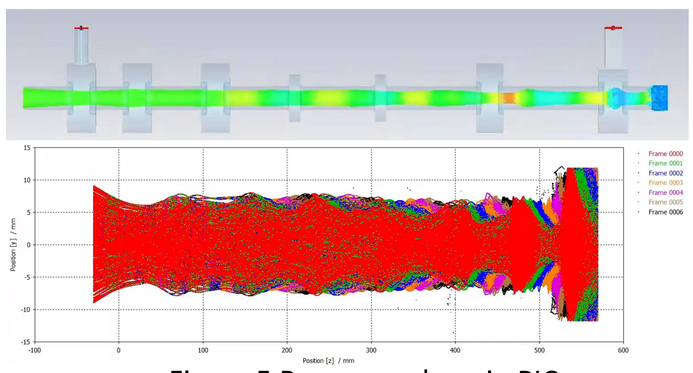

Figure 5 Beam envelope in PIC

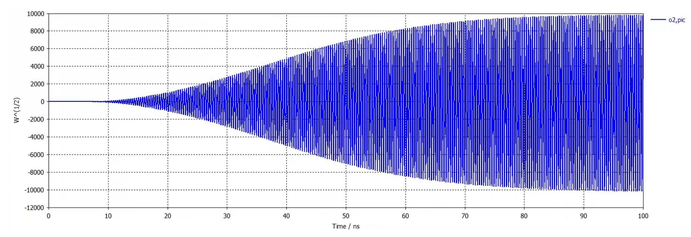

Figure 6 Output power in PIC

SUMMARY AND OUTLOOK

This study presents the design of an S-band 50 MW high-efficiency permanent magnet klystron, featuring adjacent second harmonic cavities and segmented periodic permanent magnet focusing. This configuration offers the benefits of high efficiency, simplicity, and compactness. CST simulation results indicate an output power of 50 MW with an efficiency of 55%.

The next step is to reduce the voltage requirement of the tube while maintaining this efficiency.

REFERENCES

[1] Syratchev, I. (2022). High efficiency klystrons. [PowerPoint slides]. https://indico.cern.ch/event/1138690/contributions/4782684/attachments/2435633/4171251/IFAST_2022_SI.pdf

[2] Matsumoto, H., Shintake, T., Ohkubo, Y., Taoka, H., Ohhashi, K., & Kakuno, K. (2001). High power test of the first C-band (5712 MHz) 50 MW PPM klystron. PACS2001. Proceedings of the 2001 Particle Accelerator Conference (Cat. No.01CH37268), 2, 993-995 vol.2.

[3] Chin, Y.H., Matsumoto, S., Mizuno, H., Morozumi, Y., Ohkawa, T., Ohya, K., Takata, K., Toge, N., Tokumoto, S., Kazakov, S.Y., Larionov, A., & Teryaev, V.E. (2001). X-band PPM klystron development for JLC. PACS2001. Proceedings of the 2001 Particle Accelerator Conference (Cat. No.01CH37268), 5, 3792-3794 vol.5.

[4] Sprehn, D.W., Caryotakis, G., Jongewaard, E.N., & Phillips, R.M. (1999). Periodic permanent magnet development for linear collider X-band klystrons.

[5]CST GmbH, Darmstadt, Germany.

†Work supported by Dr. Yifang Wang's Science Studio of the Thousand Talents Project

Poster ID: 10

The 2024 International Workshop on the High Energy Circular Electron Positron Collider (CEPC2024), Hangzhou, China, Oct 23-27, 2024

*Study on Arc Protection for CEPC High-Voltage Direct Current Long-Distance Transmission**

Fei Li[1] , Xinan Xu[1], Jindong Liu[1] , Dayong He[1] , Nan Gan[1] , Ouzheng Xiao[1] ,

Yu Liu[1,2] , Yajie Mu[1] , Xiuqian Shi[1,2] , Yiao Wang[1,2], Zusheng Zhou[1.2†]

1Institute of High Energy Physics, Chinese Academy of Sciences, Beijing 100049

2University of Chinese Academy of Sciences, Beijing 100049, China

中国科学院高能物理研究所
Institute of High Energy Physics
Chinese Academy of Sciences

The CEPC high-voltage direct current (HVDC) power supply and the klystron are connected via a long-distance HVDC cable. When an arc short circuit occurs in the klystron, the energy generated by the discharge of the distributed capacitance in the long-distance transmission cable can directly damage the klystron. To address this, a high-voltage direct current long-distance transmission arc protection device has been developed. This device has a voltage rating higher than 120 kV and, when an arc short circuit occurs in the klystron, triggers the Crowbar device to instantly bypass and discharge the energy. The response time of the device is less than 5 microseconds, and the energy is limited to within 10 joules. This paper will analyze the discharge energy of the distributed capacitance in long-distance cable transmission based on the layout of the CEPC HVDC power supply and the klystron, establish a circuit model, conduct system simulations and energy calculations, and systematically analyze the design principles and key technologies of the arc protection device.

INTRODUCTION

Considering klystron lifetime, power redundancy and cost, the 2 cavities of CEPC collider will be powered with one CW klystron capable to deliver more than 800 kW and the klystron frequency is 650 MHz. The high-voltage DC power supply is 130 kV/16 A, operating in a one-to-one configuration with the klystron. According to the layout in the CEPC technical design report, the high-voltage DC power supply is located on the ground, while the klystron is in the auxiliary tunnel. The calculation of the high-voltage cable length includes the distance from the ground, the length of the vertical shaft, etc., with a maximum length of 700 meters.

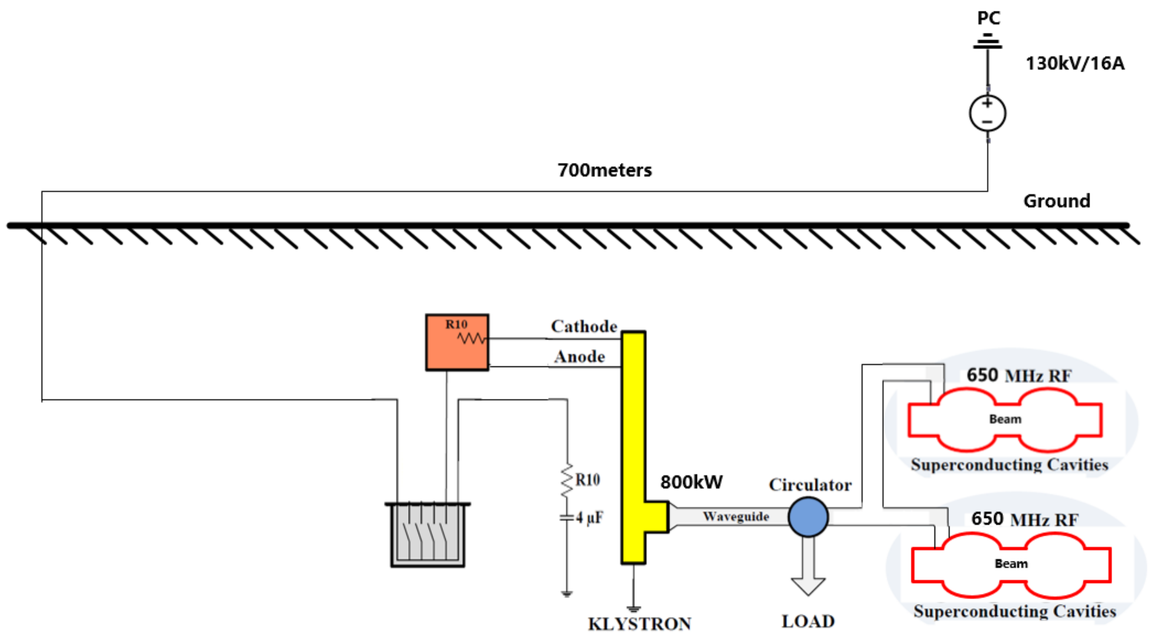

CEPC TDR high-voltage DC power supply and CW klystron structural layout diagram.

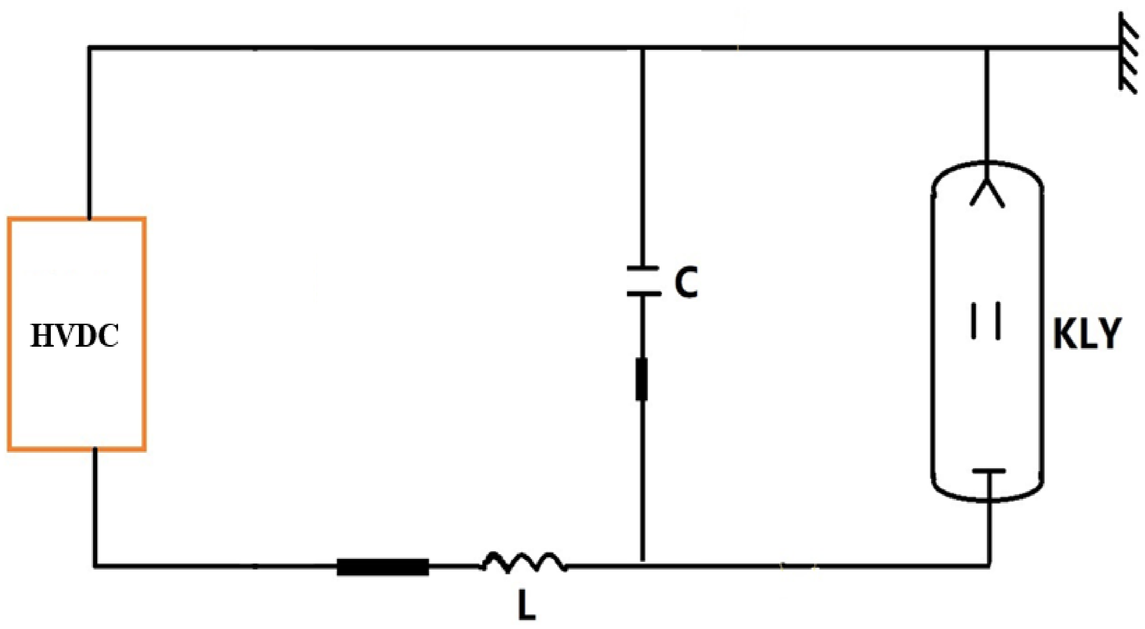

Equivalent schematic diagram for long-distance transmission of high-voltage DC.

SIMULATION ANALYSIS

The high-voltage DC power supply currently uses PSM (Pulse Switching Modulation) technology. The simulation of its output circuit shows a discharge time of approximately 110 μs. Measured discharge waveforms for the PSM high-voltage power supply at 30 kV, 60 kV, and 90 kV under no-load and load conditions were analyzed against theoretical predictions. Simulations of the natural decay of capacitance and inductance energy storage were also conducted.

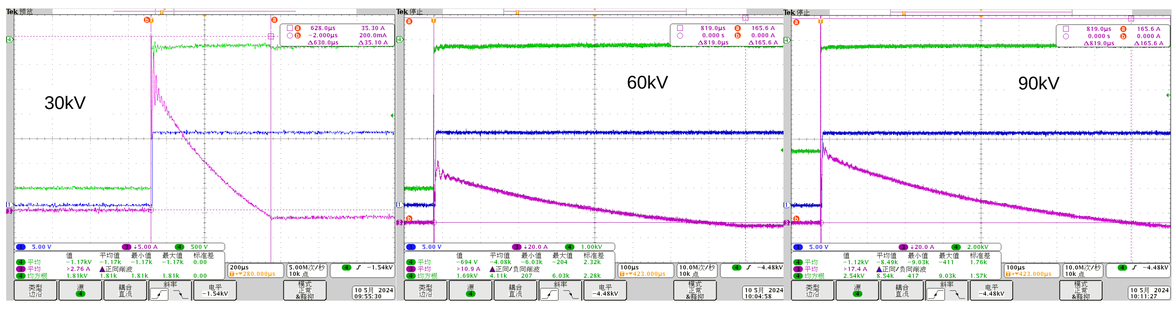

PSM power supply resistance load discharge test waveform.

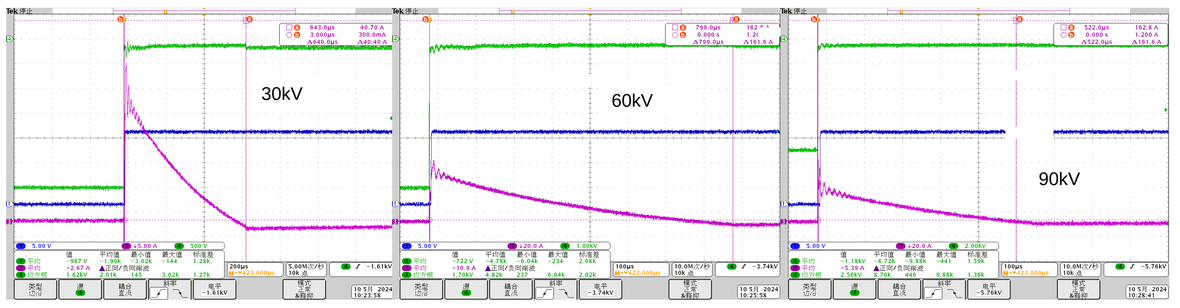

PSM power supply no-load discharge test waveform.

CROWBAR

To address the above issues, a crowbar solution is implemented by connecting a crowbar in parallel at the klystron end of the long-distance high-voltage cable, as shown in Figure 6. When a short circuit in the klystron is detected, the crowbar is quickly triggered, allowing it to instantaneously bypass and release the energy, thereby protecting the klystron load. A crowbar was designed using a series of thyristors in a solid-state configuration. The design goals are to achieve a voltage withstand capability greater than 120 kV, a response time of less than 5 μs, and an energy limit of under 10 J, meeting the transmission requirements for high-voltage DC cables with a length of 1000 meters.

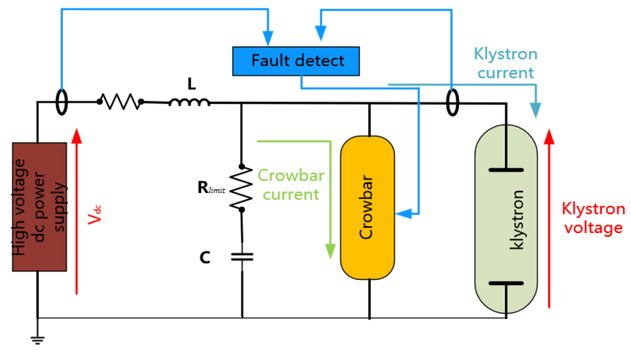

Crowbar scheme principle schematic diagram.

REFERENCES

[1] The CEPC Study Group. CEPC Technical Design Report: Accelerator[J]. Radiation Detection Technology and Methods, 2024, 8(1).
[2] Butterworth, A et al. “The LEP2 Superconducting RF System.” Nuclear instruments & methods in physics research. Section A, Accelerators, spectrometers, detectors and associated equipment 587.2 (2008): 151–177.
[3] G.Ravida,O.Brunner,D.Valuch. PERFORMANCE OF THE CROWBAR OF THE LHC HIGH POWER RF SYSTEM[C],2012.
[4] J.Li,J.M.Qiao,X.A.Xu,et al. CSNS Linac RF System Design and R&D Progress[C],2010.
[5] Tooker, J.F, P Huynh, and R.W Street. “Solid-State High-Voltage Crowbar Utilizing Series-Connected Thyristors.” 2009 IEEE Pulsed Power Conference. IEEE, 2009. 1439–1443.

*** Work supported by Yifang Wang’s Science Studio of the Thousand Talents Project**

† email address: zhouzs@ihep.ac.cn

Poster ID：11 The 2024 International Workshop on the High Energy Circular Electron Positron Collider (CEPC2024), Nanjing, China, Oct 23-27, 2024

Design and High-Power Test of the High Efficiency RF Power Source Test Stand

LIU J.D, ZHOU Z.S, GAN N, LI F, HE D.Y, XIAO O.Z. SHI X.Q, LIU Y, Li X.P, LI J.Y, CHI Y.L

1. Institute of High Energy Physics, Chinese Academy of Sciences, Beijing, China

2. University of Chinese Academy of Sciences, Beijing 100049, China

INTRODUCTION

The high-power RF power source system is the energy acquisition of particle acceleration, and is the key devices. The CEPC project planned in China, the total power requirement of the RF power system is about 110 MW, which is a huge energy consumption. Therefore, it is important to explore the ways to maximize the energy conversion efficiency of RF power systems for future advanced projects. The Institute of High Energy Physics (IHEP) has developed a high power test stand (HPTS) for high-power RF power source systems, which is used for explore topics in high-efficiency klystrons, multi-beam klystrons, multi-stage depressed collection (MSDC), energy recovery, and high-power reliability research and high power conditioning tasks. And it is also a prototype validation of the CEPC megawatt PSM high-voltage power supply.

This article provides a detailed introduction to the design and implementation of the platform. The highlight of this HPTS is that it achieves full output range of high-voltage duty cycle from pulse to DC. In continuous wave DC applications, the high voltage ripple/stability is improved from the traditional PSM power supply's 1% level to the 0.1% level, achieving an order of magnitude improvement. Compatible with pulse mode applications, the pulse width can be adjusted from 0.5ms to DC, with leading edge, flat top, and repetition stability indexes reach the level of specially designed long pulse modulators. As a result, the newly developed power supply can provide a flexible high-power test environment for the research and development of CEPC high-efficiency klystron tubes. Not only effectively reducing the probability arcing events in newly processed klystron, but also synchronizing the entire RF conditioning process, reducing consumption, and improving energy utilization efficiency. The prototype was completed in 2021 and passed a 200kW resistive load test. In 2024, full-scale power experiments were completed for CEPC high-efficiency 800kW/650MHZ klystron loads. Its RF power reaches up to 800kW, which also verifies the effectiveness of the proposed hybrid modulation high-voltage power supply and lays an excellent foundation for the subsequent high-efficiency program of RF power source.

In 2024, full-scale power experiments were completed for CEPC high-efficiency 800kW/650MHZ klystron loads.

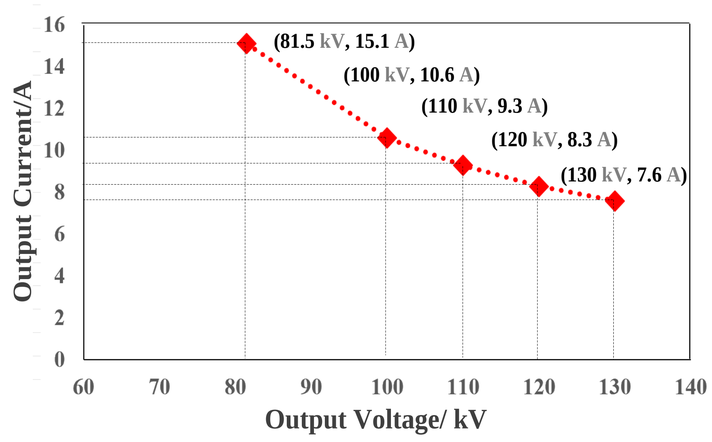

The power requirements of the operating point for the high-efficiency klystron load

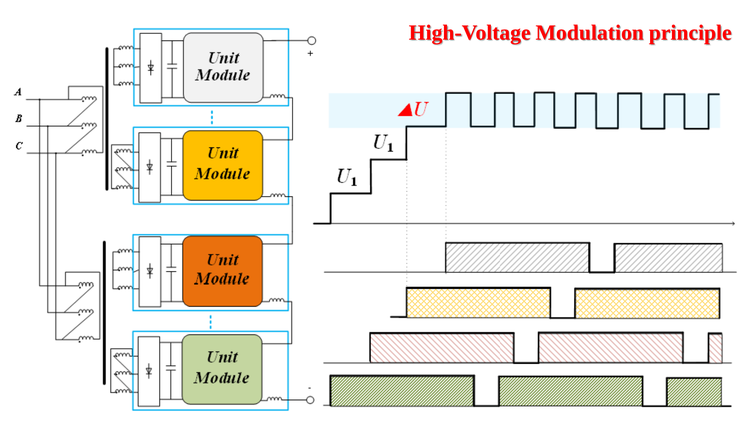

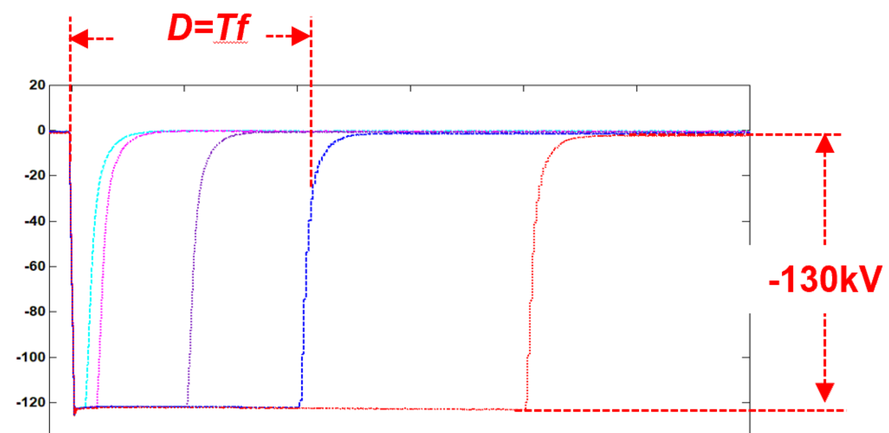

High voltage power supply system and High-Voltage output simulation（from pulse to DC）

From Resistive Loads (kW level) to Klystron Loads (MW level)

Pulse high voltage output (100kV/16A. max 200Hz)

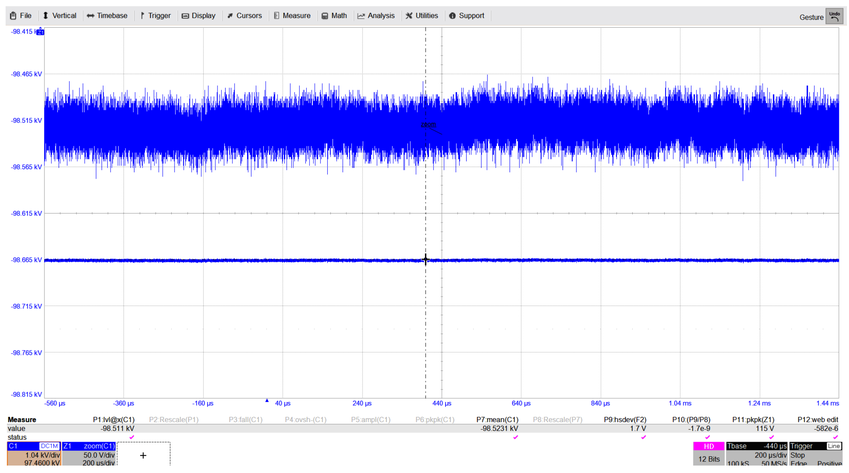

Continuous-wave DC operation mode

2021年11月
- Pulse Mode 130kV/16A
- CW 130kV/100kW

2022年1月~5月
- High-power test of the first klystron load
- PAPS High Voltage Long Cable Layout Klystron Load Short Circuit (arcing) Experiment

2023年12月~2月
- Power experiment of high-efficiency klystron (pulse mode)

1ms/110kV 800kW RF Power

2024年4月~8月
- 1‰ High voltage and RF power Duty cycle
- CW 800kW，Eff. 78%

High-power progress of HPTS

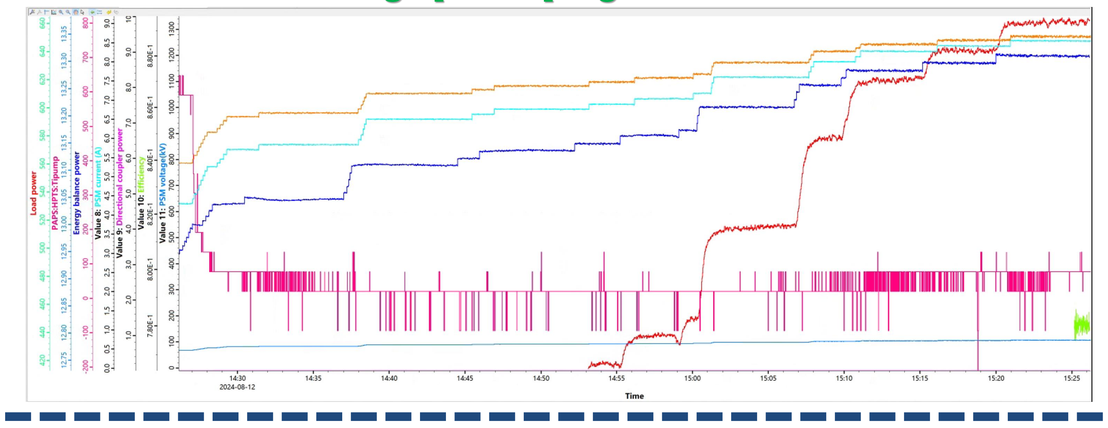

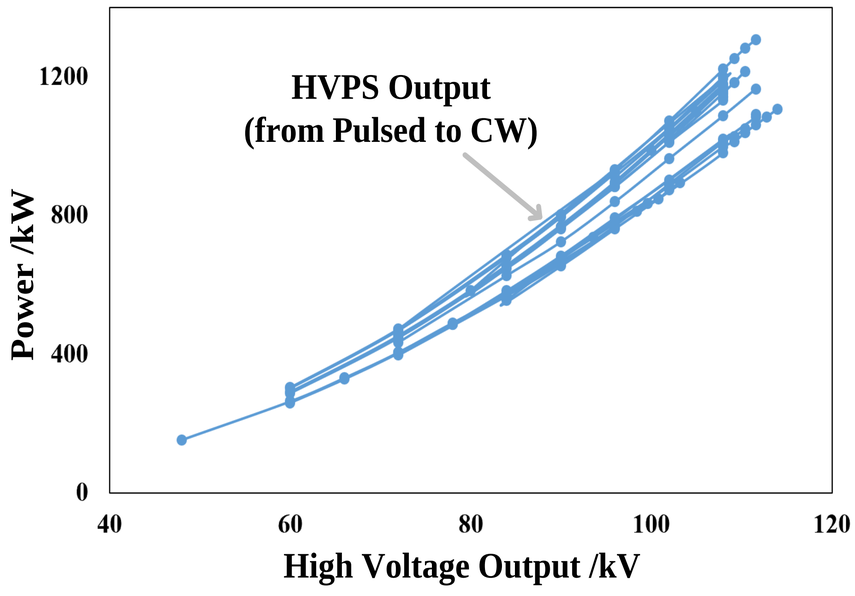

Megawatt power test data statistics

ACKNOWLEDGMENT

The future research supported by National Natural Science Foundation of China (Grant No. 12205320, Grant No.12275288); Work also supported by PAPS project and Yifang Wang's Science Studio of the Thousand Talents Project.

liujd@ihep.ac.cn, zhouzs@ihep.ac.cn, lxp@ihep.ac.cn

Poster ID:12

Design and high power test of 650MHz/800 kW high efficiency klystron for CEPC

中国科学院高能物理研究所 Institute of High Energy Physics Chinese Academy of Sciences

O. Xiao#, Z. Zhou, Y. Liu, G. Pei, Z. Lu, Munawar Iqbal, Y. Wang, H. Xiao, F. Li, F. Wang

Institute of High Energy Physics, Chinese Academy of Sciences, Beijing 100049, China

Introduction

To reduce energy consumption and operating cost for circular electron positron collider (CEPC) in China, the high efficiency klystron are being developed as a priority frontier technology at Institute of High Energy Physics, Chinese Academy of Sciences. A high efficiency 800 kW continuous wave klystron operating at frequency of 650 MHz, using a low perveance (0.25 μP) and a novel bunching method(CSM), has been successfully developed. The full 3-dimensional particle-in-cell simulation of the whole klystron in CST verified that the klystron efficiency was achieved up to 77% without instability and returning electrons. This prototype klystron has been finished high power acceptance test in August 2024. The test results show that the output power and efficiency have reached 803kW and 78%, respectively.

High efficiency klystron design

Klystron main design parameters

Parameters	Value
Operating frequency	650 MHz
Beam Voltage	113 kV
Beam Current	9.5 A
Beam Perveance	0.25 μA/V$^{3/2}$
Efficiency at rated Output Power	≥75%
Saturation Gain	≥43 dB
Output power	800 kW
1 dB Bandwidth	±0.5 MHz
Brillouin Magnetic Field	116 Gs
Number of Cavities	7

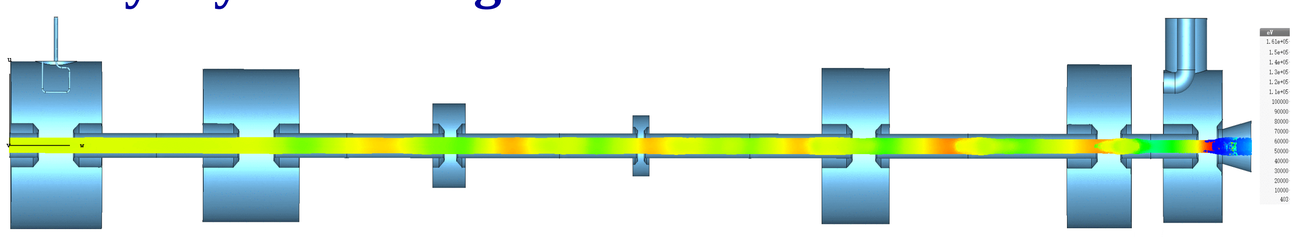

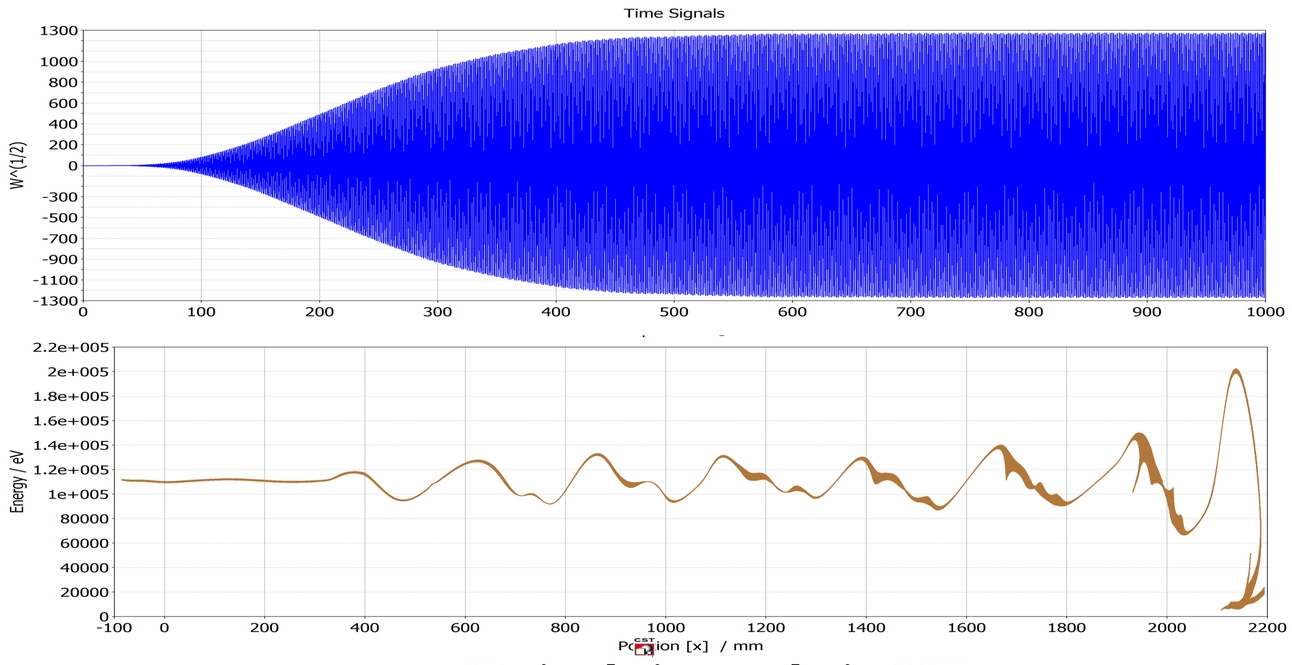

3D simulation results in CST

High efficiency klystron components manufacture

Gun

Cavity

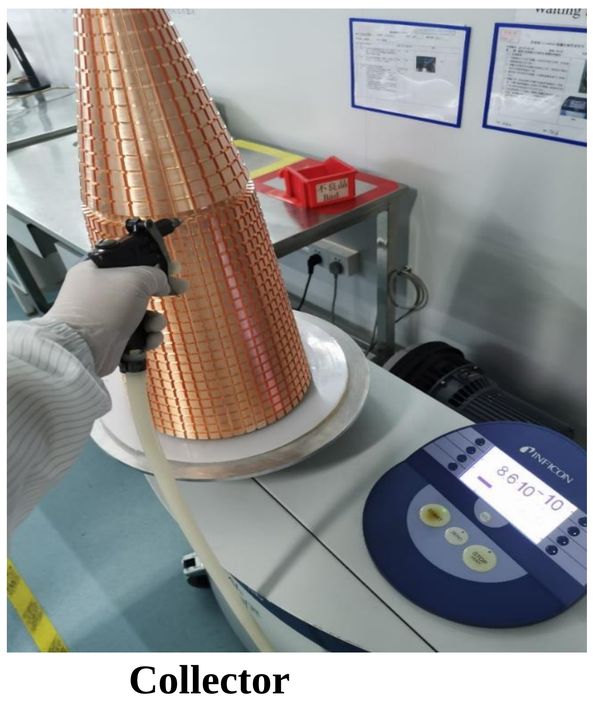

Collector

Coil

High efficiency klystron high power test

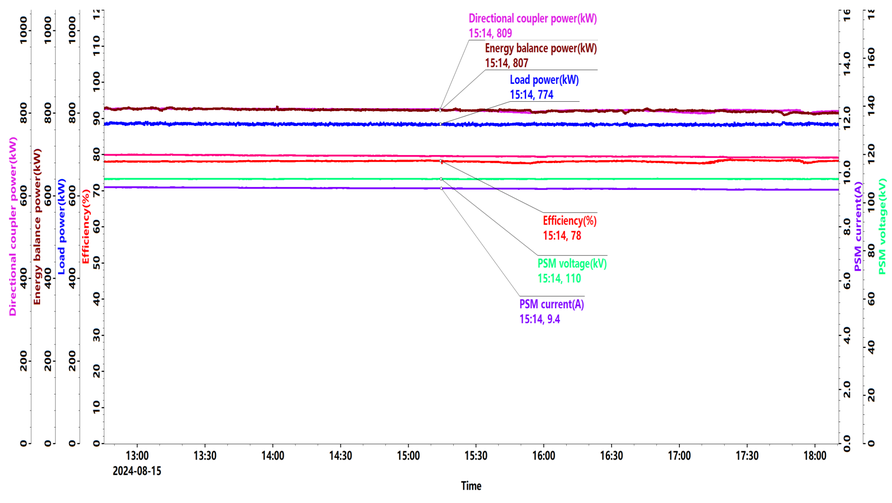

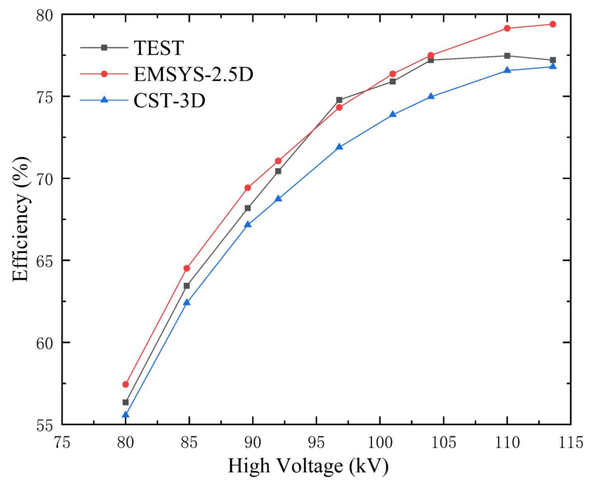

Acknowledgment

This Work is supported by Yifang Wang's Science Studio of the Thousand Talents Project. We would like to acknowledge colleague in Linac group at IHEP and Kunshan GuoLi Electronic Technology Company (GLVAC) for their great cooperation.

 # xiaooz@ihep.ac.cn

Development of 1.2 Mega-Watt P-band Travelling Wave Resonant Ring*

Fanyu Wang[1,2], Zusheng Zhou†[1,2], Ouzheng Xiao[1], Yiao Wang[1,2], Yu Liu[1,2], Wenbing Gao[1,2], Han Xiao[1,2], Fei Li[1], Nan Gan[1], Noman Habib[1,2], Munawar Iqbal[1], Abid Aleem[1]

[1]Institute of High Energy Physics, Chinese Academy of Sciences, Beijing 100049, China

[2]University of Chinese Academy of Sciences, Beijing 100049, China

中国科学院高能物理研究所 Institute of High Energy Physics Chinese Academy of Sciences

High power microwave devices, such as ceramic windows and couplers, are critical components in accelerators, where safety and reliability are paramount. To ensure their safe operation, these devices must undergo rigorous high-power testing. The Traveling Wave Resonant Ring (TWRR) is an economical and efficient device used for such testing. The Institute of High Energy Physics (IHEP) is currently designing a TWRR at the P-band frequency to support the development of klystrons in CEPC[1]. The TWRR's main components include a directional coupler, observation window, 3-stub tunner, load, and cooling system. This TWRR is capable of testing at 1.2MW(1.5 times the rated power of an 800-kW klystron), significantly reducing the risk of the window being penetrated during operation.

INTRODUCTION

A resonant ring, also known as a traveling wave resonator(TWRR), is a loop of waveguide which can amplify apparent power through the coupling of waves at its input. Figure 1 shows a basic resonant ring circuit.

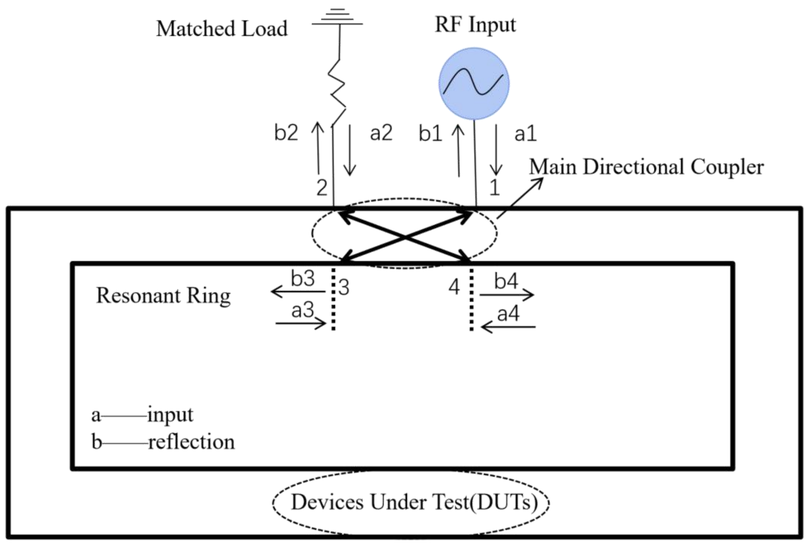

Figure 1 Basic Resonant Ring Circuit

Power is initially input to port 1 and then coupled into the ring through port 3. Uncoupled waves continue through port 2, which is typically terminated by a load, while the waves within the ring travel through ports 3 and 4. With the appropriate ring length and matching, these waves add constructively, resulting in a voltage increase that functions as power gain within the ring. Since power meters can easily measure the ring's performance, it is often the loop power "gain" that is of primary interest, which is proportional to the square of the voltage gain.From V. Veshcherevich [2],when the ring is in resonance,power gain M is:

$$M = \frac{C^2\left(1 - e^{-\alpha L}\sqrt{1-C^2}\sqrt{1-r^2}\right)^2}{\left(1 - 2e^{-\alpha L}\sqrt{1-r^2}\sqrt{1-C^2} + e^{-2\alpha L}(1-C^2)\right)^2}$$

where C is the coupling coefficient of the directional coupler; r is the reflection coefficient in the ring; $e^{-\alpha L}$ is the attenuation in the circuit; α is the effective attenuation coefficient; L is the length of the ring.

The length of the ring must be an integral number of guide wavelengths of coupled wave,which will reinforce previously coupled energy and place the ring in a state of resonance [3].

POWER GAIN

The lower the attenuation and the reflection in the resonant ring are, the higher is the power gain. Figure 2 illustrates the behavior of the M parameter for the ring with no reflection (r = 0).

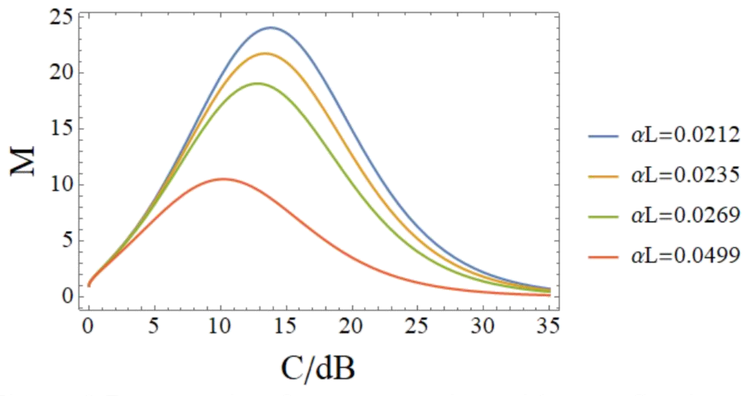

Figure 2 Power gain of a resonant ring with no reflections

For each attenuation value, there exists the optimal coupling coefficient C_{opt}, for which the power gain is maximal. For no reflection case, C_{opt} is

$$C_{opt} = \sqrt{1 - e^{-2\alpha L}}$$

and the maximal power gain is

$$M_{max} = \frac{1}{C_{opt}^2} = \frac{1}{1 - e^{-2\alpha L}}$$

Attenuation coefficient for a rectangular waveguide is

$$\alpha_w = \frac{R_{sw}}{Z_0}\frac{1 + \frac{2h}{w}\left(\frac{\lambda}{2w}\right)^2}{h\sqrt{1-\left(\frac{\lambda}{2w}\right)^w}}$$

where R_{sw} is the surface resistance of the waveguide wall material, $Z_0 \approx 377\text{Ohm}$ is the free space impedance, h is the height of the waveguide, w is its width, λ is the wave length in free space.

Table 1 shows the calculation results of 1.2 Mega-Watt P-band Travelling Wave Resonant Ring.The maximal power gain M_{max}=24 and the maximal power gain M_{max}=10.5.

Table 1 Theoretically Results of P-band TWRR

Waveguide	WR1500
Attenuation coefficient α_w	3.6×10^{-3} dB/m
Length of the ring	9.28m
Insertion loss of windows	0.05-0.3dB
Minimum total attenuation αL_{min}	0.0204
Maximum total attenuation αL_{max}	0.0499
C_{opt} at αL_{min} /C_{opt} at αL_{max}	–14dB/–10dB
M_{max}/M_{min}	24/10.5

The coupling coefficient and the power gain assuming ideal matching in the traveling wave resonator.In fact, reflections strongly affect the parameters of rings. Figure 3 illustrates this effect for the 1.2 MW P-band TWRR with αL = 0.0499.

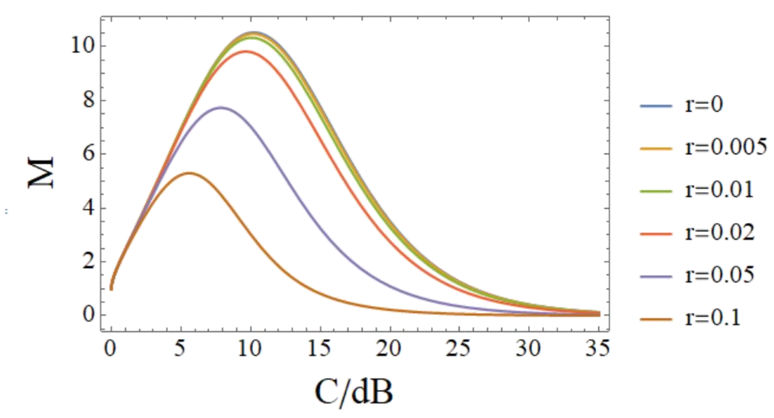

Figure 3 Power gain of a resonant ring with reflections (αL = 0.0499)

Figure 4 presents dependence of the power gain on circuit attenuation for the resonant ring with given coupling and different reflection values.It is obvious that the reflection coefficient should be below 0.02 to obtain a considerable power magnification.

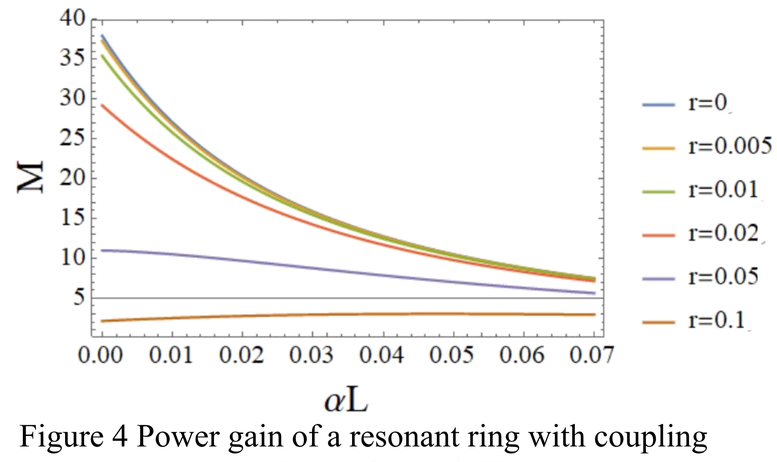

Figure 4 Power gain of a resonant ring with coupling coefficient C = –10 dB

MAIN DIRECTIONAL COUPLER

To couple the traveling wave resonator to the main transmission line, the ring requires a directional coupler with a coupling coefficient of C = –10 dB that has low reflection when the the attenuation is maximal.Scattering coefficients of that directional coupler are calculated by CST MWS[4] are presented in Figure 5. It can be observed that the directivity ($S_{41} - S_{21}$) of the directional coupler is better than 30 dB.

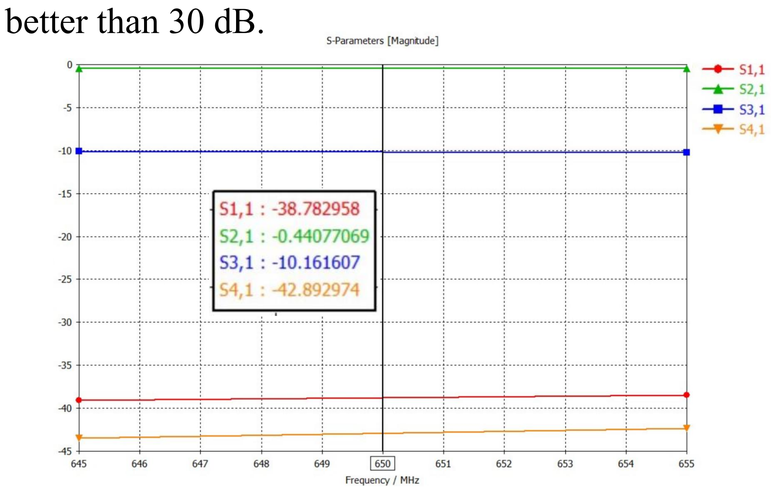

Figure 5 Main directional coupler response in CST MWS

RESONANT RING FOR WINDOW TESTS

P-band resonant ring consists of a WR1500 waveguide part, a main directional coupler, a directional coupler for power detection,a three-stub tuner for matching purposes,devices under test(DUTs), and a matched load. Configuration and the direction of power flow inside the TWRR. are showed in figure 6 and figure 7.

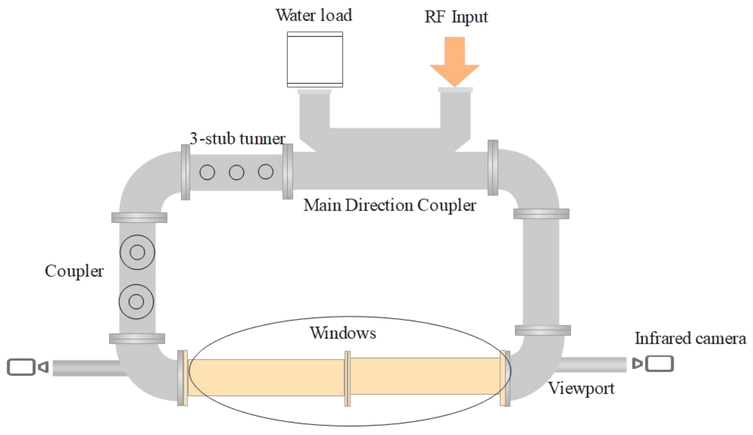

Figure 6 Configuration of P-band TWRR

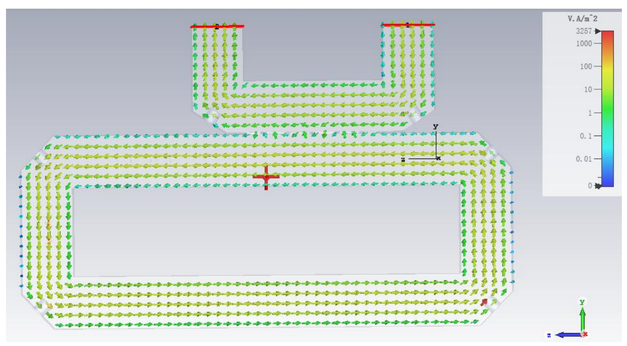

Figure 7 Power flow in P-band TWRR

SUMMARY AND OUTLOOK

This paper presents the development of a 1.2 Mega-Watt P-band Traveling Wave Resonant Ring. The power gain is analyzed theoretically, and the main directional coupler is identified. In the next phase, we will complete the design of the three-stub tuner, along with a thermal analysis of the ring.

REFERENCES

[1]Gao, J. CEPC Technical Design Report: Accelerator. Radiat Detect Technol Methods 8, 1–1105 (2024). https://doi.org/10.1007/s41605-024-00463-y

[2]"Theory and Application Instruction Manual for the Resonant Ring" I-T-E Circuit Breaker Company, Special Products Division, Philadelphia 34, Pennsylvania.

[3]Resonant Ring for High Power Tests of RF Couplers, Veshcherevich, Vadim.,Physics, Engineering,2003.

[4]CST GmbH, Darmstadt, Germany.

*** Work supported by Yifang Wang's Science Studio of the Thousand Talents Project**

† email address: zhouzs@ihep.ac.cn

Poster ID:26 The 2024 International Workshop on the High Energy Circular Electron Positron Collider (CEPC2024), Hangzhou , China, Oct 23-27, 2024

Design and simulation of Electron gun and Magnet of C-Band 80MW klystron for CEPC LINAC

Noman Habib[1,2], Zu-Sheng Zhou[1,2]*, Munawar Iqbal[1,3], Ou-Zheng Xiao[1], Yu Liu[1,2], Yi-Ao Wang[1,2], Abid Aleem[1], Wen -Bing Gao[1,2], Han Xiao[1,2], Fan-Yu Wang[1,2]

[1]Institute of High Energy Physics, Chinese Academy of Sciences, Beijing-China

[2]University of Chinese Academy of Sciences, Beijing-China

[3]Centre for High Energy Physics, University of the Punjab, Lahore-Pakistan

*Corresponding Author Email: zhouzs@ihep.ac.cn

Abstract

The design and simulation of the complete electron gun and electromagnet for 80 MW C-band klystron of CEPC LINAC. At an acceleration potential of 425 kV, a space charge beam current of 425A is achieved with an average cathode loading of less than 9.0 A/cm^2. It has been calculated that the maximum surface electric field at the high voltage ceramic seal and beam optics is less than 23 kV/mm and 4.80 kV/mm, respectively. With an average beam radius of 5.40 mm, the electron beam is successfully transported to the interaction cavity with a beam ripple rate of around 5.0%. The 3-D CST simulation validates and finds agreement with the results of the 2D-GUN, and POISSON simulations.

Klystron Fundamentals

Definition: Klystron is an electron-beam vacuum tube in which the beam interacts with standing-wave RF fields in several consecutive & collinear RF cavities to produce high power RF wave.

Madidate : RF Amplifier of the accelerator to accelerate the particles close to the velocity of light.

Principle: 1.Electron Gun: The cathode is heated to ~1000C and applied (Pulsed or DC) to several 100kV. Electrons are accelerated from the cathode towards the anode at ground, which is isolated from the cathode by the high voltage ceramics. The electron beam passes the anode hole and drifts in the drift tube, **2. Magnet :** The beam is focused by the cathode coil and a solenoid, **3. Cavities:** By applying RF power to input cavity , the beam is velocity modulated. On its way to the out put cavity, the velocity modulation converts to density modulation due to additional buncher cavities. The beam is decelerated in the out put cavity by applying a negative electrode. The electrons lost energy which is converted into RF power, **4. Window:** This RF power is coupled out by a window through a wave guide, **5 Collector:** The residual beam is dumped in the collector. Fig 1, is the cross-sectional view of the Klystron.

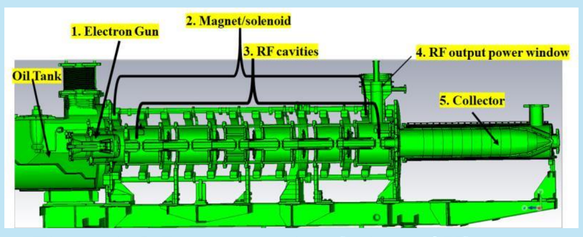

Figure 1: 3-D cross sectional view of Klystron.

Applications:

Some important application are mentioned as below:

1.Colliders: Particles are accelerated at High Energy through Klystrons and then collided to explore the mysteries of the Universe. LHC,CERN, SUPERKEKB, JAPAN, BESIII, China, etc. are Colliders.

2. Linear Accelerators : Accelerate particles at high energy by Klystron to produce electrons and photons for *Medical Applications* like cancer diagnosis and treatment.

3. Free Electron Lasers: High energy electron beam produced through LINAC is used both for lasing & pumping by itself produced *high power LASER light* while passing through a undulator magnet.

4.RADARs: The main applications are defense surveillance systems, navigation and locating enemy targets. High frequency radars are also used to plot or to map the terrain in the area. The transmitter produces the microwave pulses emitted by the radar which propagates through Antenna. The transmitter's main components is Klystron.

Electron Gun Design

Table 1: Beam Optics Design Parameters

Parameters	Units	Values
Anode Diameter	mm	120
Focusing electrode diameter	mm	68.304
Cathode - anode spacing	mm	76.1
Cathode - focusing electrode spacing	mm	1.1
Cathode diameter	mm	87.8

A 2D & 3D view of the Klystron electron gun shown in figure 2, was modeled in DGUN & CST Code with parameters given in table 1. This is a thermionic diode gun having cathode, focusing electrode and anode.

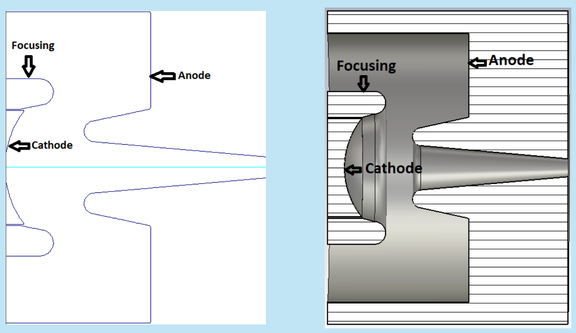

Figure 2: 2-D & 3-D model of the gun produced by DGUN &CST.

Magnet Design

We used POISSON and CST code to design solenoid as given in Fig. 3(a , b) with a Reverse Current Coil at the cathode for beam trajectories matching in the field free region. The obtained magnetic field comparison of POISSON and CST in Excel is given in Fig 4.

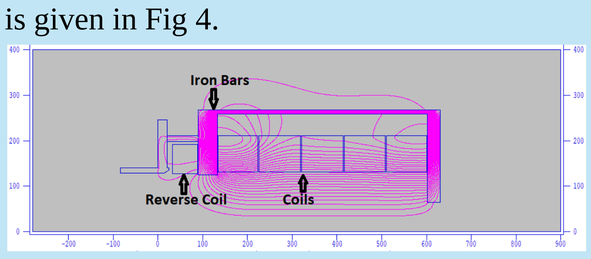

Figure 3a:Design of the solenoid in POISSON

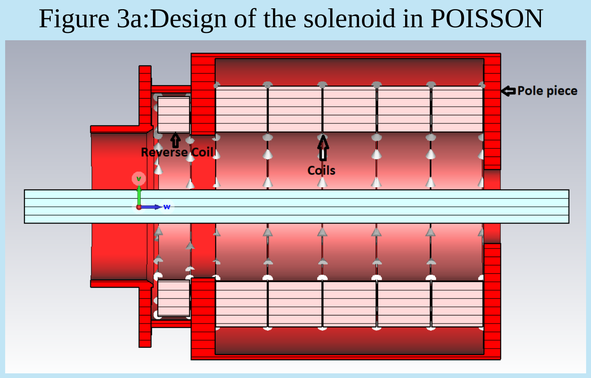

Figure 3b:Design of the solenoid in CST

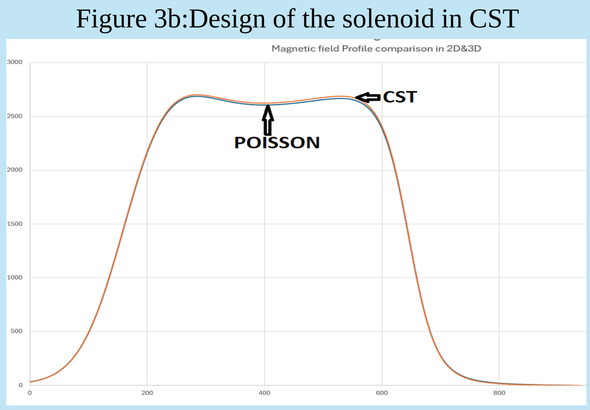

Figure 4:Axial Magnetic field profile Comparison of the Magnet(CST&POISSON)

Beam Optics Simulation

Table 2. Simulation parameters

Parameter	Units	Values
Cathode voltage	kV	0
Anode voltage	kV	425
Magnetic field	Gauss	2687

The gun was then simulated in DGUN and CST Codes for the beam optics analysis. To get the maximum beam convergence, high emission density and low perveance in the field free region we used the parameters as listed in table2.

We obtained an electron beam of average radius of 5.55 mm in DGUN and 5.73 mm in CST. The electron beam trajectories are shown in figure 5(a , b).

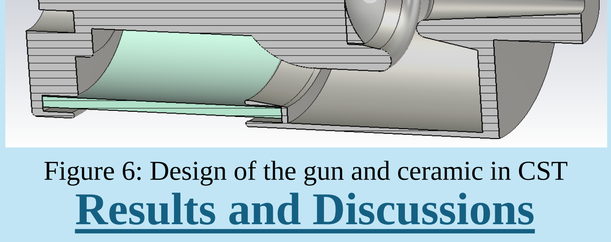

Figure 5(a): Beam trajectories of Klystron electron beam gun under magnetic field in DGUN

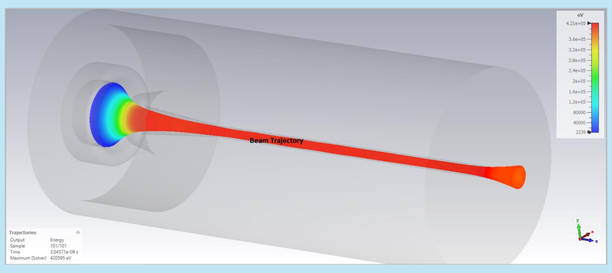

Figure 5(b): Beam trajectories of Klystron electron beam gun under magnetic field in CST

Gun Ceramic

We used POISSON and CST code to design Gun envelope and calculate its electric field as shown below.

Figure 6: Design of the gun and ceramic in CST

Results and Discussions

A maximum electric field value of 22.7 kV/mm at the focusing electrode is obtained as the potential lines are spaced very close to each other as can be seen in the Figure 5(a). A space charge current of 418A is obtained as can be seen in the Figure 7. The perveance is calculated to be 1.5 µP.

Figure 7: Space charge beam current

The values of the maximum & minimum beam size under the magnetic field is also shown in Figure 8. Transmission of the beam in the downstream is given in Figure 8 which shows the size and the ripple of the beam. The beam is laminar with reduced size under the obtained magnetic field.

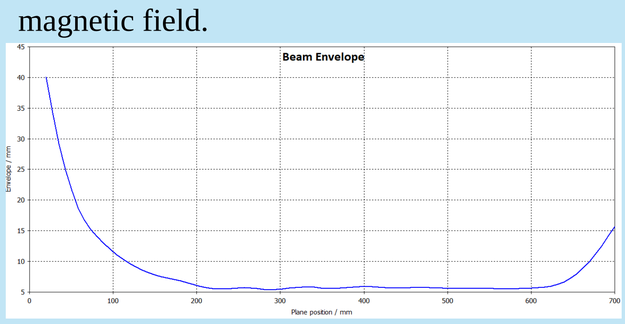

Figure 8: Envelope vs. plane position

Figure 9 represents the dotted line which shows the current density on cathode. The current density value almost uniform, and it drops at the edges of the cathode due to lower heating. The maximum value obtained is around 8.8 A/cm^2.

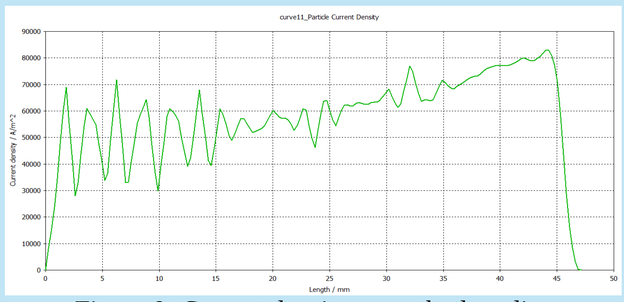

Figure 9: Current density vs. cathode radius

Summary

A thermionic high-power diode electron gun in a simple structure is designed (modeled), simulated and analyzed. Simulation values verified from the two codes, DGUN and CST agree. High emission current, low perveance of the source have been obtained.. Close agreement of simulated results depicts that the DGUN and CST are best suited software's for complete design and analyses of electron beam guns of klystron for linear accelerators applications. Magnetic field of strength 2687 Gauss is used to focus the beam at the target The electron beam is focused on the target with the desired size of the radius of the beam. The percentage current error between DGUN and CST results was about 0.83 %. A summary of the calculated parameters are given in table 3.

Table 3: Emission Characteristics of the Gun

Parameters	Units	CST	DGUN	POISSON
Acceleration voltage	kV	420.7	425	425
Current	A	418	425.1	NA
Maximum Cathode current density	A/cm^2	8.8	8.8	NA
Perveance	µP	1.5	1.5	NA
Maximum radius	mm	6.04	5.86	NA
Minimum radius	mm	5.3	5.239	NA
Average radius	mm	5.67	5.54	NA
Ripple rate	%	6.5%	5.6%	NA
Electric field @ focusing electrode	kV/mm	22.7	19.3	22.7
Electric Field @ ceramic	kV/mm	4.7	NA	4.7
Maximum Magnetic field @ drift tube	Gs	2687	2687	2687

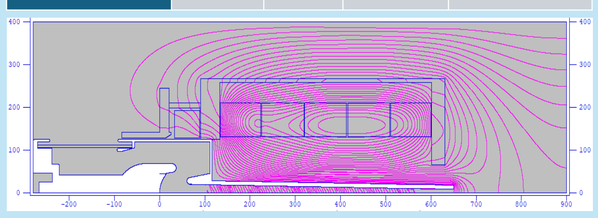

Figure 10a:Design of the Gun, solenoid and ceramic seal in POISSON

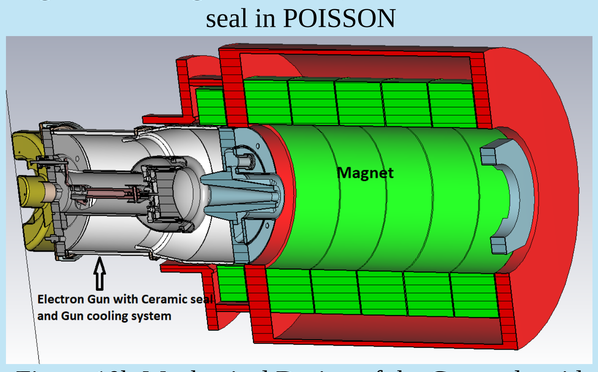

Figure 10b:Mechanical Design of the Gun, solenoid and ceramic seal in CST

Figure 10(a , b) shows the Mechanical Design of the Gun, solenoid and ceramic seal in POISSON and CST software.

The gun, magnet and the ceramic are designed for 80MW klystron and now under fabrication in the Chinese company.

References

1- A Microwave Source of Surprising Range and Endurance* George Caryotakis Stanford Linear Accelerator Center, Stanford University, Stanford CA 94309.

2- A. Larionov, K. Ouglekov, DGUN-code for simulation of intensive axial-symmetric electron beams, in: Proceedings of 6th ICAP, Darmstadt, Germany, 2000, p. 172.

3- POISSON Code, Los Alamos National Laboratory Report, 1987, LA-UR-87-126.

4- User Manual, CST-Particle Studio, Darmstadt, Germany, 2020.

5- Gao, J. CEPC Technical Design Report: Accelerator. Radiat Detect Technol Methods 8, 1–1105 (2024)

*** Work supported by Yifang Wang's Science Studio of the Thousand Talents Project**

中国科学院高能物理研究所
Institute of High Energy Physics, Chinese Academy of Sciences

The 2024 international workshop on the high energy Circular Electron Positron Collider
Track： Accelerator technology Poster ID:75

Superconducting quadrupole magnets in the interaction region of CEPC and BEPCII-U

Jieru Geng [a, b], Yingshun Zhu [a], Chuang Shen [a], Xiangchen Yang [a], Yingzhi Wu [a], Zilin Chen [a],

Wan Chen [a], Xiaojuan Bian [a], Jianxin Zhou [a], Fusan Chen [a], Yuhui Li [a, b]

a Institute of High Energy Physics, Chinese Academy of Sciences, 19B Yuquan Road, Beijing, 100049, China

b University of Chinese Academy of Sciences, 19A Yuquan Road, Beijing, 100049, China

Jieru Geng, IHEP&UCAS
gengjieru@ihep.ac.cn

Abstract

This poster presentation includes research progress on superconducting quadrupole magnets in the interaction region for two current Chinese electron positron collider projects. One section describes the study on CCT ironless dual aperture superconducting quadrupole magnets in the interaction region being designed for the CEPC. And the other section describes the combined superconducting magnets in the interaction region being manufactured for the BEPCII Upgrade project.

Introduction

The accelerator of CEPC is now in the engineering design phase, which places more stringent requirements on the design of the superconducting quadrupole magnets in the interaction region. The need to reduce both the weight of the superconducting magnets and the deformation of the cantilevered support has led to the proposal of an ironless magnet solution. As the dual aperture magnets are not shielded by iron yokes, crosstalk will affect the magnetic field quality. For this reason, we propose the ironless dual aperture superconducting quadrupole magnet without correction coils.

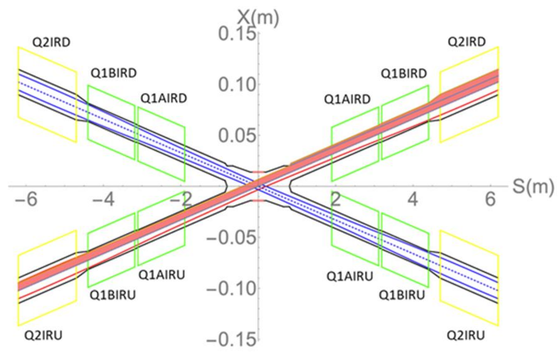

Layout of SCQ magnets in the interaction region.

Purpose

The dual-aperture superconducting quadrupole magnet Q1a, with the interaction region closest to the interaction point and the smallest distance between the two apertures in the Higgs mode, is taken as an example. The magnetic field quality problems caused by crosstalk and edge effects between the two apertures of the magnet are solved to meet the EDR requirements for the Q1a magnet.

Item	Value	Unit
Position from the IP	1900	mm
Magnetic field gradient	142.3	T/m
Reference radius	7.46	mm
Magnetic length	1210	mm
Distance between two aperture beam lines at tip	62.71	mm
Integrated field harmonics	≤ 3×10-4	-
Dipole field in aperture	≤ 300	G

Requirements of Q1a magnet.

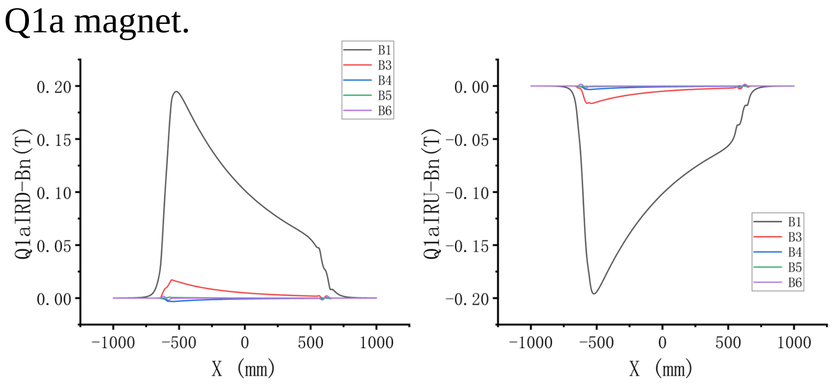

Uncorrected CCT Q1a magnet multipole components.

Method

The CCT coil path can be expressed by the equation, and the surface current density is used to derive the corresponding current density distribution of the coil and the magnetic field it generates. Therefore, by modifying the coil path equation, the current density distribution of the coil can be adjusted and new multipole magnetic fields can be added without the corrector coils.

Modified CCT coil path equation:

$$\vec{P}(\theta) = \begin{cases} R\cos\theta \\ R\sin\theta \\ \dfrac{R}{\mathrm{n}\tan(\alpha)}\sin(\mathrm{n}\theta) + \dfrac{\mathrm{w}\theta}{2\pi} + z' \end{cases}, -\pi N \le \theta \le \pi N$$

$$z' = \sum\nolimits_{n_1}\left(C_m \frac{R\sin(n_1\theta)}{n_1 \tan\alpha}\right) + \sum\nolimits_{n_2}\left(D_m \frac{R\cos(n_2\theta)}{n_2 \tan\alpha}\right)$$

$$\begin{cases} C_A = (-1)^{n-1} C_{n+m-1}^{n-1} \dfrac{I_B}{I_A}\left(\dfrac{R}{x}\right)^{n+m} \\ C_B = (-1)^{2n+m-1} C_{n+m-1}^{n-1} \dfrac{I_B}{I_A}\left(\dfrac{R}{x}\right)^{n+m} \end{cases}$$

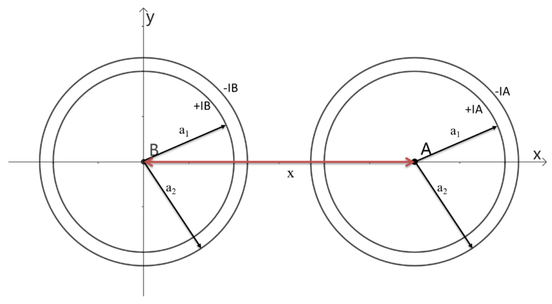

R: coil radius (a1,a2), w: turn advance, θ: azimuthal angle around the cylinder, α: inclination angle, n: multipole order, x: distance between the centres of the apertures, +IA /+IB: inner current of A/B, -IA /-IB: outer current of A/B.

An additional 2n-pole magnetic field is generated to correct the interference field generated by another aperture 2m-pole magnetic field.

Result

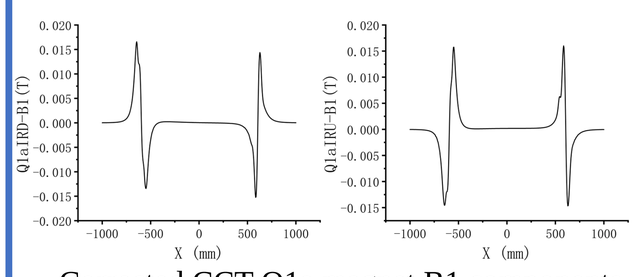

Corrected CCT Q1a magnet B1 components.

The critical aspect of the magnet combination analysis is to determine whether the magnitude of the dipole field amplitude meets the physical requirements after combining Q1a, Q1b, and Q2.

n	B_n/B_2 (Higgs Mode) ≤ 3×10^{-4}					
	Q1AIRD	Q1AIRU	Q1BIRD	Q1BIRU	Q2IRD	Q2IRU
	R_{ref}=7.46mm		R_{ref}=9.085mm		R_{ref}=12.24mm	
2	1	1	1	1	1	1
3	8.54E-05	-1.00E-04	6.13E-06	-2.20E-05	-1.20E-04	9.89E-05
4	-7.90E-06	-2.70E-05	-5.70E-07	-4.60E-06	1.47E-05	1.34E-05
5	-1.40E-04	1.39E-04	-2.70E-05	2.64E-05	-9.80E-06	9.98E-06
6	1.56E-05	1.57E-05	-3.40E-07	-3.10E-07	-3.00E-06	-3E-06
7	-2.90E-06	3.11E-06	-2.70E-07	2.80E-07	-2.30E-07	5.44E-08
8	2.76E-07	6.23E-07	2.34E-08	2.40E-08	-4.00E-08	-7.8E-08
9	-9.00E-10	-7.30E-08	5.86E-08	8.81E-09	1.17E-07	3.75E-08
10	2.94E-08	2.08E-07	-2.10E-08	5.11E-08	-5.70E-08	1.88E-07

Harmonics of Q1a, Q1b, Q2.

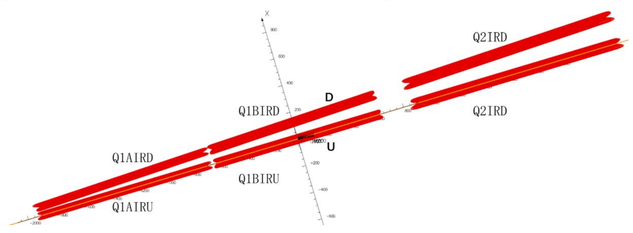

Q1a, Q1b, Q2 magnets 3D model.

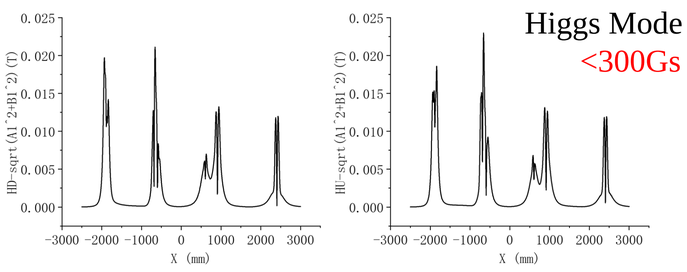

Higgs Mode <300Gs

Amplitude of Q1a, Q1b, Q2 dipole field.

BEPCII-U

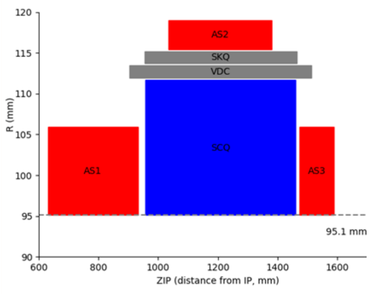

The BEPCII-U aims to extend the beam energy to 2.8 GeV and to enhance the luminosity at the optimized energy of 2.35 GeV from 3.5×10^{32} $cm^{-2}s^{-1}$ to 3.5×10^{32} $cm^{-2}s^{-1}$. It requires the development of combined superconducting magnets with higher magnetic field gradients for the interaction region. The challenge lies in producing combined superconducting magnets that meet high magnetic field precision requirements, it is essential to ensure that the coil winding process is both stable and precise. Using the developed direct winding system, the combined superconducting magnets were manufactured and passed the process tests.

Direct wind system

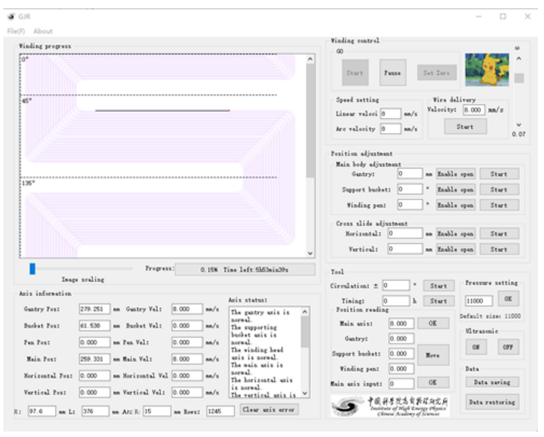

GUI of direct wind system.

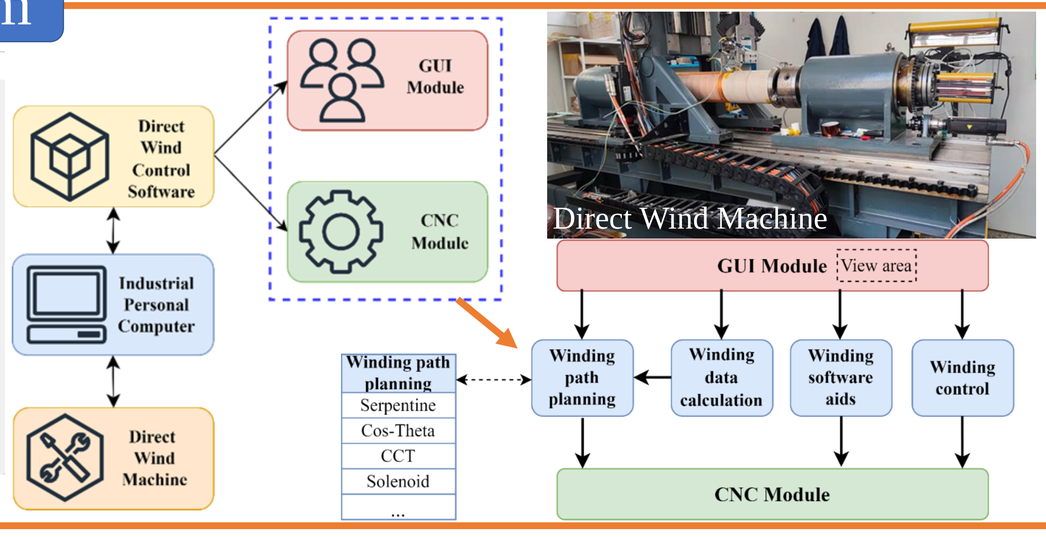

Manufacture

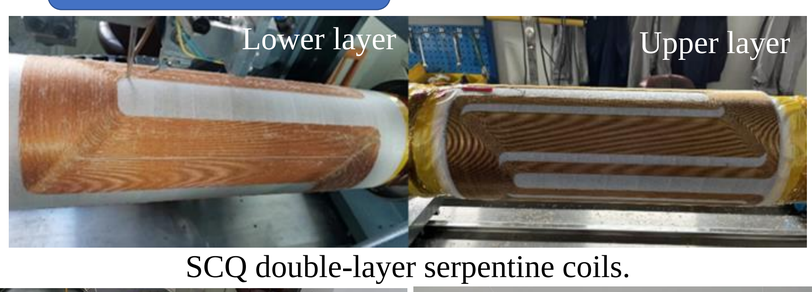

SCQ double-layer serpentine coils.

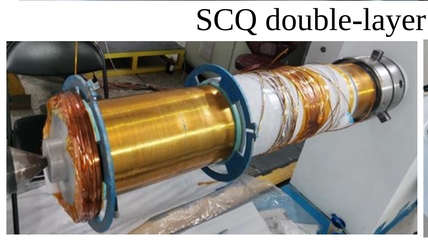

AS1 solenoid coil winding.

Finished superconducting magnet

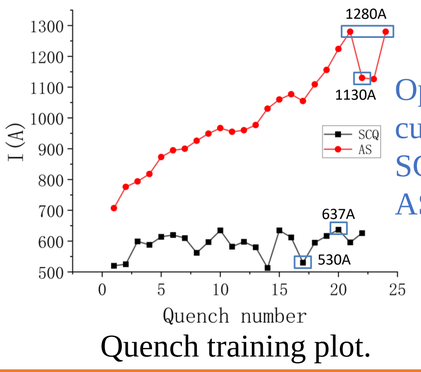

Operating current: SCQ-530A AS-1130A

Quench training plot.

n	B_n/B_2 (SCQ)		
	530A	600A	630A
2	1	1	1
3	1.15E-04	1.17E-04	1.15E-04
4	1.12E-04	1.06E-04	1.03E-04
5	3.38E-05	3.65E-05	3.45E-05
6	1.15E-04	1.24E-04	1.30E-04
7	2.62E-05	1.47E-05	8.93E-06
8	2.33E-05	2.58E-05	2.31E-05
9	2.01E-05	3.30E-05	2.69E-05
10	5.88E-05	6.08E-05	7.49E-05

$B_n/B_2 \le 3\times10^{-4}$

SCQ magnet harmonics.

No. 95

Design and development of CEPC control system

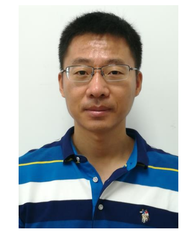

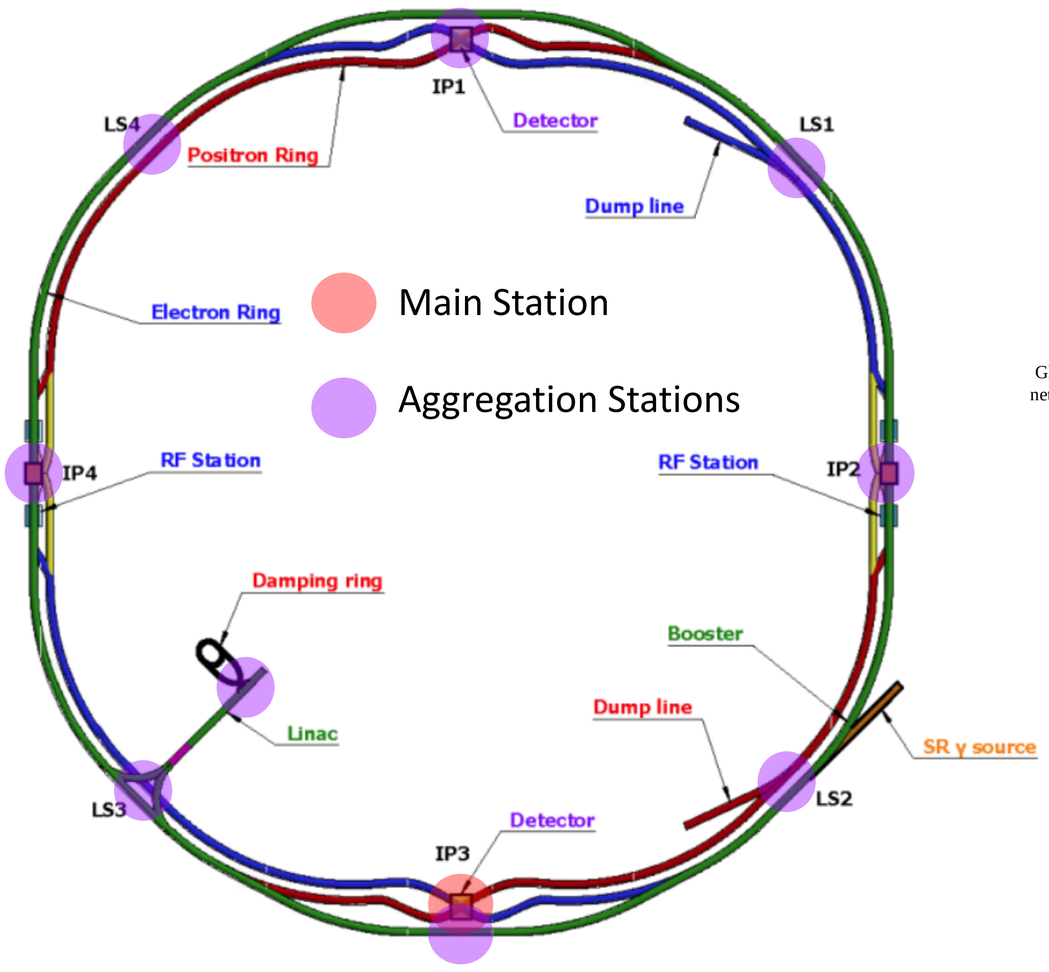

Timing/clock/network, optical-fiber-based connections

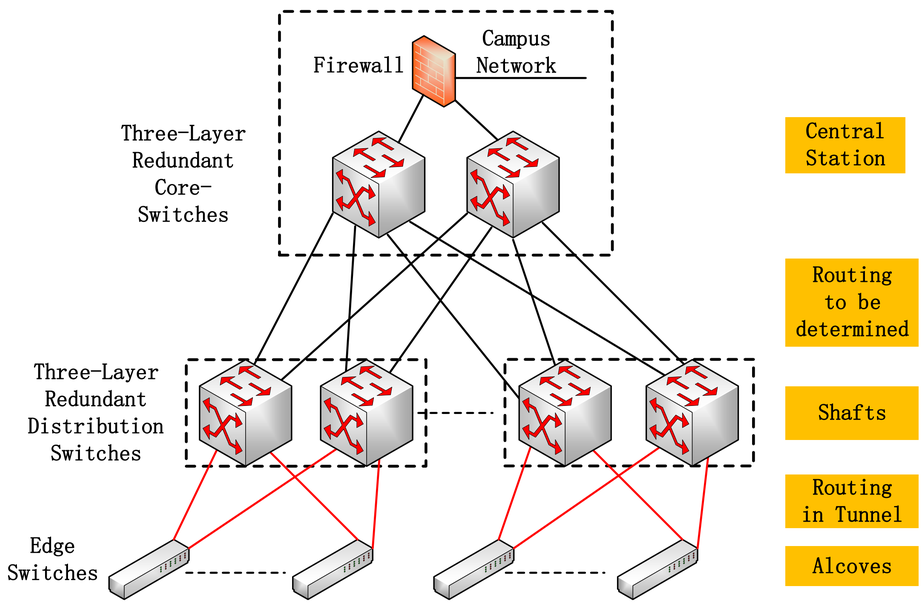

Network structure of the CEPC control system

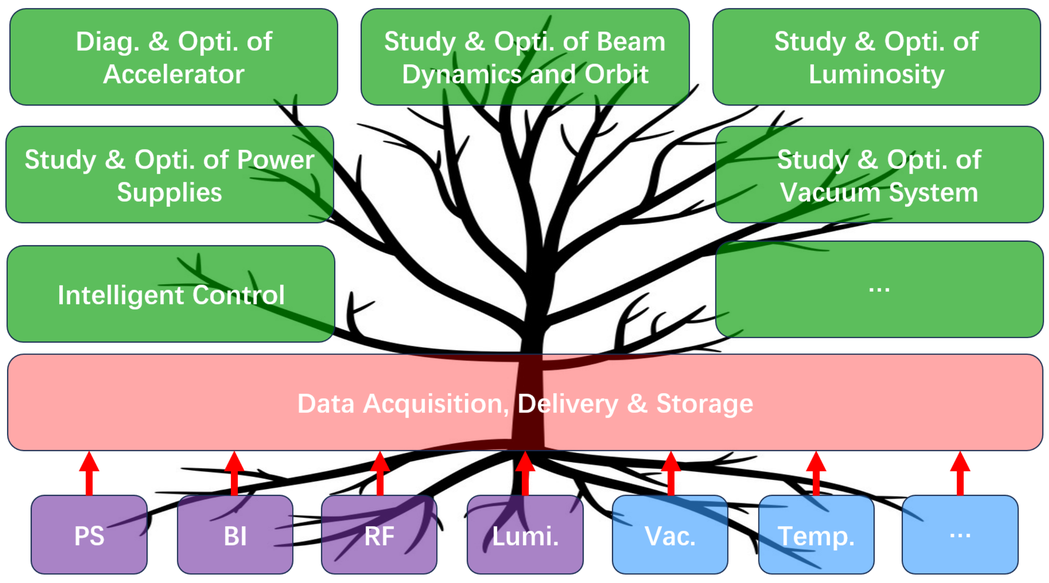

Application of artificial intelligence based on high-quality data

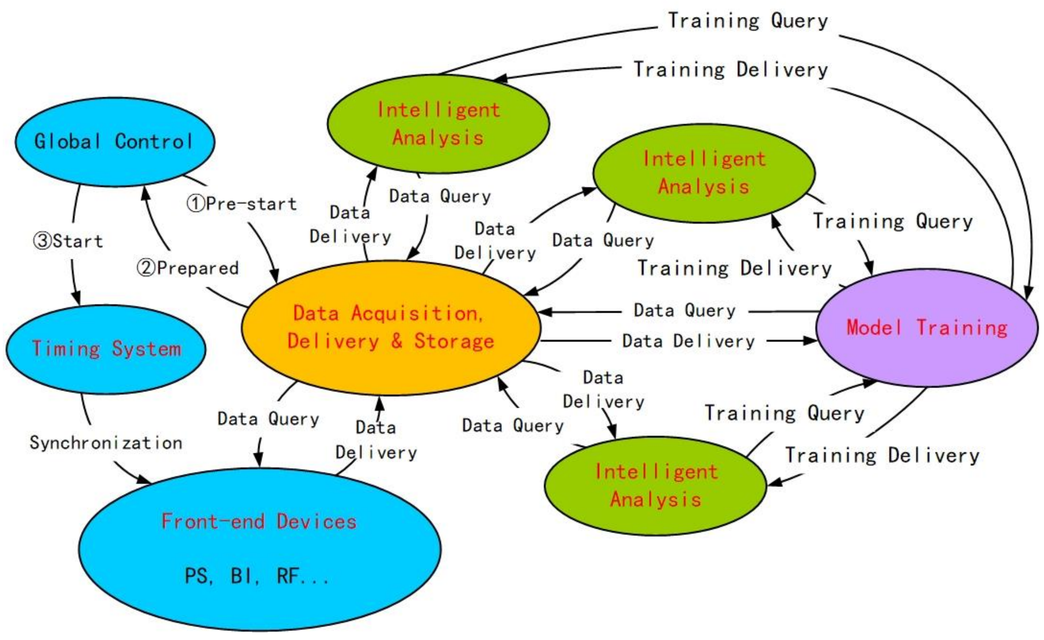

Dataflow of data acquisition & analysis

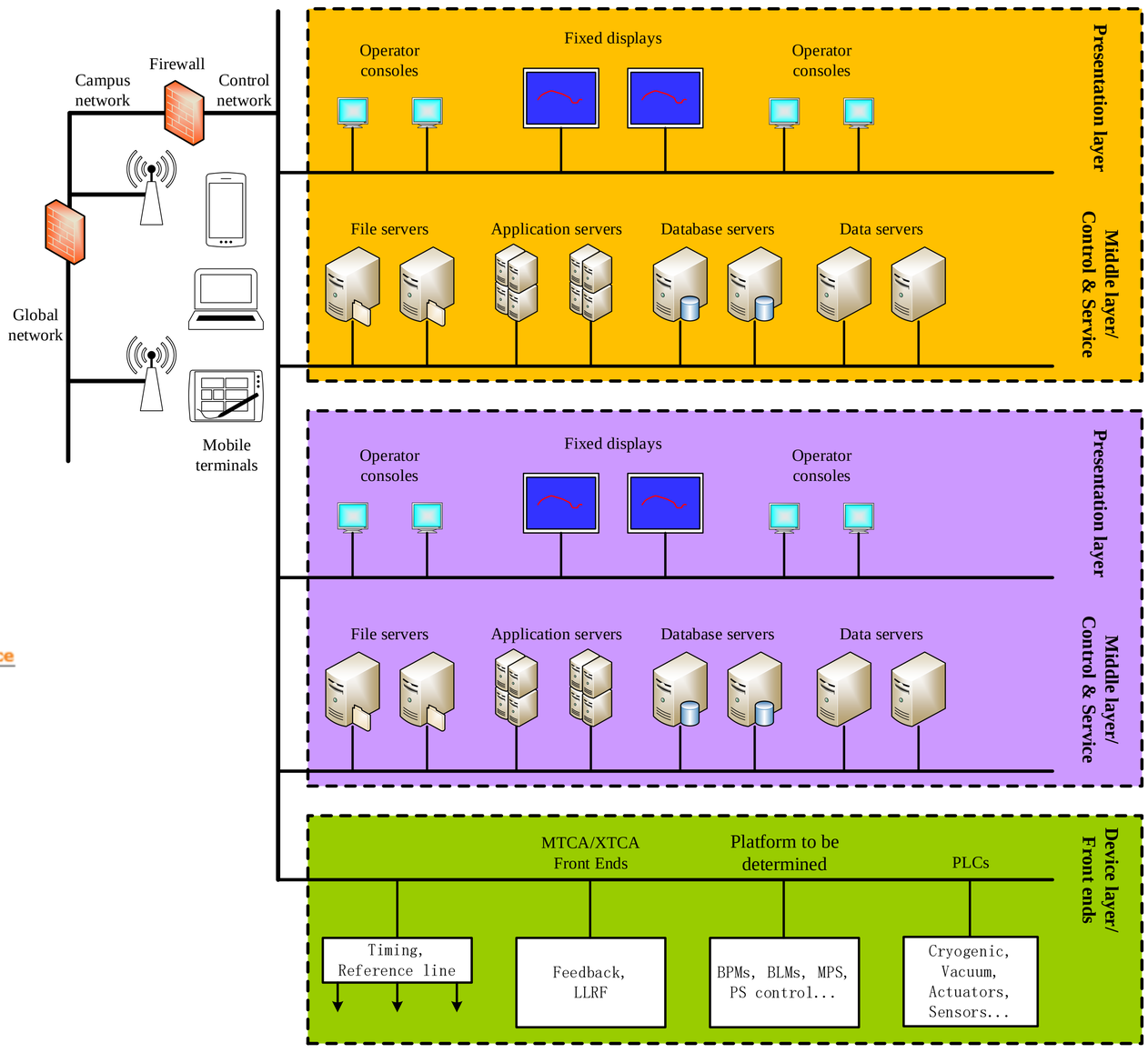

Structure of CEPC control system

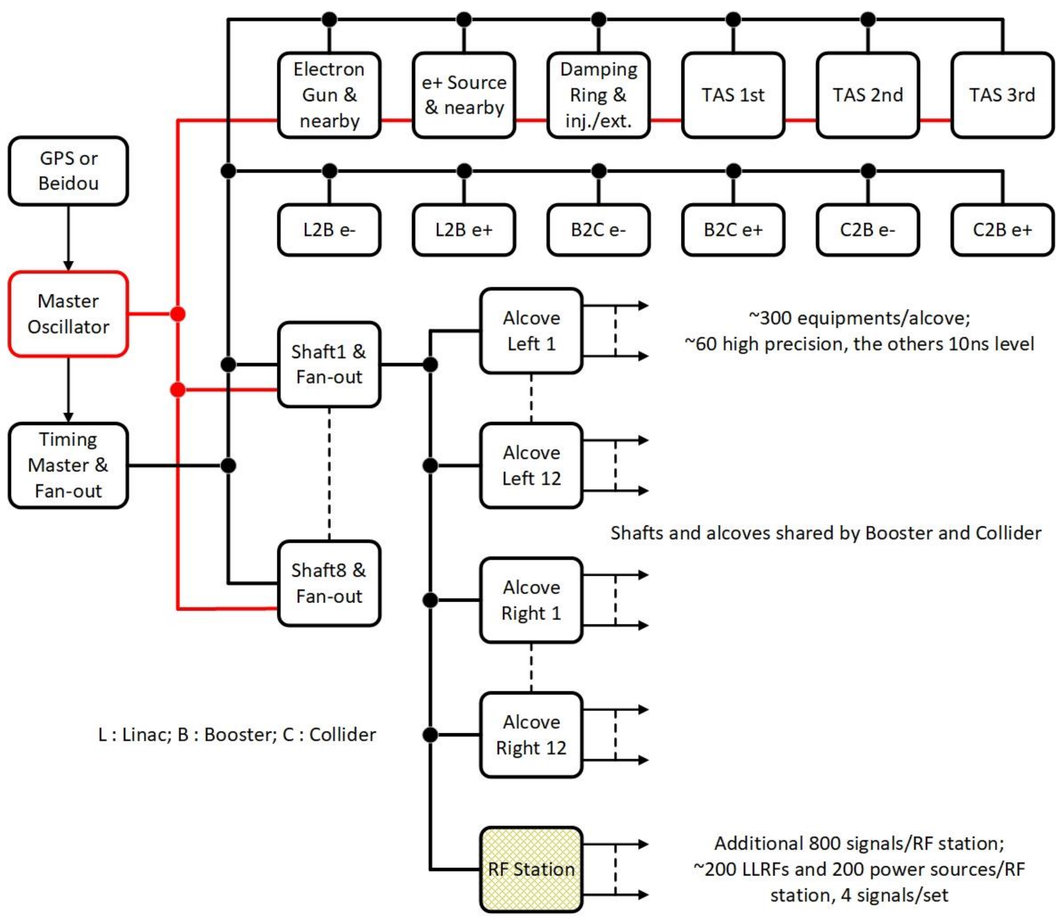

Structure of the timing system and clock reference

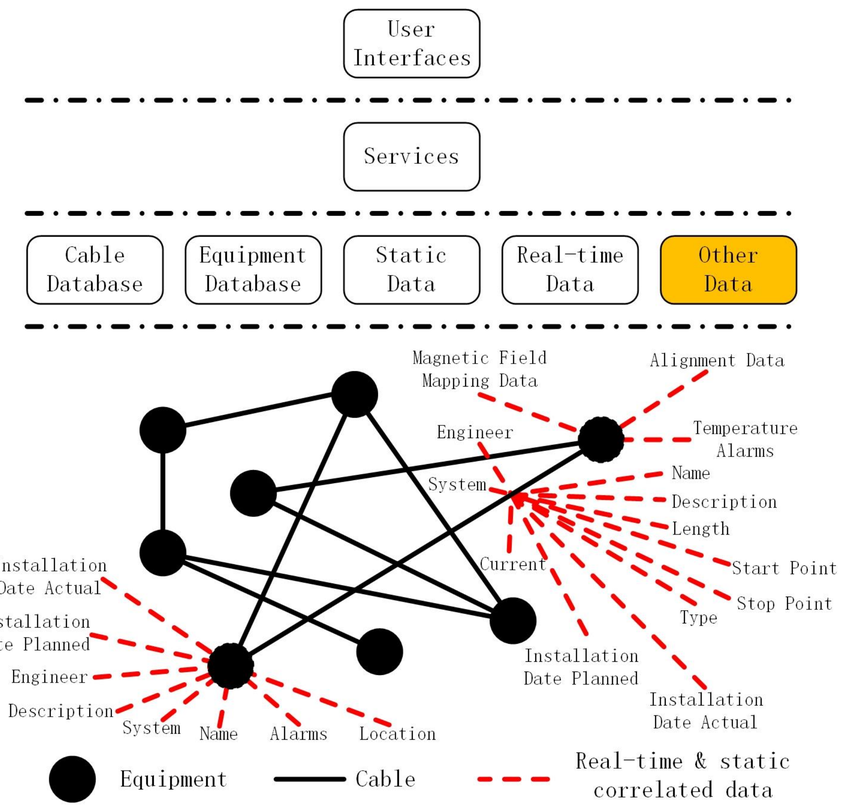

Information management system

With the huge size, there come some critical issues for CEPC related to the reliability, availability, maintainability and so on. Long distance means large temperature-variation induced time drift, which is essential for the clock reference and timing system. Large amount of equipment means large amount of data to be acquired and analyzed, and large amount of information to be managed.

High quality highly-correlated data is the base for machine performance improvement and fault prediction. High quality static & dynamic information management is the base for both of the facility construction and operation.

Besides those shown in this poster, there are many other control tasks, such as personnel protection, machine protection, global orbit feedback, power-supply remote control, vacuum control, environment monitoring, data archiving, system alarm …

Dapeng Jin, IHEP, Beijing, China. E-mail : jindp@ihep.ac.cn

Poster ID:126

Phase and Amplitude Calibration of the Sub-harmonic Buncher for the High Energy Photon Source Linac

Z. T. Liu[1], W. Li[1], X. Zhang[1], C. Meng[1], O. Z. Xiao, N. Gan, J. He, Y. Y. Du, L. Du, J. R. Zhang, J. Y. Li

Institute of High Energy Physics, Chinese Academy of Sciences, Beijing 100049, China

[1]also at University of Chinese Academy of Sciences, Beijing 100049, China

Abstract

The High Energy Photon Source (HEPS) Linac is a normal conducting electron linear accelerator capable of producing high bunch charge beam. Two Sub-harmonic bunchers (SHB) are included in its bunching system for longitudinal bunching to increase the bunch charge. The phase and amplitude of the SHB is crucial for achieving high-quality electron beam in Linac. This paper presents a method for calibrating the phase and amplitude of the SHB using the time-of-flight technique, and experiments were conducted based in the HEPS Linac and employing two Beam Position Monitors (BPMs). This paper presents detailed insights into both the simulation and experimental procedures

Calibration Theory

A. Single-particle Model

$$E_2 - E_1 = eV_{eff}cos(\phi + \phi_0)$$

$$t_{ToF} = \frac{L_1}{v_1} + \frac{L_2}{v_2} + \Delta t$$

B. Particle-bunch Model

$$\langle E_{2i} - E_{1i} \rangle = e\kappa V_{eff}cos(\phi + \phi_0 + \Delta\phi)$$

$$\kappa = \sqrt{\left(\frac{1}{N}\sum_{i=1}^{N} sin\Delta\phi_i\right)^2 + \left(\frac{1}{N}\sum_{i=1}^{N} cos\Delta\phi_i\right)^2}$$

$$\Delta\phi = arctan\left(\frac{\sum_{i=1}^{N} sin\Delta\phi_i}{\sum_{i=1}^{N} cos\Delta\phi_i}\right)$$

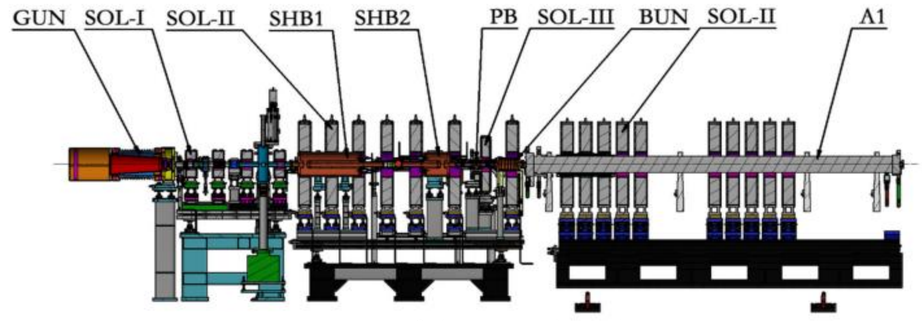

Fig. 1 Layout of the HEPS bunching system

Simulation Results

Beam dynamics simulations using ASTRA were conducted at bunch charges of 1.0 nC, 5.0 nC, and 9.0 nC with FWHM bunch lengths of 500 ps, 1000 ps, and 1500 ps. ToF was extracted using two methods—global averaging and truncated averaging—and their results are presented.

- **Global Averaging Method:**

  All particles are included in the calculation of the average Time of Flight.

Truncated Averaging Method:

- Only particles with densities above a specified threshold on the particle distribution are included in the average ToF calculation.

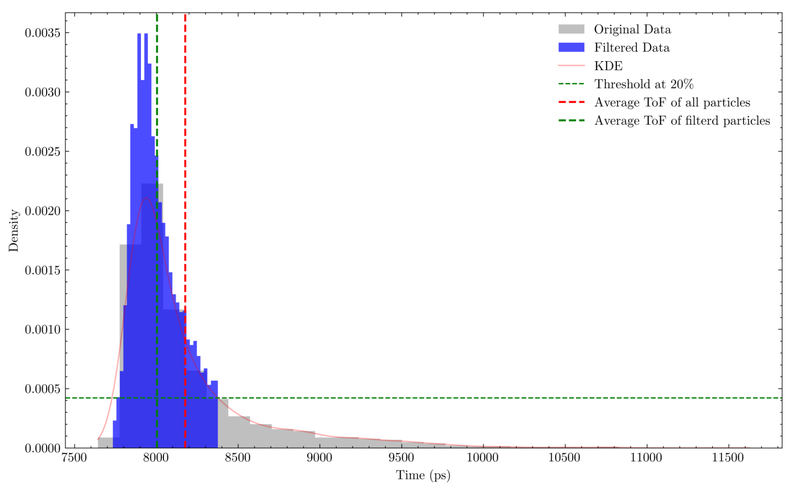

Fig.4 Difference between global averaging method and truncated averaging method

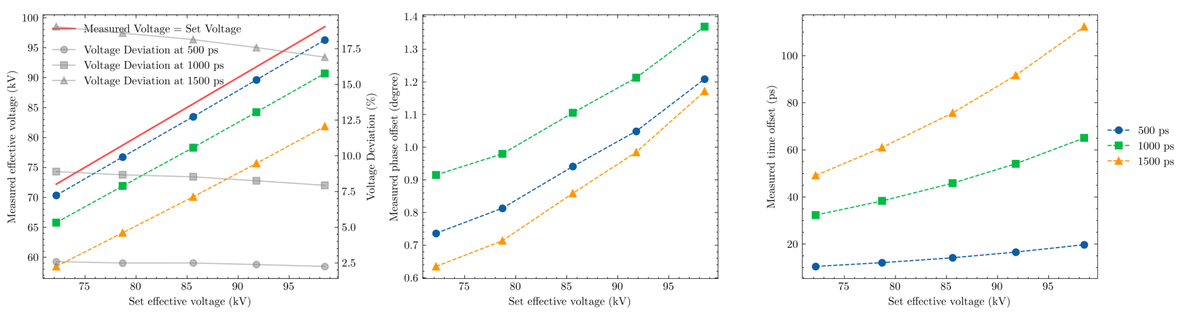

Fig.2 Simulation results. Single-particle model with global averaging method

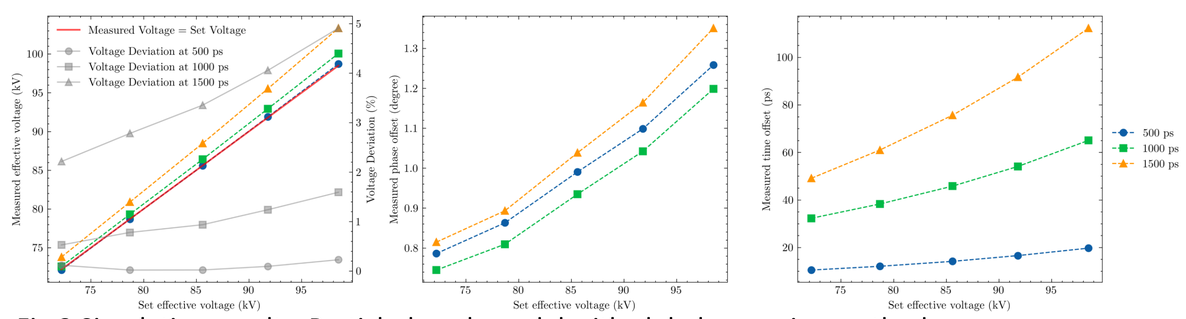

Fig.3 Simulation results. Particle-bunch model with global averaging method

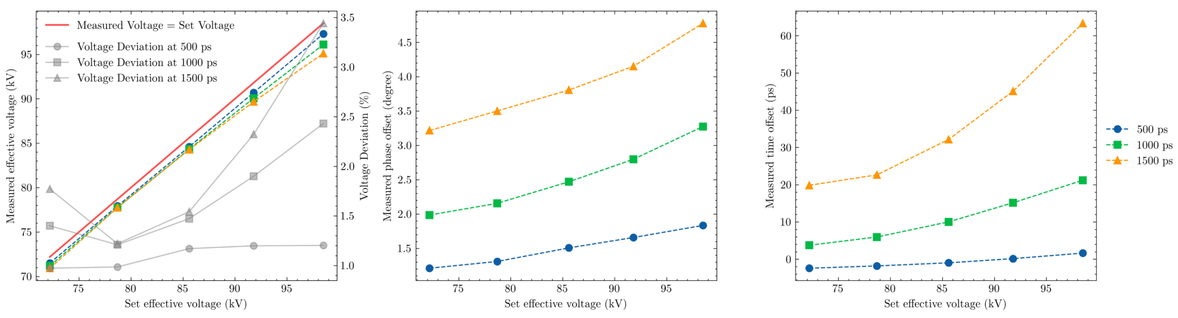

Fig.5 Simulation results. Single-particle model with truncated averaging method

Experimental Results

Multiple approaches were employed to extract the ToF data and derive the phase scan curve, including the use of peak, valley, and zero-crossing points to determine the time of flight.

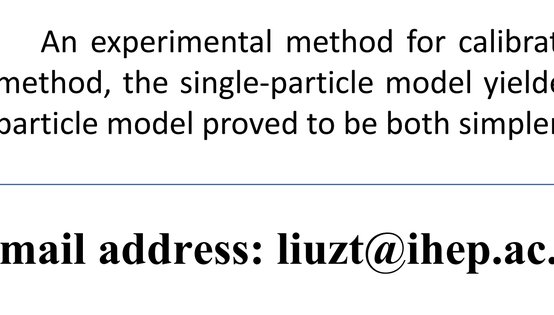

Fig.6 Signals from BPM1 and BPM2

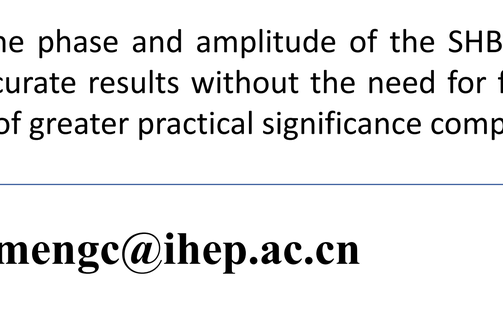

Fig.7 Integrated signals from BPM1 and BPM2

Fig.8 Comparison of phase scan curves obtained using different methods with 0.6nC bunch charge

Fig.9 Comparison of phase scan curves obtained using different methods with 9.0nC bunch charge

As seen in Fig. 10, the time offset and its error bars show significant variation when the truncation percentage is below 20%. However, beyond 20%, these fluctuations become minimal. Thus, the truncation percentage was set to 20%.

Fig.10 Timeoffset as a function of truncation percentage

Fig.11 Experimental Results

Conclusion

An experimental method for calibrating the phase and amplitude of the SHB using two BPMs has been presented. For ToF extraction using the truncated averaging method, the single-particle model yielded accurate results without the need for further refinement. The combination of the truncated averaging method with the single-particle model proved to be both simpler and of greater practical significance compared with the particle-bunch model.

† email address: liuzt@ihep.ac.cn, mengc@ihep.ac.cn

Poster ID:334

The Integration of Feedback System with Machine Learning

Di Yin*, Junhui Yue, Liang Xu, Fangqi Huang,
IHEP, Beijing, P. R. China

*yind@ihep.ac.cn

Abstract

For accelerators like CEPC, which have extremely large storage rings, there is a significant issue with beam instability, By utilizing appropriate machine learning techniques, it is possible to train on a large dataset of beam oscillation signals to directly compute the feedback signals required for the beam, significantly shortening the data acquisition time, achieving faster damping times than traditional feedback systems, and even realizing single-turn feedback.

Introduction

The damping time that feedback system can provide includes the time for signal acquisition and processing. In traditional bunch-by-bunch feedback systems, the filter processes signals that require data collection over multiple turns. The effect of this data acquisition time on the damping time is not prominent in smaller circumference storage rings, but it can become a major issue in the CEPC, potentially resulting in damping times comparable to the instability growth times.

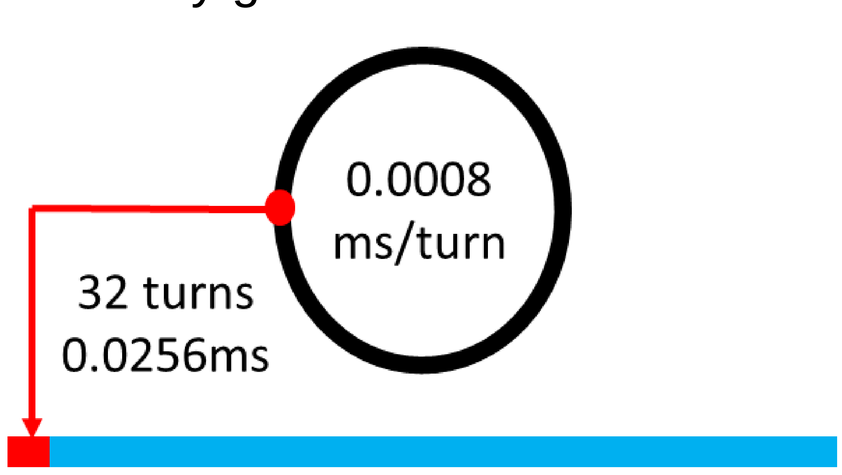

BEPCII Damping Time 0.5ms

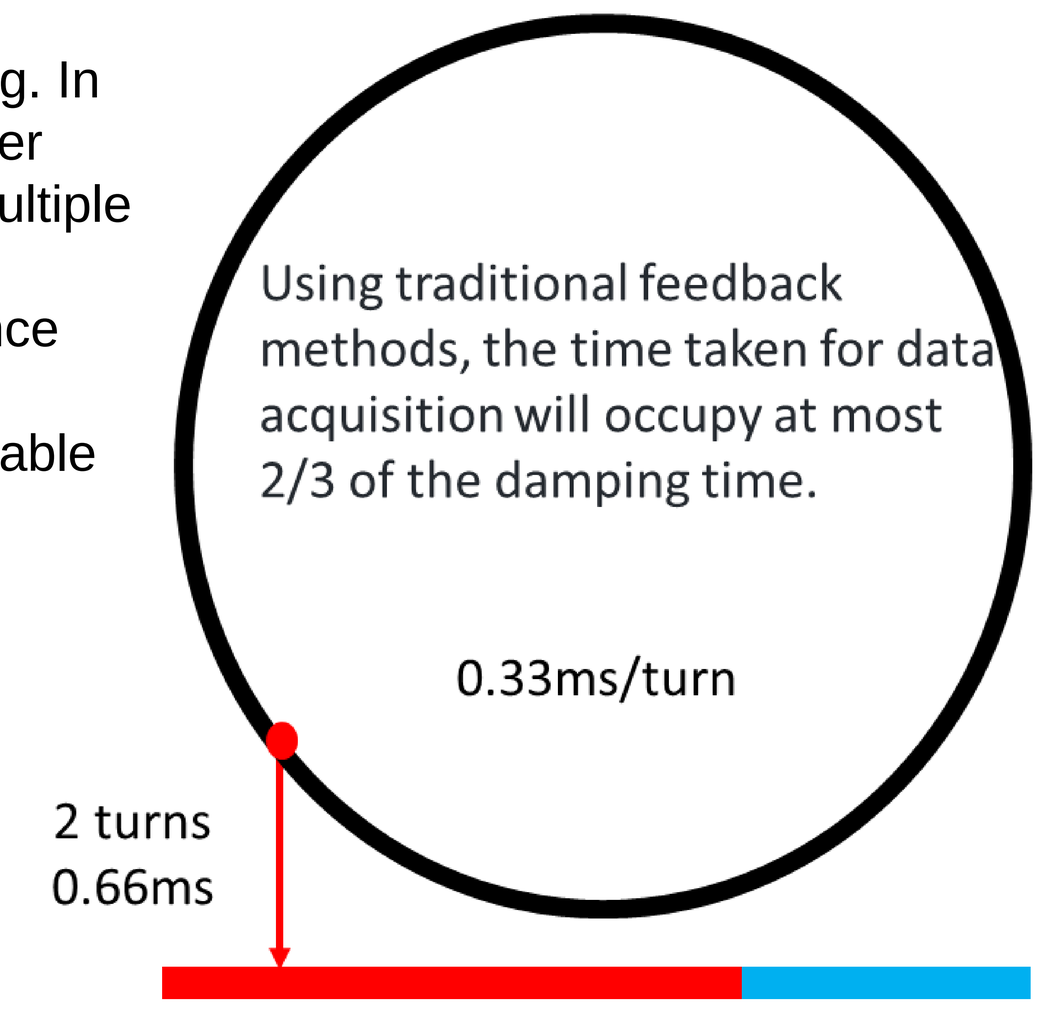

CEPC Damping Time 1ms

Comparison of the time taken for data acquisition by the feedback systems in small rings (BEPCII) and large rings (CEPC) relative to the damping time.

Method

- **Implementation of Closed-orbit Signal Cancellation based on Digital/Analog Circuits**
- **Oscillation Information Acquisition Based on Machine Learning**

Acquire the dataset of X and Y direction signals calibrated by the oscillation signals, and select an appropriate neural network to perform machine training on the dataset. Establish a suitable machine learning model, test its signal processing effectiveness in software, and compare it with actual signals. Subsequently, optimize the processing speed and the machine learning model.

- **Debugging of the Signal Processing Card and FPGA Implementation**

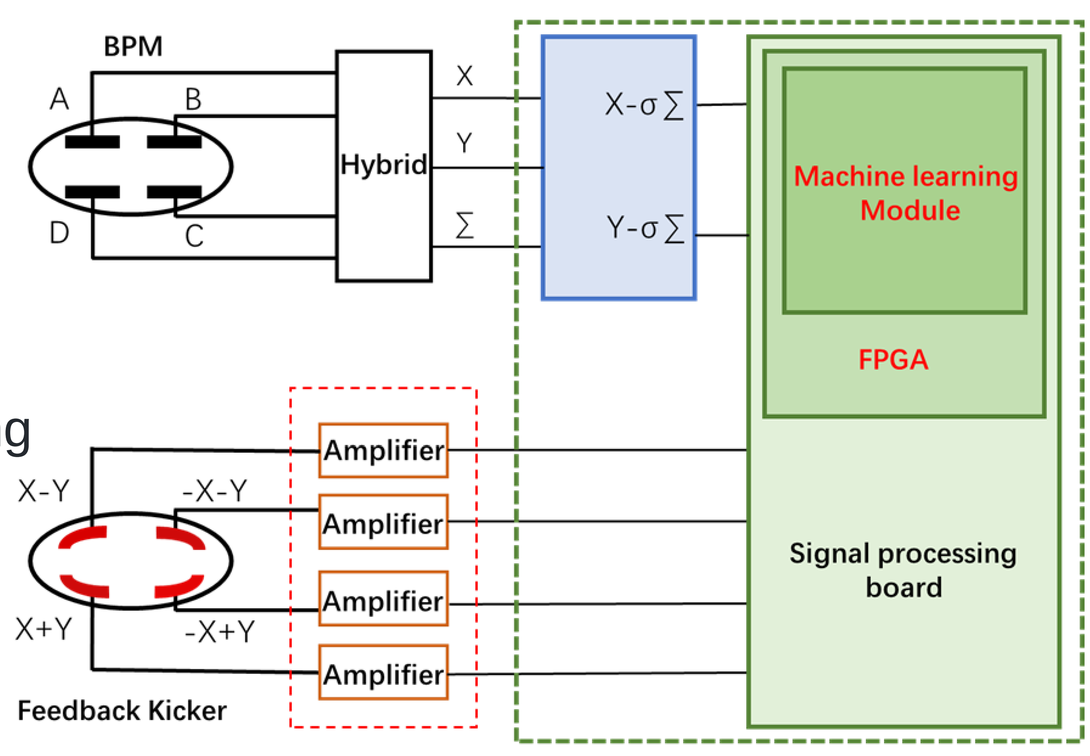

Implement the machine learning model in the FPGA

Work support by Jialin Xie Fundation

Poster ID :349

Design of Collimator Control System for PWFA

Shutao Zhao, Ningchuang Zhou, Dapeng Jin, Dou Wang, Yanru Wei, Guangyi Tang, Xiaoping Li, Dazhang Li
Institute of High Energy Physics, Chinese Academy of Sciences, Beijing 100049, China

ABSTRACT

The primary function of the collimator in the PWFA project is to reduce the lateral dimensions of the beam bunch and select a very small and precise beam bunch through the high-precision movement of its scraping elements. The control system employs EtherCAT bus technology to enable precise motion control of the collimator's scraping components. Given the intense radiation environment, Linear Variable Differential Transformers (LVDTs) are utilized for position feedback, replacing conventional optical encoders. Furthermore, the system incorporates multiple levels of safety protection, ensuring operational safety. Using Safety-over-EtherCAT, a safety integrity level of SIL-3 can be achieved.To facilitate remote operation, the system adopts the Experimental Physics and Industrial Control System (EPICS) framework and communicates with EPICS Input/Output Controllers (IOCs) using the MODBUS TCP protocol.

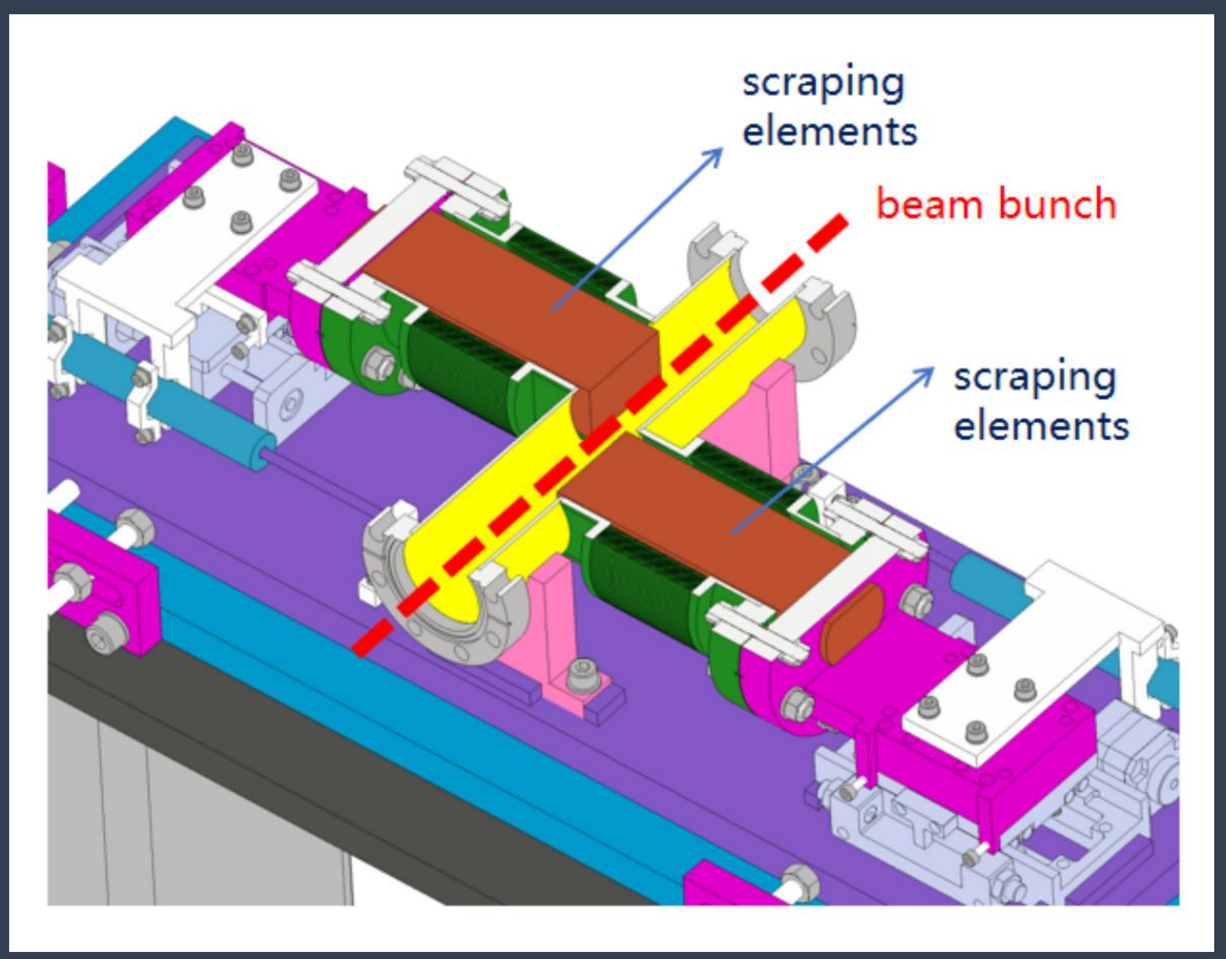

Scraping elements of collimator

SYSTEM DESIGN

- EtherCAT Control Architecture: distributed system design based on EtherCAT industrial Ethernet bus technology, leveraging its capabilities for high-speed data transmission and high-precision synchronization to ensure precise control of the collimator. The system consists of a master station and multiple slave stations, where the master station is responsible for issuing control commands and collecting feedback information; the slave stations include drive units for stepping motors and I/O modules for sensor signal acquisition.
- Absolute Position Calibration: In a high-radiation environment, an LVDT sensor is used to achieve high-precision positioning instead of a linear encoder.
- Safety System Design: Multiple layers of safety protection, including software limits, mechanical limit switches, and emergency stop switches.Functions such as emergency stop for motors, motor temperature monitoring, and PLC software protection are all integrated into the safety system. Using Safety over EtherCAT, a safety integrity level of SIL-3 can be achieved
- Remote Control:Realization of remote control via MODBUS TCP protocol communication between Beckhoff PLC and EPICS IOC. The EPICS OPI interface is developed using Phoebus CSS.

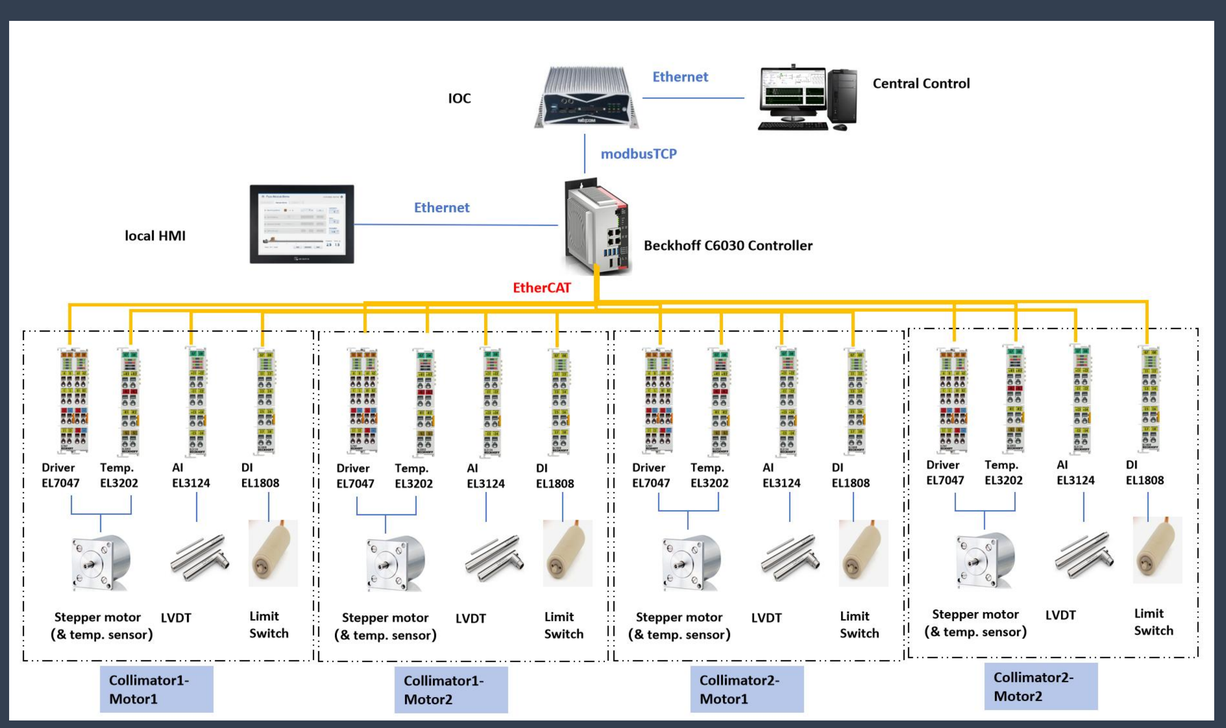

EtherCAT Control Architecture

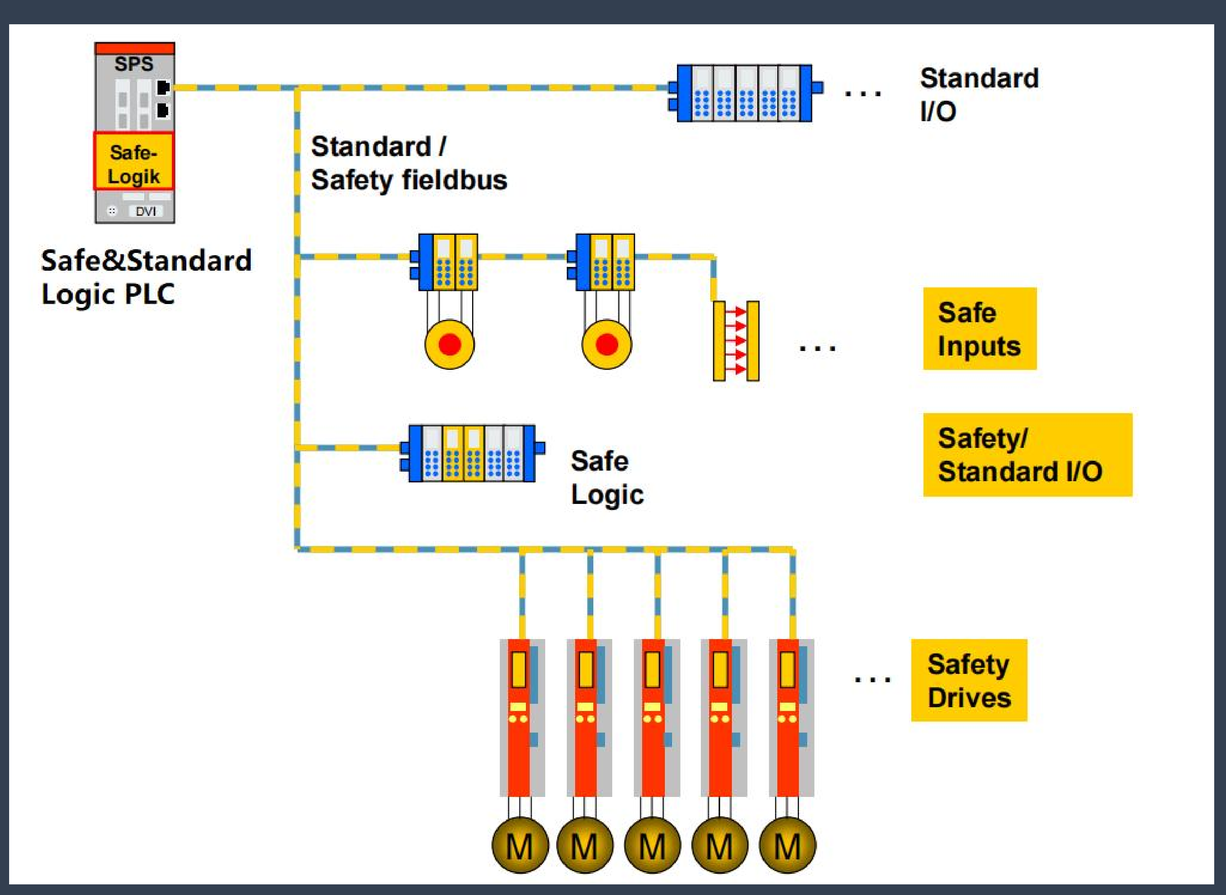

Safe-Over-EtherCAT Safety Architecture

zhaost@ihep.ac.cn 13811064581

The 2024 international workshop on the high energy Circular Electron Positron Collider

Poster ID: 350

Oct 22 - 27, 2024

CEPC Carbon Footprint and CO2 Reduction Optimization

中国科学院高能物理研究所
Institute of High Energy Physics
Chinese Academy of Sciences

Dou Wang#, Jie Gao, Yuhui Li, Jinshu Huang, Song Jin, Manqi Ruan, Mingshui Chen, Shanzhen Chen

Abstract

The Higgs factory is a kind of special energy consumer and the environmental impact for the given scientific outcome must be optimized carefully. The carbon footprint of CEPC was estimated based on simplified model including both construction process and operation process. The environmental impact of CEPC with different circumference, different energy source, different SR power and different Higgs number was studied. The carbon intensity of China electric grid will be reduced rapidly by 2040 due to the development of renewable energies. Some results to compare the future colliders, including linear colliders and circular colliders, are given. Assuming all the colliders will use the same clean energy (20 ton CO2e/GWh), CEPC has the lowest carbon emission to produce one Higgs boson.

• Current Status of Chinese Electricity Grid

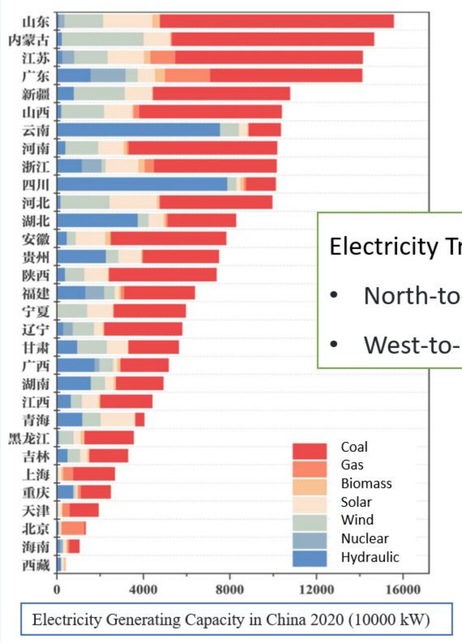

Electricity Generating Capacity in China 2020 (10000 kW)

Electricity Transmission:
- North-to-South
- West-to-East

Carbon intensity (kgCO2/kWh)

省份	2010 年	2012 年	2018 年	2020 年	
辽宁	0.836	0.775	0.722	0.91	
吉林	0.679	0.721	0.615	0.839	
黑龙江	0.816	0.797	0.663	0.814	
北京	0.829	0.776	0.617	0.615	
天津	0.873	0.892	0.812	0.841	
河北	0.915	0.898	0.903	1.092	Qin Huang Dao
山西	0.88	0.849	0.74	0.841	
内蒙古	0.85	0.929	0.753	1.000	
山东	0.924	0.888	0.861	0.742	
上海	0.793	0.624	0.564	0.548	
江苏	0.736	0.75	0.683	0.695	
浙江	0.682	0.665	0.525	0.532	Hu Zhou
安徽	0.791	0.809	0.776	0.763	
福建	0.544	0.551	0.391	0.489	
江西	0.764	0.634	0.634	0.616	
河南	0.844	0.806	0.791	0.738	Zheng Zhou
湖北	0.372	0.353	0.357	0.316	
湖南	0.552	0.517	0.499	0.487	Chang Sha
重庆	0.629	0.574	0.441	0.432	
四川	0.289	0.248	0.103	0.117	
广东	0.638	0.591	0.451	0.445	Shen Shan
广西	0.482	0.495	0.394	0.526	
海南	0.646	0.686	0.515	0.459	
贵州	0.656	0.495	0.428	0.42	
云南	0.415	0.306	0.092	0.146	
陕西	0.87	0.769	0.767	0.641	
甘肃	0.612	0.573	0.491	0.46	
青海	0.226	0.232	0.26	0.095	
宁夏	0.818	0.779	0.62	0.872	
新疆	0.764	0.79	0.622	0.749	

• “Double Carbon Target” in China

- **Peak Carbon Dioxide Emissions**: China has pledged to reach carbon peak by 2030, and then gradually reduce carbon dioxide emissions.
- **Carbon neutrality:** achieve a relative "zero emissions" before 2060 by planting trees and forests, saving energy and reducing emissions

2021~ 2030: realize peak carbon emissions

↓

2031~ 2045: rapid reduction of carbon emissions

↓

2046~ 2060: deep decarbonization, achieving carbon neutrality

Solar (t CO2/GWh)	Wind (t CO2/GWh)	Hydroelectric (t CO2/GWh)	nuclear(t CO2/GWh)
30	15	25	5

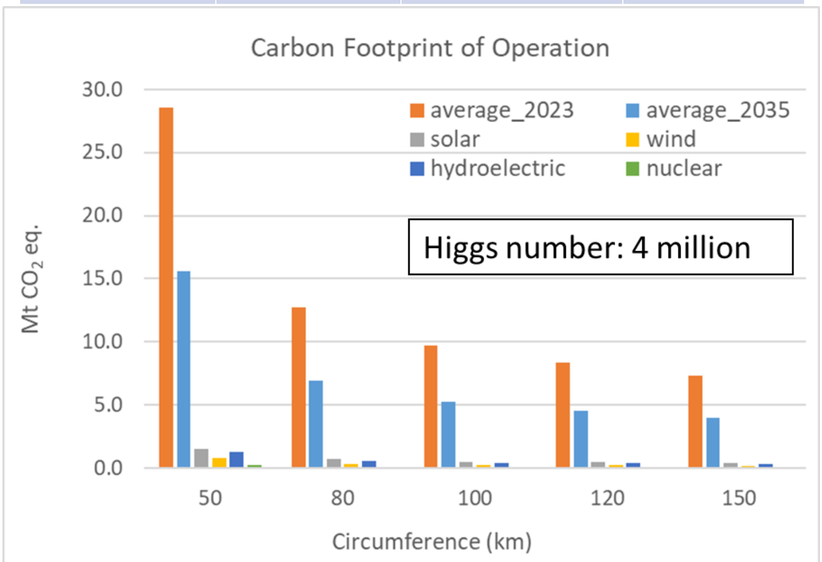

• Electricity Grid Carbon Intensity in China (2025-2035)

省份	2025 年	2030 年	2035 年
辽宁	0.578 (0.528-0.664)	0.496 (0.432-0.571)	0.371 (0.342-0.408)
吉林	0.564 (0.559-0.594)	0.43 (0.384-0.472)	0.216 (0.210-0.281)
黑龙江	0.654 (0.648-0.683)	0.599 (0.590-0.621)	0.504 (0.467-0.528)
北京	0.595 (0.573-0.612)	0.519 (0.476-0.532)	0.289 (0.208-0.299)
天津	0.688 (0.668-0.709)	0.536 (0.53-0.584)	0.418 (0.413-0.448)
河北	0.736 (0.714-0.784)	0.683 (0.666-0.733)	0.544 (0.512-0.571)
山西	0.707 (0.69-0.738)	0.7 (0.684-0.738)	0.598 (0.583-0.633)
内蒙古	0.8 (0.791-0.836)	0.792 (0.783-0.836)	0.673 (0.665-0.714)
山东	0.546 (0.536-0.56)	0.498 (0.489-0.506)	0.383 (0.36-0.386)
上海	0.333 (0.321-0.464)	0.325 (0.312-0.432)	0.281 (0.259-0.349)
江苏	0.601 (0.579-0.639)	0.512 (0.489-0.539)	0.411 (0.386-0.435)
浙江	0.418 (0.412-0.427)	0.386 (0.381-0.402)	0.307 (0.289-0.314)
安徽	0.755 (0.725-0.758)	0.694 (0.65-0.757)	0.596 (0.546-0.644)
福建	0.363 (0.346-0.379)	0.33 (0.322-0.358)	0.27 (0.266-0.293)
江西	0.474 (0.451-0.498)	0.436 (0.414-0.444)	0.354 (0.334-0.359)
河南	0.599 (0.553-0.621)	0.49 (0.462-0.512)	0.389 (0.356-0.409)
湖北	0.31 (0.307-0.317)	0.254 (0.247-0.316)	0.202 (0.19-0.261)
湖南	0.453 (0.447-0.46)	0.409 (0.397-0.422)	0.312 (0.3-0.331)
重庆	0.363 (0.231-0.396)	0.256 (0.193-0.304)	0.179 (0.131-0.226)
四川	0.104 (0.103-0.107)	0.075 (0.073-0.075)	0.04 (0.04-0.04)
广东	0.369 (0.359-0.382)	0.332 (0.318-0.351)	0.276 (0.269-0.295)
广西	0.336 (0.316-0.363)	0.334 (0.317-0.373)	0.279 (0.26-0.308)
海南	0.326 (0.312-0.332)	0.224 (0.188-0.236)	0.115 (0.11-0.143)
贵州	0.398 (0.393-0.408)	0.276 (0.26-0.278)	0.204 (0.146-0.206)
云南	0.1 (0.093-0.102)	0.062 (0.05-0.075)	0.025 (0.022-0.03)
陕西	0.607 (0.533-0.623)	0.601 (0.528-0.619)	0.515 (0.446-0.53)
甘肃	0.443 (0.433-0.469)	0.407 (0.391-0.439)	0.279 (0.223-0.285)
青海	0.067 (0.048-0.078)	0.032 (0.027-0.041)	0.01 (0.01-0.013)
宁夏	0.724 (0.703-0.758)	0.665 (0.643-0.714)	0.459 (0.452-0.551)
新疆	0.720 (0.601-0.745)	0.713 (0.595-0.745)	0.573 (0.516-0.599)

➢ The carbon intensity will be reduced rapidly until 2035 in China.

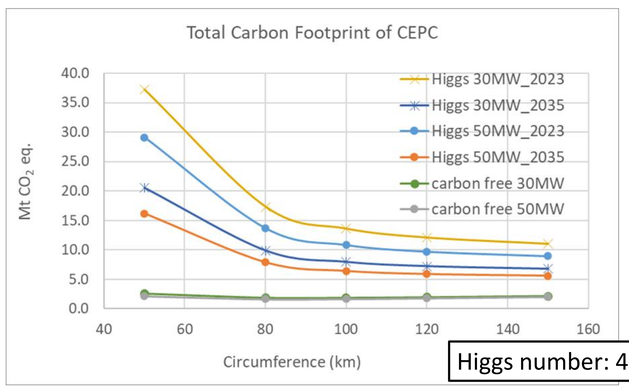

Higgs number: 4 million

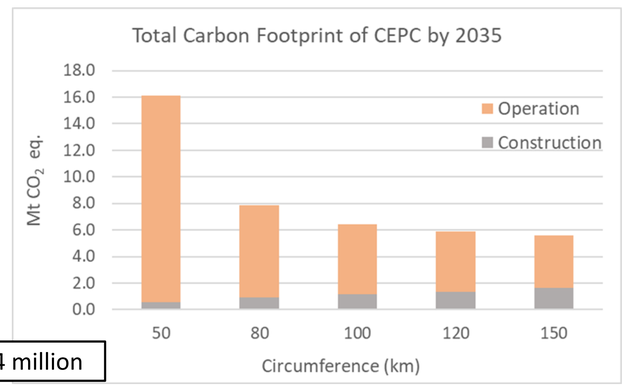

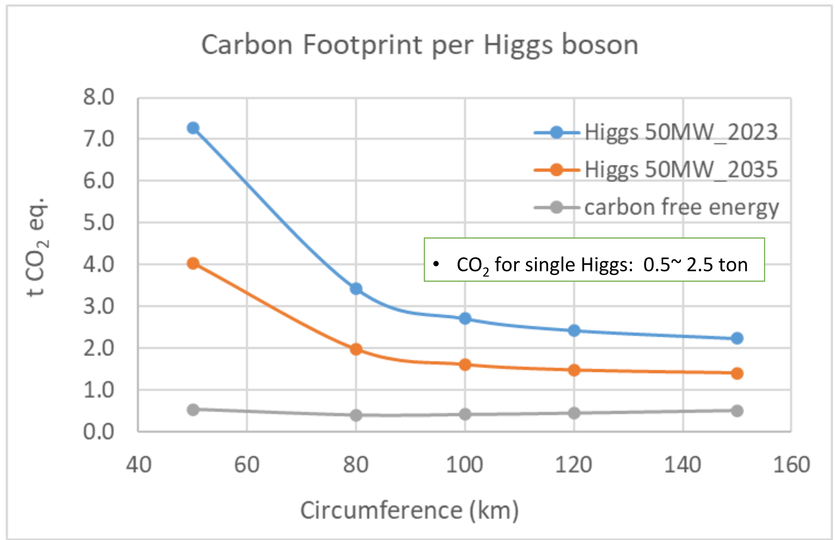

• Total Carbon Emissions of Future Colliders

	ILC-250	CLIC-380	C3-250	CEPC-240	FCCee-240
Instantaneous power (MW)	111	110	150	340	290
Annual collision month	6.2	4.6	6.2	5.0	4.2
Annual collision time (E7 s)	1.6	1.2	1.6	1.3	1.1
Operational efficiency	0.75	0.75	0.75	0.57	0.75
Higgs operation time (years)	11.5	8	11.5	10	3
Higgs number (million)	0.5	0.25	0.5	4	1

Assumption: All the projects can use the same clean energy (20 ton CO2e/GWh (solar & nuclear))

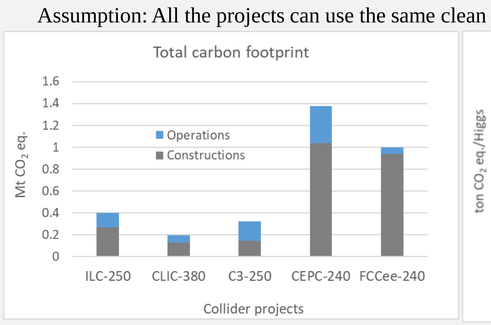

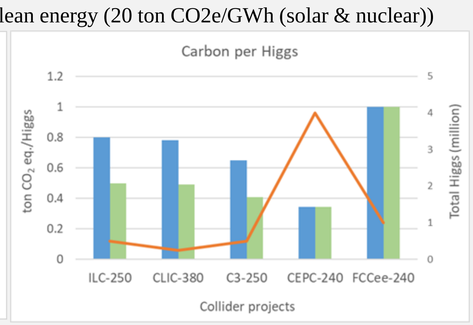

• Total Carbon emissions with different physics goal

Assumption: All the projects have same Higgs number.

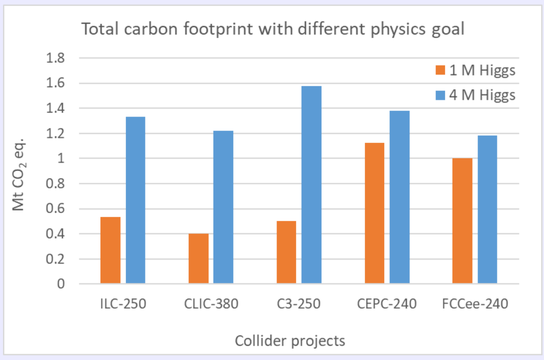

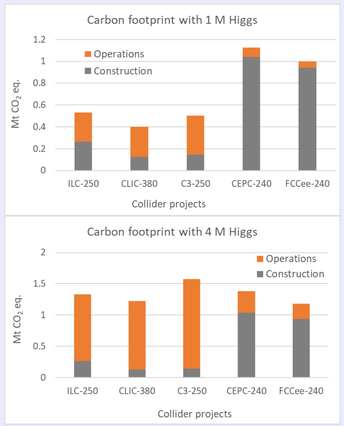

- The carbon footprint of CEPC was estimated based on simplified model including both construction process and operation process.
- The environmental impact of CEPC with different circumference, different energy source, different SR power and different Higgs number was studied.
- The carbon intensity of the electric grid will be reduced rapidly by 2040 due to the development of renewable energies. And it is possible to consider using the dedicated renewable electricity plants for each collider project.
- Assuming all the colliders will use the same clean energy (20 ton CO_2e/GWh), CEPC has the lowest carbon emission to produce one Higgs boson.
- The environmental impact of CEPC and strategies to lower the carbon footprint will be studied continuously.

#wangd93@ihep.ac.cn

Institute of High Energy Physics (IHEP), Beijing, China